YGS Field Trip Guidebook

Magmatic-hydrothermal deposits in central Yukon: Variations on a theme

Patrick Sack and Maurice Colpron

with contributions from:
Helena Kuikka – Eagle mine
Al McOnie – Keno district
Nikolett Kovacs – Minto Mine and Carmacks Copper deposit
Tony Barresi, Jesse Halle and Emily Halle – Freegold district

Published under the authority of the Department of Energy, Mines and Resources, Government of Yukon yukon.ca.

Printed in Whitehorse, Yukon, 2022.

Publié avec l'autorisation du Ministères de l'Énergie, des Mines et des Ressources du gouvernement du Yukon, yukon.ca.

Imprimé à Whitehorse (Yukon) en 2022.

This, and other Yukon Geological Survey publications, may be obtained from:
Yukon Geological Survey
102-300 Main Street
Box 2703 (K-102)
Whitehorse, Yukon, Canada Y1A 2C6
email geology@gov.yk.ca

Yukon Geological Survey website https://yukon.ca/en/science-and-natural-resources/geology.

In referring to this publication, please use the following citation:

Sack, P. and Colpron, M., 2022. Magmatic-hydrothermal deposits in central Yukon: Variations on a theme. Yukon Geological Survey, Field Trip Guidebook, 73 p.

Cover photo: Participants of a 2019 Keno Hill district field trip run by Alexco Resources Corp. and the Yukon Geological Survey.

Preface

This field trip guidebook was prepared for the 100th Anniversary Meeting of the Society of Economic Geologists originally planned to be held in Whistler, British Columbia, September 15–18, 2020. The meeting was postponed because of the global COVID-19 pandemic and was rescheduled to September 14–17, 2021, but the field trips were canceled due to travel uncertainty at the time. Victoria Gold Corp. (Eagle mine), Alexco Resource Corp. (Keno Hill district), Pembridge Resources (Minto mine), Copper North Mining Corp. (Carmacks Copper deposit) and Triumph Gold Corp. (Mount Freegold district) generously agreed to host the field trip and enabled their geologists to contribute to this guidebook. Anyone wanting to follow this guidebook is advised to contact the companies regarding access.

Patrick Sack
Metallogenist
Yukon Geological Survey

Table of Contents

Introduction

This five-day field trip through central Yukon examines five magmatic-hydrothermal deposits hosted in two distinct geological domains delimited by the Tintina fault in the northern Cordillera (Fig. 1; Table 1). The domain northeast of the Tintina fault is primarily underlain by Neoproterozoic to Paleozoic sedimentary rocks that were deposited along the western continental margin of ancestral North America (or Laurentia in the Paleozoic). This domain is characterized by extensive shale successions and epigenetic deposits hosted in these basinal rocks are typically Au, W or Ag-Zn-Pb deposits that formed from reduced mineralizing fluids (Table 2). The first two days of the excursion focus on two distinct types of mineralization. On Day 1, we visit the mid-Cretaceous reduced intrusion-related gold system on the Dublin Gulch property, including the Eagle Gold Mine of Victoria Gold Corp. (Tables 1 and 2). On Day 2, we tour the historic Keno Hill silver district, where Late Cretaceous high-grade Ag-Pb-Zn vein systems are inferred to be also derived from reduced mineralizing fluid (e.g., Lynch, 1989; Beaudoin and Sangster, 1992).

Southwest of the Tintina fault, the Intermontane terranes comprise variably metamorphosed volcanic, plutonic and sedimentary rocks that formed in magmatic arc environments between the mid-Paleozoic and Mesozoic. In this domain, magmatic-hydrothermal mineral systems consist mainly of porphyry-style Cu (Au, Ag ± Mo) deposits that are the product of oxidized mineralizing fluids (Table 2). These styles of deposits are the focus of the second part of the field trip (Table 1). Days 3 and 4 tour the Minto Mine and Carmacks Copper deposit, where Late Triassic porphyry Cu (Au-Ag) mineralization has been variably modified by post-mineral deformation and subsequent metamorphism/migmatization associated with intrusion of younger Early Jurassic batholiths. These two tours will illustrate the range of textural and mineralogical modification of the host rock and ore, and review the evidence leading to interpretation of these enigmatic deposits as metamorphosed alkalic(?) porphyry Cu deposits.

On the last day, we visit a more classic porphyry system in the Mount Freegold district. There, Cu (Au, Ag ± Mo) mineralization is related to Late Cretaceous intrusions, similar to the large Casino deposit, and controlled by a dextral strike-slip fault system. Throughout the excursion, the regional tectonic and metallogenetic controls on the various styles of mineralization are also discussed.

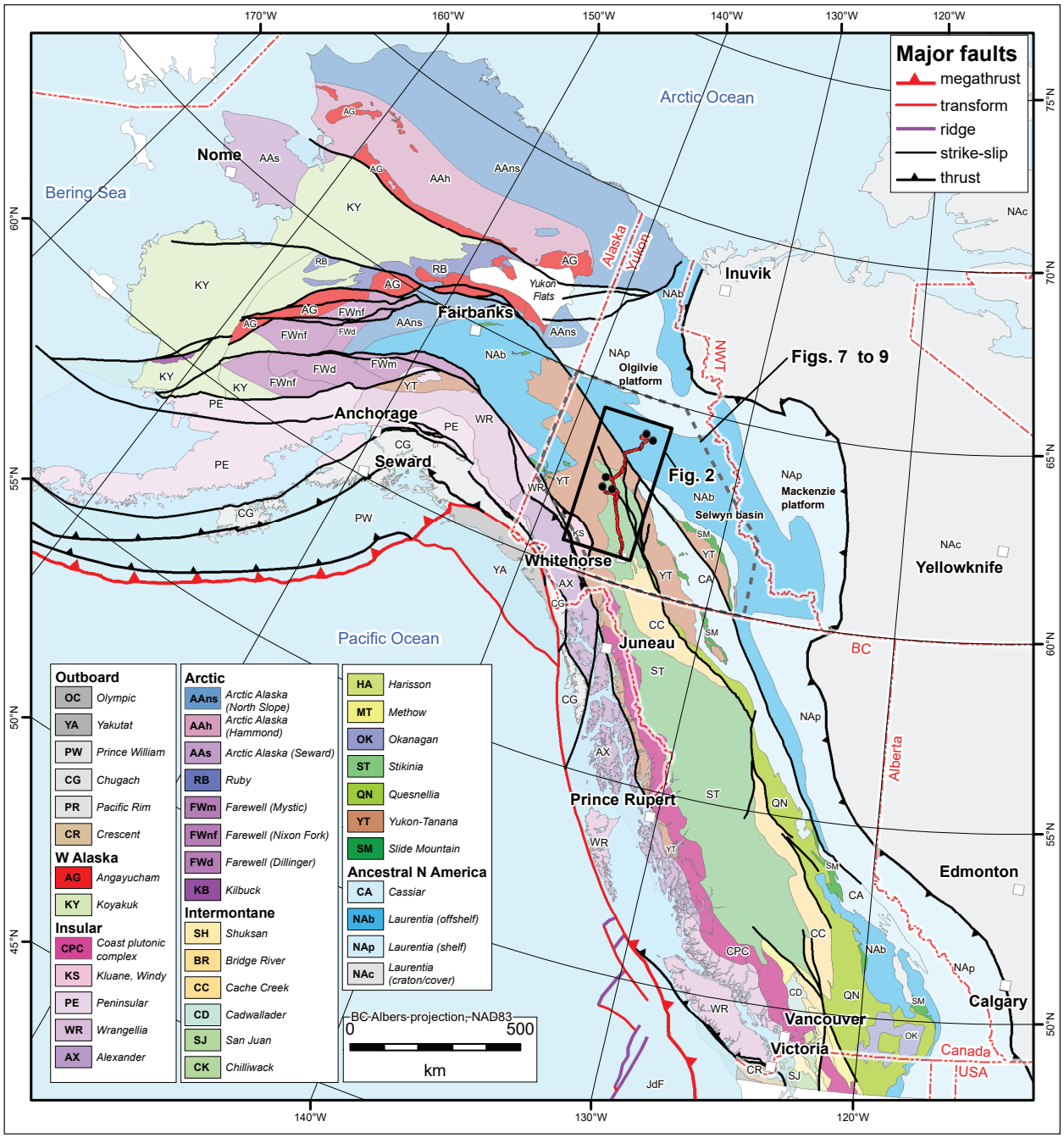

Figure 1. *Terrane map of the northern Cordillera (YGS, 2020d). Field trip route shown by red line, field trip locations by black circles.*

Table 1. *Summary of distances travelled.*

Day	Location	Driving (km)	Driving (hours)	Touring (hours)	Length of day (hours)
0	Whitehorse				
1	Eagle deposit tour	150	3	5	8
2	Keno district tour	20	0.5	8	8.5
3	Minto deposit tour	325	5.5	6	11.5
4	Carmacks Copper deposit tour	120	3	6	9
5	Freegold district tour	330	6	6	12
6	Whitehorse				

Table 2. *Summary of characteristics of the deposits and districts on the field trip. Compiled from references in text.*

Deposit/district	Eagle/Dublin Gulch	Keno Hill	Minto	Carmacks Copper	Nucleus & Revenue/ Mount Freegold
Deposit model	reduced intrusion-related gold system (RIRGS)	veins (at least some magmatic input)	metamorphosed alkalic (?) porphyry	metamorphosed alkalic (?) porphyry	calc-alkalic porphyry system
Host rock unit and lithology	Yusezyu Formation: metasandstone and shale	Keno Hill Quartzite	Minto suite: granodiorite	Minto suite: granodiorite	Whitehorse suite: granodiorite
Host rock age	Neoproterozoic	Mississippian	Early Jurassic	Early Jurassic	mid-Cretaceous
Age of mineralization	93.2 ± 0.3 Ma	ca. 89–68 Ma?	ca. 215 Ma?	ca. 215 Ma	mostly ca. 76–72 Ma; minor ca. 105 Ma
Age of magmatism	96–93 Ma	94–89 Ma	Late Triassic to Early Jurassic; 205–194 Ma	Late Triassic to Early Jurassic; 205–194 Ma	Early Jurassic, mid and Late Cretaceous (ca. 105 and 75 Ma)
Oxidation state of magma and mineralizing fluid	reduced	reduced	oxidized	oxidized	oxidized
Metal assemblage	Au-(As)-Bi-Te-W	Ag-Pb-Zn-(As)-Sb ± Cu ± Bi	Cu-Au-Ag ± Mo	Cu-Au-Ag ± Mo	Cu-Au-Ag-Mo ± W
Post-mineralization modification	brittle faulting	brittle faulting	ductile fabric, metamorphism, folding, migmatization, brittle faulting	ductile fabric, metamorphism, folding, migmatization, brittle faulting	brittle faulting

Data sources

Regional geology maps are made using the Yukon Geological Survey bedrock geodatabase (YGS, 2020a). This dataset can be downloaded online at http://data.geology.gov.yk.ca/Compilation/3. Legends for geology maps show layered rocks with rectangular patches and plutonic rocks with oval patches.

Radiometric ages are primarily from the Yukon Geological Survey geochronology database (YGS, 2020b). This database can be downloaded online at http://data.geology.gov.yk.ca/Compilation/22.

Mineral occurrences are referenced with a unique identifier comprising the 1:250 000 NTS sheet and a three-digit inventory number from Yukon MINFILE (YGS, 2020c). These are referenced in the text with square brackets e.g., [115I 021]. Further information on each occurrence can be found online at http://data.geology.gov.yk.ca/Occurrences/.

Regional geologic setting

The northern Cordillera is an accretionary orogen that has developed along the western edge of the North American continental plate at its boundary with the oceanic Pacific plate (Fig. 1). The eastern part of the orogen is underlain by parautochthonous, mainly sedimentary rocks that were deposited along the continental margin of western Laurentia. To the west, large parts of the Intermontane Plateaus and Pacific Mountains systems of British Columbia, Yukon and most of Alaska are comprised of allochthonous terranes (Monger and Price, 2002; Colpron *et al.*, 2007; Nelson *et al.*, 2013; Colpron and Nelson, 2021). The allochthonous terranes include volcanic, plutonic, sedimentary, and metamorphic assemblages that originated as parts of microcontinents, magmatic arcs, accretionary complexes, and segments of ocean basins. They were accreted to western North America mainly in the Mesozoic and Cenozoic. Parts of the northern Cordillera are overlain by Jurassic and younger syn and post-accretionary siliciclastic deposits (e.g., Whitehorse trough). Syn to post-accretionary plutons intrude the allochthonous terranes and the western part of the continental margin succession; in Yukon, the Cretaceous magmatic front extends farther east into the continental margin than in the southern part of the orogen in British Columbia. A series of post-accretionary, mainly dextral strike-slip faults dissect the interior of the orogen and mark its western boundary in coastal British Columbia and southeast Alaska (Fig. 1).

In central Yukon, the Tintina fault is a major strike-slip fault with approximately 430 km of dextral offset since the latest Cretaceous (<64 Ma; Gabrielse *et al.*, 2006). It juxtaposes rocks of the western Laurentian continental margin, to the northeast, to the allochthonous Intermontane terranes to the southwest (Fig. 2).

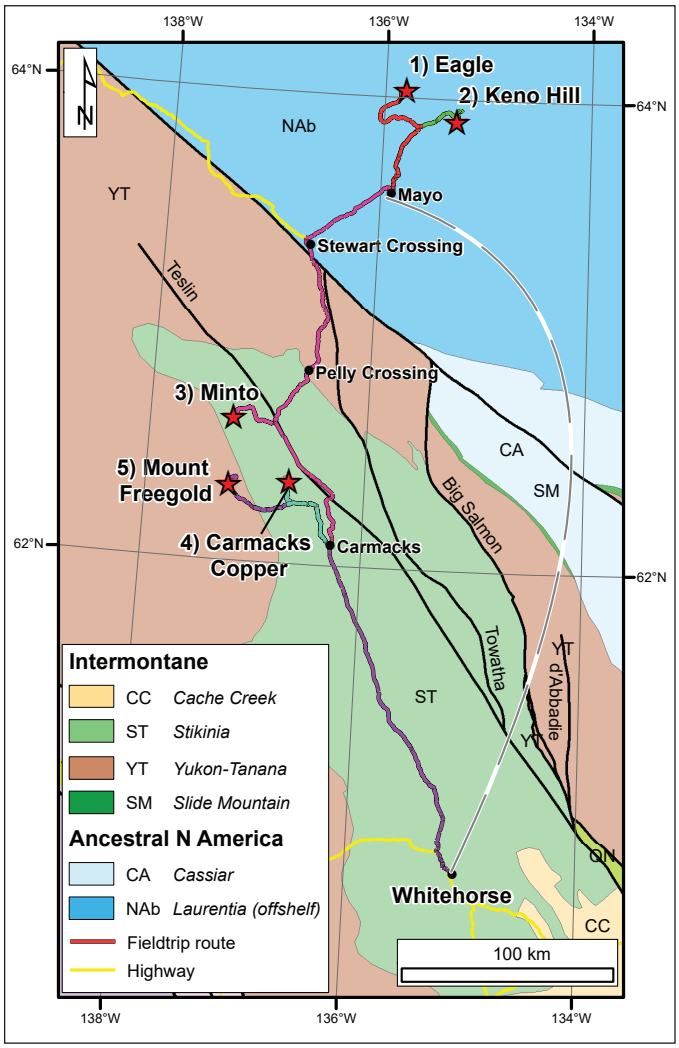

Figure 2. *Field trip route in south and central Yukon. Numbered locations refer to order of field trip days in Table 1. Dashed grey line illustrates flight from Whitehorse to Mayo. Highways colour coded to days driving: red = day 1, green = day 2, pink = day 3, aquamarine = day 4 and purple = day 5.*

Continental margin strata

Neoproterozoic to lower Paleozoic strata deposited along the western margin of Laurentia record rifting associated with breakup of the supercontinent Rodinia (Hyland Group on Fig. 3) and subsequent development of a passive continental margin (Abbott and Turner, 1990; Moynihan et *al.*, 2019). In central Yukon, Cambrian to Lower Devonian strata were deposited in an offshelf, basinal setting (Selwyn basin) and comprise predominantly shale, calcareous shale, sandstone and chert, with local occurrences of alkalic volcanic rocks (Gull Lake Formation to Road River Group on Fig. 3; Gordey and Anderson, 1993). Coeval, shallow-water shelf carbonate was deposited on the Mackenzie platform to the east and Ogilvie platform to the north (Fig. 1). Passive margin sedimentation was interrupted in the Middle to Late Devonian and strata of the upper Earn Group unconformably overlie various older strata of Selwyn basin across central Yukon (Gordey et *al.*, 1987). The Earn Group comprises black shale, chert sandstone and conglomerate, and locally calc-alkaline magmatic rocks. The sub-Earn unconformity and Late Devonian magmatism are inferred to correspond with the onset of active margin tectonism along western Laurentia, including initial arc magmatism in the Yukon-Tanana terrane and opening of the Slide Mountain ocean in Late Devonian to Early Mississippian (Mortensen, 1992; Nelson et *al.*, 2006; Colpron et *al.*, 2007; Colpron and Nelson, 2009; Cobbett et *al.*, 2021).

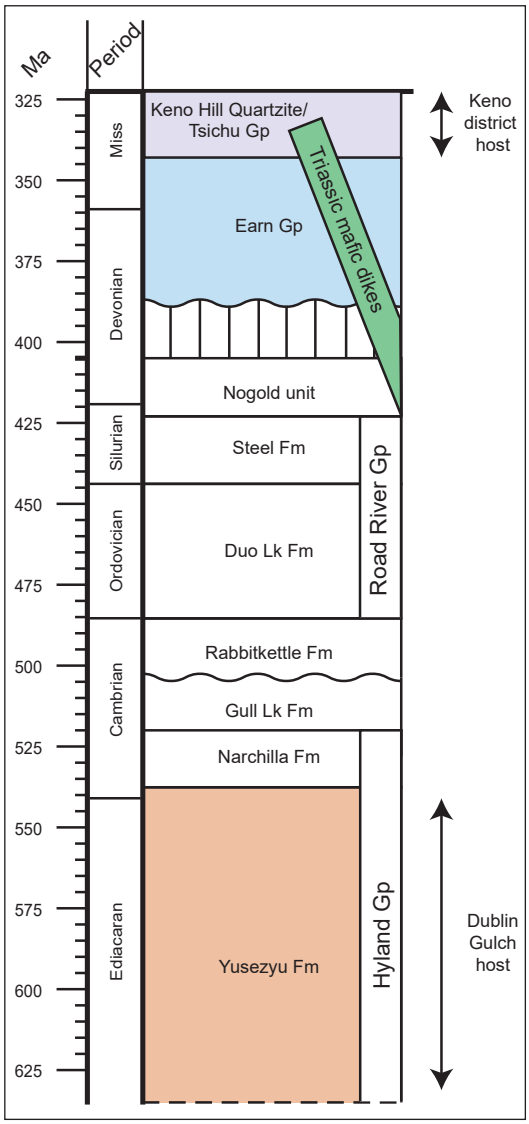

Figure 3. *Composite regional stratigraphic column for the McQuesten-Keno area from Roots (1997) and Murphy (1997). Timescale from Cohen et al. (2013). Gp = group, Fm = formation. Coloured background shows the units we will see on this field trip, colours correspond to map units on Figure 4.*

Strata of the Neoproterozoic-Cambrian Hyland Group (primarily the Yusezyu Formation) and Devonian-Carboniferous Earn Group and Keno Hill Quartzite are most relevant to this field trip as they are hosts to mineralization at the Eagle deposit and in the Keno Hill district (Figs. 3 and 4). The Yusezyu Formation rocks consists of fine to coarse-grained metaclastic rocks, primarily greenish, quartz-rich chlorite-muscovite schist, locally with schistose quartz grit (Murphy, 1997). The Earn Group comprises primarily dark coloured shale (phyllite) with lesser chert, siltstone, sandstone, limestone, felsic metavolcanic rocks (chlorite-muscovite phyllite) and chert-pebble conglomerate (Murphy, 1997). In the Keno Hill silver district, the chlorite-muscovite phyllite is thick enough to map and occurs near the top of the unit, below the Keno Hill Quartzite (Murphy, 1997). The Keno Hill Quartzite is a thick bedded to massive, medium to dark grey quartzite (Murphy, 1997).

Intermontane terranes

In the northern Cordillera, the Intermontane terranes include the Yukon-Tanana, Slide Mountain, Stikinia, Quesnellia and Cache Creek terranes (Fig. 1). These terranes record development of overlapping mid-Paleozoic to early Mesozoic magmatic arcs (Yukon-Tanana, Stikinia and Quesnellia), a marginal ocean basin (Slide Mountain) and the accretionary complex (Cache Creek) that was adjacent to the Stikinia-Quesnellia arc system. The second part of this field trip focuses on porphyry deposits that are either hosted by, or closely related to Yukon-Tanana and Stikinia (Fig. 5).

The Yukon-Tanana terrane consists of mid to late Paleozoic metavolcanic, metaplutonic and metasedimentary rocks that record development of a series of magmatic arcs that were constructed on a metasedimentary sequence of western Laurentian affinity (Mortensen, 1992; Colpron, 2006; Nelson et *al.*, 2006; Colpron et *al.*, 2007; Piercey and Colpron, 2009). The Yukon-Tanana terrane comprises the oldest rocks in west-central Yukon, southwest of the Tintina fault (Figs. 1 and 5). In the region northwest

of Carmacks, where deposits visited by this field trip are located, the main Yukon-Tanana units present are part of the Snowcap assemblage and Simpson Range plutonic suite (Colpron et *al.*, 2006). The Snowcap assemblage is pre-Late Devonian in age and consists of a metasedimentary sequence including psammitic schist and quartzite. The Simpson Range plutonic suite (355–345 Ma) comprises mainly fine to medium-grained, foliated and locally gneissic metaplutonic rocks of tonalite to granodiorite composition.

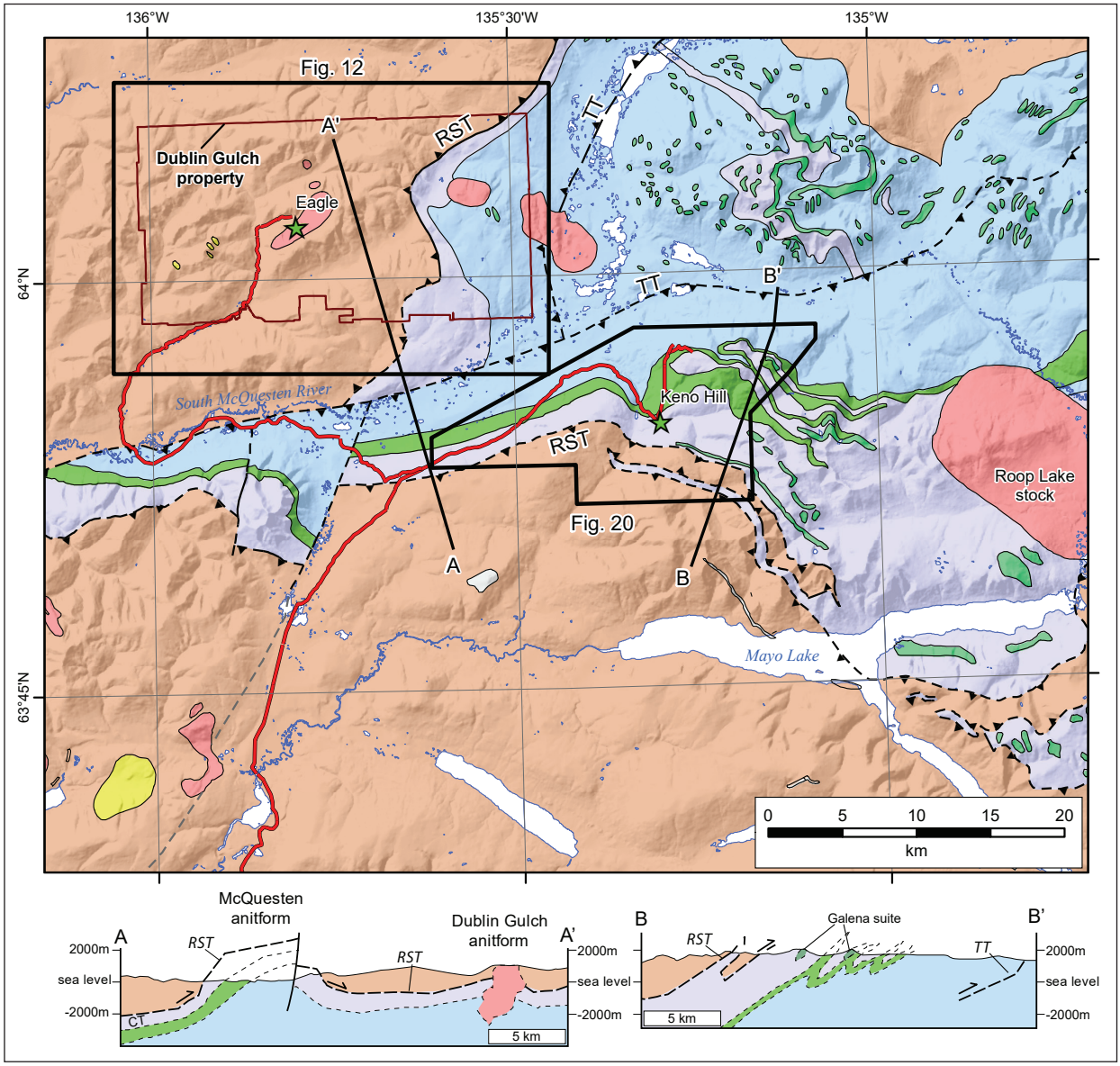

Figure 4. *Simplified regional geological map of the Eagle-Keno City area showing siliciclastic country rocks and plutonic suites relative to sites on this field trip. Geology from YGS (2020a). RST = Robert Service Thrust fault, TT = Tombstone Thrust fault. Cross sections A–A' from Murphy (1997) and B–B' from Roots (1997).*

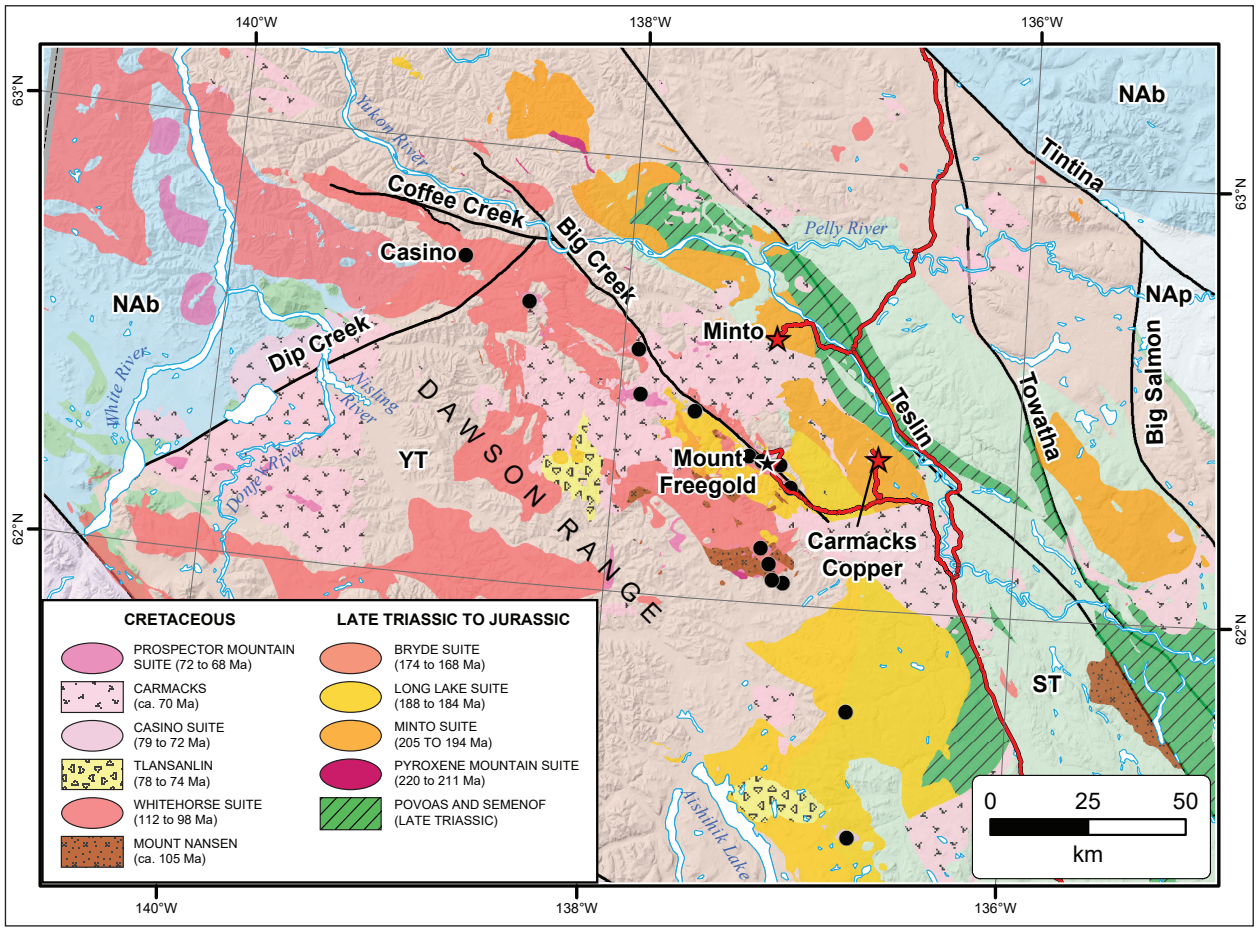

Figure 5. *Simplified regional geological map of the Dawson Range showing plutonic suites and volcanic rocks relative to significant Late Triassic (red) and Late Cretaceous (black) mineral occurrences. Geology from YGS (2020a). Stars show occurrences included on the field trip. Underlying terrane colours as in Figure 1.*

In Yukon, Stikinia is represented by the Upper Triassic volcanic and associated sedimentary rocks of the Lewes River Group (Wheeler, 1961; Tempelman-Kluit, 1984, 2009; Hart, 1997). The northernmost exposures of these Upper Triassic rocks occur in the area visited for this field trip. Northwest of Carmacks, volcanic rocks of the Lewes River Group are assigned to the Povoas formation and consist of mainly mafic to intermediate, calc-alkaline basalt and basaltic-andesite with common pyroxene and plagioclase phenocrysts. The rocks are generally foliated and metamorphosed to greenschist facies (chlorite grade). Amphibolite and schist xenoliths that host the mineralization at the Carmacks Copper deposit are interpreted to be derived from rocks of the Lewes Group that were metamorphosed to higher grade during intrusion of the younger plutonic rocks of the Granite Mountain batholith (Kovacs, 2018; Kovacs *et al.*, 2020). Coarse-grained,

Late Triassic pyroxenite bodies (locally coarse-grained amphibolite) that intrude the Yukon-Tanana terrane northwest of Carmacks suggest that these older Paleozoic rocks form the basement to Stikinia in this region (Nelson *et al.*, 2013; Sack *et al.*, 2020).

Regional deformation

Central Yukon was affected by multiple episodes of syn to post-accretionary deformation. Southwest of the Tintina fault, rocks of the Yukon-Tanana terrane were deformed and metamorphosed at mid to lower crustal levels (~5–7 kbar) during Early Jurassic arc-continent collision (*ca.* 195–185 Ma; Berman *et al.*, 2007; Clark, 2017; Gaidies *et al.*, 2021). Early Jurassic deformation is inferred to be related to a series of southwest-verging thrust sheets in the Yukon-Tanana terrane. Plutons of the Minto suite were emplaced during this phase of deformation (Sack *et al.*, 2020). Early Jurassic mica cooling ages suggest that the Yukon-Tanana terrane was exhumed to upper crustal levels shortly after burial and development of the penetrative foliation.

Northeast of the Tintina fault, thrust imbrication of continental margin strata and the leading edge of the accreted terranes (Yukon-Tanana and Slide Mountain in southeastern Yukon; Fig. 1) is generally thought to have occurred in the Jura-Cretaceous. Emplacement of the accreted terranes post-dates Upper Triassic (Norian) strata in the footwall of the Inconnu thrust (Murphy *et al.*, 2006) and the fault is intruded by the *ca.* 100–98 Ma Orchay batholith north of Ross River. Near Mayo, major regional structures include the Robert Service and Tombstone thrust faults (Fig. 4; Murphy, 1997). The Robert Service thrust emplaces rocks of the Hyland Group in its hanging wall over shale and quartzite of the Earn Group and Keno Hill Quartzite in the footwall along much of its strike length. To the west, near the Dempster Highway, Triassic and Jurassic shale occupy the footwall of the Robert Service thrust (Tempelman-Kluit, 1970). The Robert Service thrust is intruded by the *ca.* 94 Ma Roop Lake stock east of Keno Hill (Roots, 1997).

Deformation associated with the Tombstone thrust to the north resulted in development of a several kilometres-thick greenschist facies strain zone in its hanging wall and folding of the Robert Service thrust (Murphy, 1997; Read *et al.*, 2020). The Tombstone thrust imbricates Devonian and Carboniferous strata containing Triassic gabbro sills over much of its strike length. Like the Robert Service, the Tombstone thrust is northeast-striking near the Dempster Highway where it juxtaposes the Keno Hill Quartzite in its hanging wall with the Jurassic (Oxfordian) “Lower Schist” in its footwall (Thompson *et al.*, 1992). The Tombstone thrust and ductile fabrics in the overlying Tombstone strain zone are also intruded by *ca.* 94–92 Ma plutons. Ductile fabrics in the Tombstone strain zone are characterized by a penetrative transposition foliation, boudinage of transposed beds, and northwest-directed extensional shear bands (Murphy, 1997). Mair *et al.* (2006) suggested that muscovite with $^{40}Ar/^{39}Ar$ ages of 104–100 Ma cooled shortly after cessation of deformation in the Tombstone strain zone. Northwest-verging deformation in the Tombstone thrust sheet has been linked to west-northwest-striking dextral strike slip faults to the south (Murphy, 1997; Gabrielse *et al.*, 2006; Nelson *et al.*, 2013). Ductile fabrics and fault surfaces in the Mayo area are folded by the west-southwest-plunging McQuesten antiform (Murphy, 1997).

Dextral strike slip faults developed between 105 and 95 Ma, and occur on both sides of the Tintina fault. These structures are inferred to form part of the northwest-directed extrusion of the core of the northern Cordillera, in which the northwest-verging Tombstone thrust is part of the frontal thrust system (Nelson *et al.*, 2013).

Emplacement of mid to Late Cretaceous plutons northeast of the Tintina fault is inferred to have been facilitated by extension after the end of ductile deformation. Similarly, vein faults in the Keno Hill district are thought to have developed in an extensional regime resulting in oblique-left normal to dip slip faults (Read *et al.*, 2021).

Southwest of the Tintina fault, displacement along dextral strike slip faults locally persisted into the Late Cretaceous (*e.g.*, Big Creek fault, *ca.* 73 Ma; Mottram *et al.*, 2020). Development of northeast-striking normal faults could be related to these younger strike slip faults, or they are younger normal faults associated with emplacement of the *ca.* 70 Ma Carmacks Group basalts. All of these elements were offset by ~430–490 km of Paleocene-Eocene dextral displacement along the Tintina fault (Gabrielse *et al.*, 2006).

Tectonomagmatic setting

Mesozoic magmatic rocks in the northern Cordillera are broadly the products of two arc cycles corresponding to periods of orogen normal compression related to the accretion of outboard terranes onto the western continental margin of Laurentia (Armstrong, 1988; Monger and Gibson, 2019). In both cycles, magmatism began as subduction-related, evolved to post-subduction settings, and was associated with significant intrusion-related mineralization (Fig. 6). In the earlier Late Triassic to Jurassic cycle, magmatism initiated as island arc magmatism related to subduction beneath the Intermontane terranes. In Yukon, this magmatism rapidly evolved into syn-collisional magmatism by the Early Jurassic, possibly as a result of orocline development (*e.g.*, Mihalynuk *et al.*, 1994) and was increasingly contaminated by continental crust through the Jurassic (Sack *et al.*, 2020). The record of this magmatic event in Yukon is primarily mid-crustal plutons. Farther south in British Columbia, there are higher-level plutons and coeval volcanic rocks (Nelson *et al.*, 2013) with preserved porphyry systems (Logan and Mihalynuk, 2014).

In the case of the second cycle, mid-Cretaceous magmatism began as widespread continental arc and back-arc magmatism related to renewed, east-dipping subduction beneath the Intermontane terranes (Rasmussen, 2013). This magmatic event evolved into volumetrically minor, but economically significant, Late Cretaceous magmatism coeval with the accretion of the Insular terranes to the western margin of the Intermontane terranes *ca.* 80 Ma (Vice, 2017). Between the two magmatic arc cycles, there was a magmatic lull, *ca.* 160 to 120 Ma that was broadly coeval with strike-slip transpression throughout the northern Cordilleran orogen (Fig. 6; Monger and Gibson, 2019).

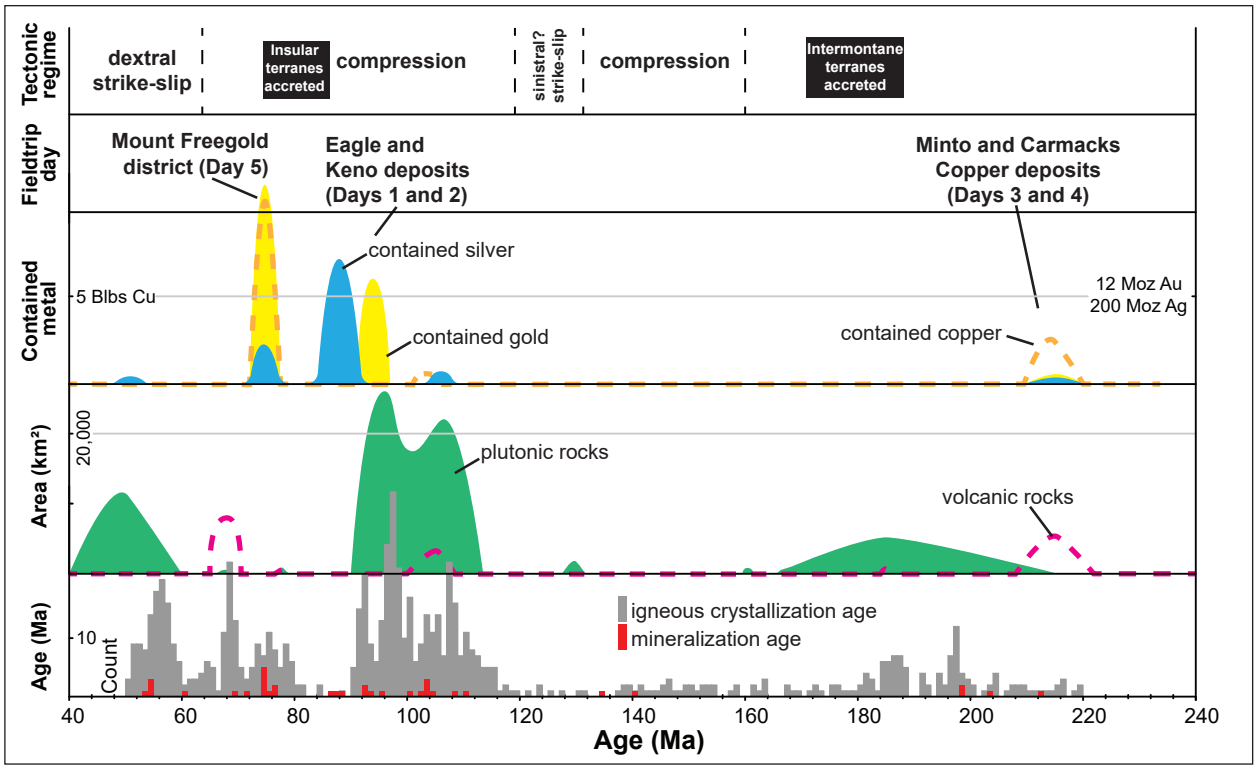

Figure 6. *Schematic framework for central Yukon showing the coeval occurrence of magmatism, compressional tectonics and metal endowment. Igneous crystallization (grey) and mineralization (red) age frequency histogram from YGS (2020b). Mapped area of volcanic (pink dash) and plutonic (green solid) rocks calculated from YGS (2020a). Amount of contained copper (orange dash), gold (yellow solid) and silver (blue solid) calculated from deposits in Casselman (2018). Contained metals are predominantly within intrusion-related deposits except gold, which includes mid-Cretaceous orogenic gold deposits. Tectonic regime from Monger and Gibson (2019), Insular terrane accretion age from Vice (2017).*

Late Triassic to Jurassic (218–168 Ma)

In Yukon, the Late Triassic to Jurassic magmatic rocks are subdivided into nine plutonic suites and three formations of volcanic rocks (Fig. 7). From oldest to youngest, Late Triassic to Jurassic magmatic rocks in Yukon are the:

- Late Triassic Pyroxene Mountain (218–214 Ma), Stikine (217–214 Ma) and Headless (208–207 Ma) suites and Povoas (ca. 237–209 Ma) and Semenof formations, interpreted to have formed in an island arc setting;
- latest Triassic to Early Jurassic Minto (205–194 Ma), Lokken (195–184 Ma), Long Lake (188–183 Ma) and Bennett (178–175 Ma) suites and Nordenskiöld tuffaceous facies of the Laberge Group (188–184 Ma), interpreted to have formed in a syn-collisional setting; and
- Middle Jurassic Bryde suite (174–168 Ma), interpreted to have formed in a post-collisional setting.

For the purposes of this field trip, we will focus on the Late Triassic mafic volcanic rocks, the likely protolith for rafts of porphyry mineralization at the Minto and Carmacks Copper deposits, and the latest Triassic to Early Jurassic Minto plutonic suite that hosts the deposits.

In general, the Late Triassic to Jurassic plutons lack an association with coeval volcanic rocks in Yukon. The exceptions to this are the plutons of the Stikine and Pyroxene Mountain suites which are broadly coeval with volcanic and volcaniclastic rocks of the Povoas formation in Stikinia (Bordet *et al.*, 2019; Hart, 1997; Tempelman-Kluit, 1984; Wheeler, 1961), and small plugs of the Headless suite which intrude coeval

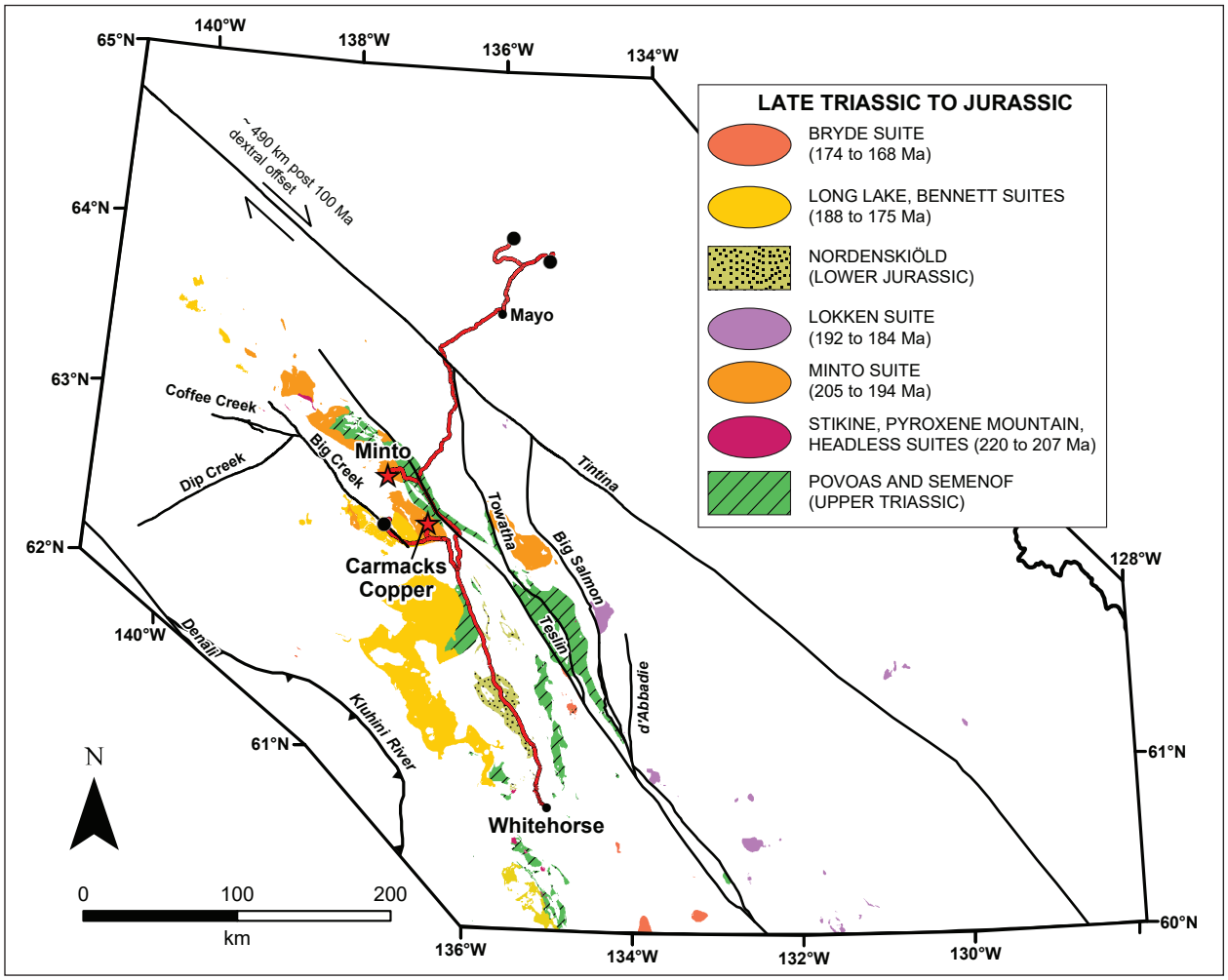

Figure 7. *Late Triassic to Jurassic plutons and volcanic rocks (215–168 Ma) in southern and central Yukon. Geology from YGS (2020a). Field trip route in red, Late Triassic deposits included on field trip shown by red stars, other deposits included on field trip shown by medium black circles. Dextral offset on Tintina fault from Gabrielse et al. (2006).*

rocks of the Upper Triassic Semenof formation east of the Teslin fault (Simard, 2003; Tempelman-Kluit, 1984). There are also Early Jurassic pyroclastic rocks of the Lower Jurassic Nordenskiöld facies in the Whitehorse trough (Colpron and Friedman, 2008). No record of Jurassic volcanism is known outside of Whitehorse trough in Yukon, the closest preserved volcanic rocks of this age are the Hazelton Group in northern British Columbia (Nelson et *al.*, 2013). The lack of volcanic equivalents suggests the plutonic record during the latest Triassic to Jurassic is confined to deeper levels of the crust. This is corroborated by the abundance of magmatic epidote in all Minto suite plutons and portions of Long Lake suite plutons (Sack et *al.*, 2020) which is indicative of emplacement depths below ~6.5 kbar (25 km; Zen and Hammarstrom, 1984). Geobarometry using Al-in-hornblende in the plutons confirms these field observations with nearly all plutons emplaced between 7 and 3 kbar (25 and 11 km depth; Sack et *al.*, 2020). These emplacement depths are also consistent with regional metamorphic studies that indicate amphibolite facies assemblages developed at pressures of 4–9 kbar between 195 and 187 Ma (Berman et *al.*, 2007; Clark, 2017; Gaidies et *al.*, 2021). These data indicate that Late Triassic magmatic rocks preserve the appropriate upper crustal level for porphyry systems whereas Early Jurassic magmatic rocks in Yukon were likely emplaced too deep for porphyry mineralization to have occurred. Not discussed here, are post-collisional, Middle Jurassic plutons (Bryde suite) which appear to have been emplaced at shallow crustal levels and have minor porphyry-style occurrences associated with them (Sack et *al.*, 2020).

mid-Cretaceous (117–90 Ma)

Mid-Cretaceous plutons are grouped into eight plutonic suites and two volcanic formations (Rasmussen, 2013; Fig. 8). This field trip focuses on mid-Cretaceous plutonic rocks formed in continental arc and post-arc settings. From oldest to youngest, Rasmussen (2013) has summarized the following mid-Cretaceous suites in Yukon:

- Whitehorse suite (112–98 Ma) and volcanic rocks of the Mount Nansen formation (108–104 Ma) interpreted to have formed in a continental arc setting;
- Anvil (110–104 Ma), Hyland (106–100 Ma) and Cassiar (117–104 Ma) suites interpreted to have formed in a back-arc setting; and
- Seagull (103–94 Ma), Tay River (99–95 Ma), Tungsten (98–96 Ma), Mayo (98–93 Ma), Tombstone (94–90 Ma) suites and South Fork volcanic rocks (*ca.* 98 Ma) interpreted to have formed in a post-arc setting.

Whitehorse suite and volcanic equivalents are continental arc rocks associated with minor epithermal mineralization in the Freegold district. Plutons of the post-arc Mayo suite are the causative intrusions of reduced intrusion-related gold system north of Mayo, including the Eagle gold deposit, and are the closest intrusive rocks to the Keno Hill silver district (Fig. 8).

Most mid-Cretaceous plutonic rocks were derived from continental arc magmas, emplaced during orogenesis (Armstrong, 1988), when deformation was broadly orogen normal throughout the Cordillera (Monger and Gibson, 2019). The magmatic rocks in south Yukon are subduction-related with the main magmatic arc axis likely demarcated by the Dawson Range batholith and back-arc plutons farther to the east (Fig. 8). The mid-Cretaceous subduction zone was likely east dipping and located between the Insular and Intermontane terranes, possibly near what is now the Denali fault. Mid-Cretaceous plutons are found from the Dawson Range batholith to past the Yukon–NWT border, some 300 km to the northeast. The farthest north of these, the Mayo and Tombstone suites, are notably younger (ca. 98–90 Ma) than the arc and back-arc

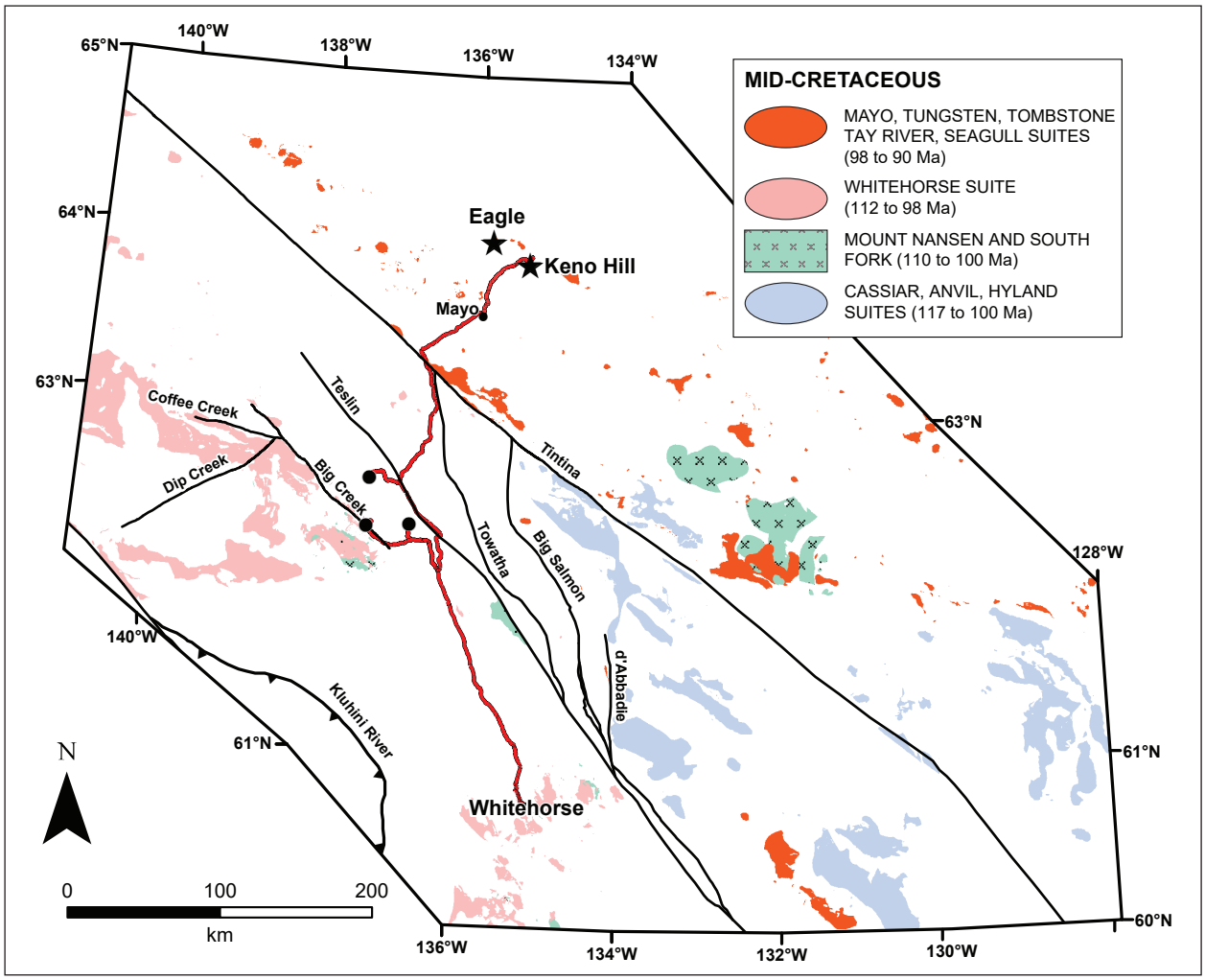

Figure 8. *Mid-Cretaceous (117–90 Ma) plutons in southern and central Yukon. Geology from YGS (2020a). Field trip route in red, mid-Cretaceous deposits included on field trip shown by black stars, other deposits included on field trip shown by medium black circles. Grouping of plutonic suites based on tectonic setting from Rasmussen (2013). Dextral offset on Tintina fault from Gabrielse et al. (2006).*

plutons and were emplaced in a post-arc extensional setting related to early dextral strike-slip movement along the Tintina fault (Gabrielse *et al.*, 2006; Rasmussen, 2013). In addition to being relatively late in arc formation, plutons northeast of the Tintina fault were also emplaced into parautochthonous Paleozoic and older rocks with significant amounts of reduced sedimentary strata (*e.g.*, black shale of the Earn and Road River groups) and these plutons have significant crustal contamination. As a result, many of these plutons are muscovite-bearing, ilmenite or ilmenite/magnetite transition series granitoids with low magnetic susceptibility ($<3 \times 10^{-3}$ SI units) which crystallized under reduced to weakly oxidized magmatic conditions (Hart, 2007).

Late Cretaceous (82–64 Ma)

Late Cretaceous plutons are subdivided into four plutonic suites, and three volcanic formations (Fig. 9). From oldest to youngest, the Late Cretaceous suites are:

- Rancheria suite (82–77 Ma) and Open Creek formation (*ca.* 80 Ma);
- Casino suite (79–72 Ma) and Tlansanlin formation (*ca.* 79–75 Ma);
- Prospector suite (72–68 Ma) and Carmacks Group (*ca.* 70–68 Ma); and
- McQuesten suite (67–64 Ma).

For this field trip, we will focus on the Casino suite as it includes the causative plutons for most of the porphyry systems in the Freegold district.

Late Cretaceous magmatism is also continental arc-related and may have initiated late or immediately post-subduction (*e.g.*, Mezger et al., 2001) with emplacement of the early Late Cretaceous calc-alkaline Rancheria and Casino suites and eruption of the Tlansanlin and Open Creek intermediate to felsic volcanic rocks. Magmatism evolved to the weakly alkalic late Late Cretaceous Prospector Mountain suite and coeval alkaline Carmacks Group volcanic rocks which are dominated by olivine basalts but also include minor felsic to intermediate volcanic rocks. The setting of these late Late Cretaceous magmatic rocks was also likely post-subduction, but their petrogenetic origin is poorly documented and understood. The petrogenetic origin of the latest Cretaceous McQuesten suite is also poorly understood, but the plutons are aligned northeast across the structural grain of the region and are likely not related to subduction.

Late Cretaceous magmatism initiated as the Insular terranes accreted to the Intermontane terranes *ca.* 80 Ma (Vice, 2017; Vice *et al.*, 2020). This magmatism either just proceeds, or is synchronous with, a major change from dominantly orogen normal deformation to dominantly orogen oblique, dextral strike-slip deformation throughout the Cordillera (Monger and Gibson, 2019). In Yukon, the ~430 km of strike-slip displacement on the Tintina fault is post 67–64 Ma as indicated by the truncation of McQuesten suite plutons (Gabrielse *et al.*, 2006). However, a further 60 km of pre-67 Ma offset is required to restore the Jurassic Inconnu thrust across the Tintina fault and likely occurred between *ca.* 100 Ma and 67 Ma (Gabrielse *et al.*, 2006). Thus the switch to, and initial stages of a dominantly dextral strike-slip tectonic regime in southern Yukon was broadly coeval with mid and Late Cretaceous magmatism.

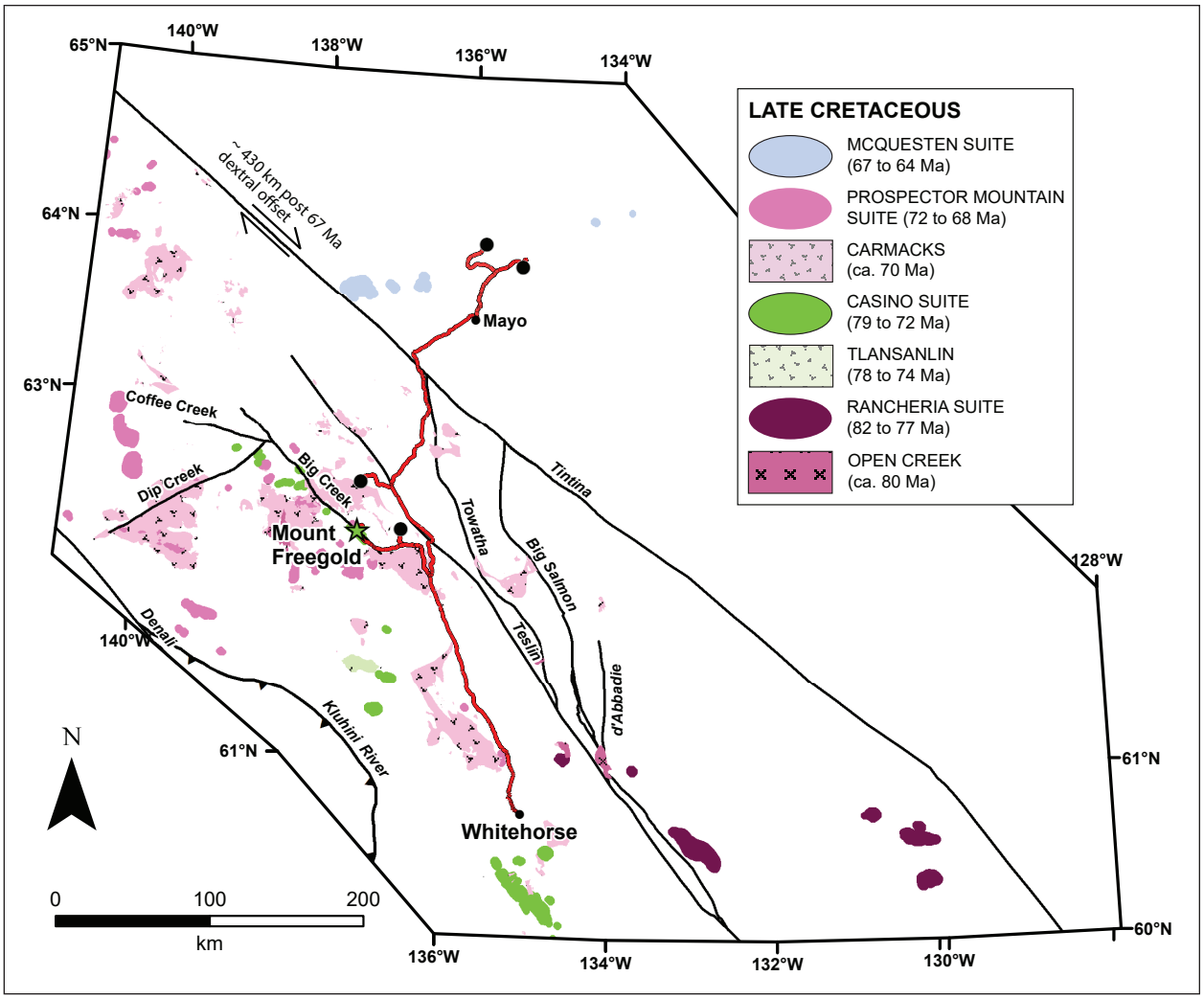

Figure 9. *Late Cretaceous (79–66 Ma) plutons in southern and central Yukon. Geology from YGS (2020a). Field trip route in red, Late Cretaceous deposits included on field trip shown by green star, other deposits included on field trip shown by medium black circles. Dextral offset on Tintina fault from Gabrielse et al. (2006).*

Days 1 and 2 – McQuesten River area

McQuesten River area geology

The first two days of the field trip focus on the Dublin Gulch reduced intrusion-related gold system and the Keno Hill silver district (Fig. 10), on the north and south sides of the South McQuesten River, respectively (Fig. 4). This area is underlain by parautochthonous strata, primarily Neoproterozoic to Mississippian clastic rocks, and is intruded by Middle Triassic mafic sills and mid-Cretaceous intermediate plutons (Murphy, 1997; Roots, 1997). Neoproterozoic-Cambrian rocks of the Yusezyu Formation (Hyland Group) are thrust over Devonian to Mississippian rocks of the Earn Group and Keno Hill Quartzite along the Robert Service thrust fault (Fig. 4). The younger Tombstone strain zone has penetratively deformed the rocks in the McQuesten River area resulting in higher metamorphic grade compared to exposures of equivalent rocks regionally (Murphy, 1997). Ductile deformation was likely complete by 104 to 100 Ma (Mair et *al.*, 2006). The McQuesten antiform broadly folds strata, the Robert Service and Tombstone thrusts and foliations within the Tombstone strain zone about a southwest-trending hinge located in the South McQuesten River valley (Murphy, 1997; Fig. 4). Mid-Cretaceous intrusions of the Mayo suite (Hart et *al.*, 2004a) are undeformed, crosscut all structural features, and were emplaced between 94 and 89 Ma (Murphy, 1997; Roots, 1997; YGS, 2020b).

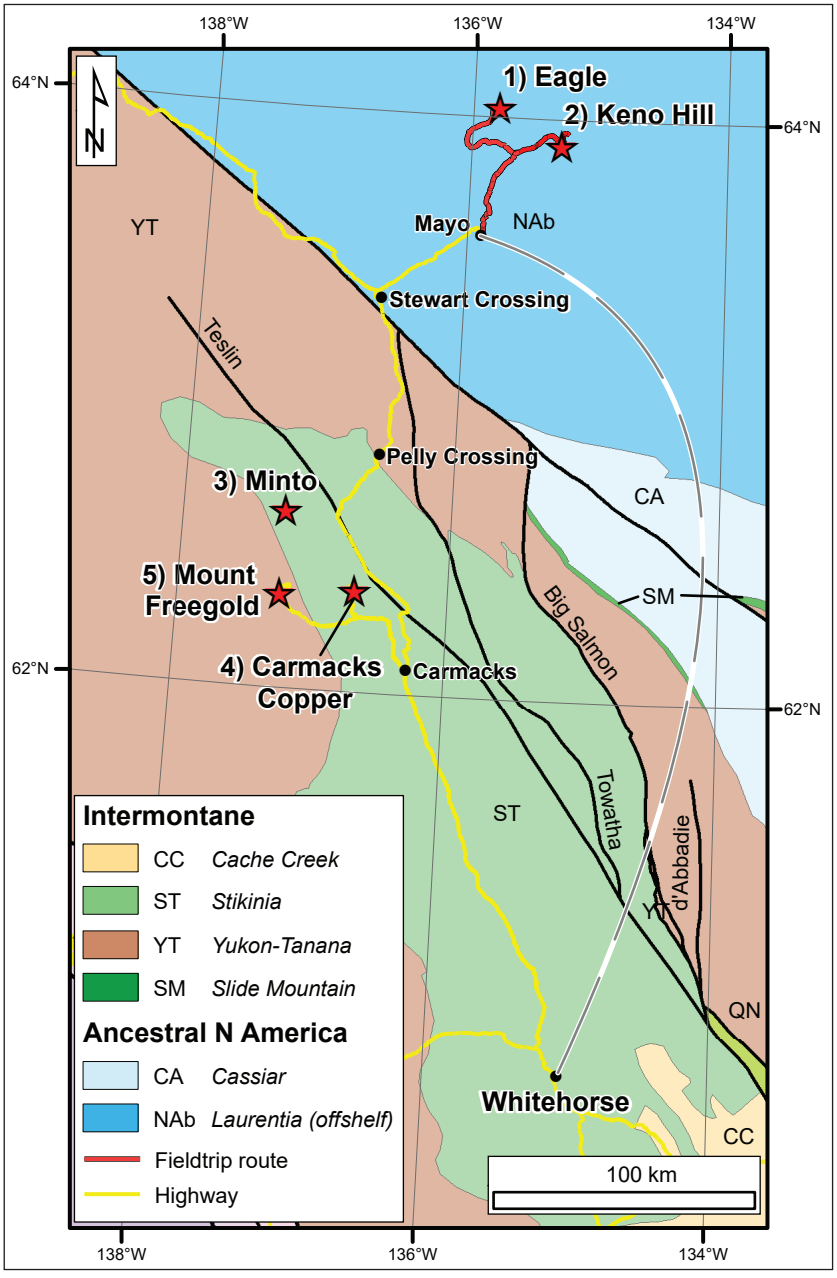

Figure 10. *Field trip route for Days 1 and 2. Numbered locations refer to order of field trip days in Table 1. Dashed grey line illustrates flight from Whitehorse to Mayo.*

Reduced intrusion-related gold systems

Mineralization at the Eagle gold deposit and the surrounding Dublin Gulch property is interpreted as part of a reduced intrusion-related gold system (RIRGS; Fig. 11) associated with the Dublin Gulch stock, part of the Mayo plutonic suite (Fig. 12). The Mayo suite is part of the larger Tombstone-Tungsten belt which forms a narrow belt of intrusions extending 550 km across north-central Yukon and into eastern Alaska (Hart et *al.*, 2004b). Like the majority of gold deposits in RIRGS, gold at the Eagle deposit occurs primarily within the stock, although minor mineralization is noted within surrounding hornfelsed country rock.

Reduced intrusion-related gold systems are characterized by widespread arrays of sheeted auriferous quartz veins with sulphide assemblages characterized by pyrrhotite-arsenopyrite (Hart, 2007). The vein arrays preferentially form in the brittle carapace at the top of stocks and plugs, at depths of 5 to 7 km, where they form bulk-tonnage, low-grade Au deposits characterized by a Au-Bi-Te-W metal assemblage (Hart, 2007). Reduced intrusion-related gold systems also include other intrusion-related mineral deposit styles such as skarns, replacements and polymetallic veins (Hart, 2007). This collection of deposit styles is characterized by proximal Au-W-As and distal Ag-Pb-Zn metal associations (Fig. 11; Hart, 2007). Associated magmas are diverse with characteristics of I, S and A-type granitoids, but one commonality between systems is the reduced ilmenite-series nature of the causative plutons (Hart, 2007).

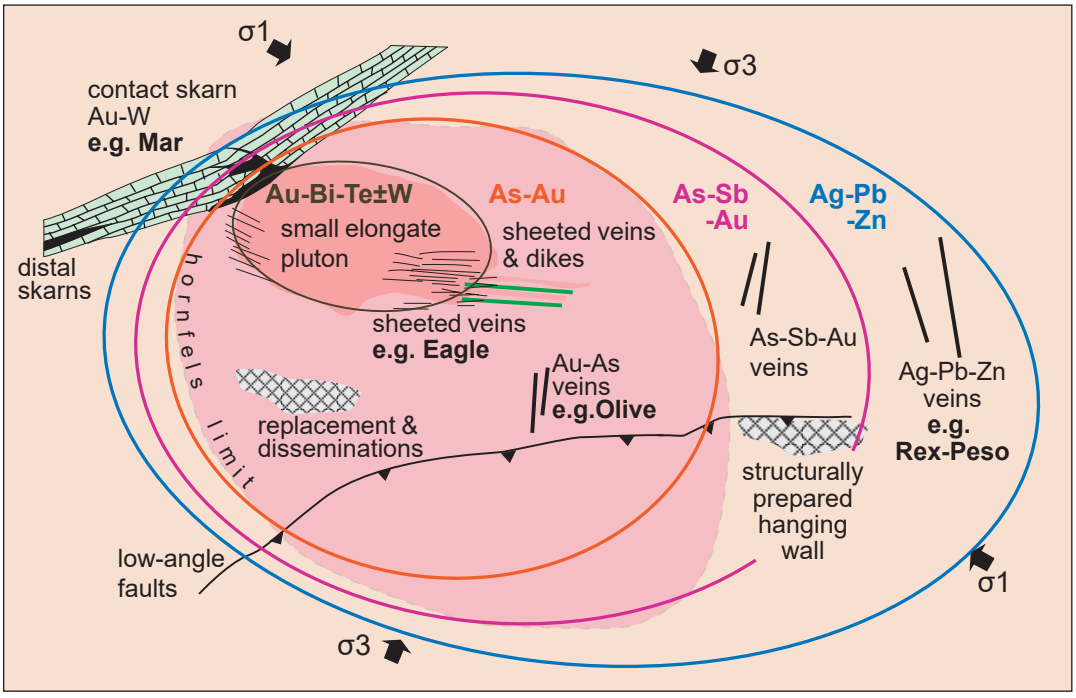

Figure 11. *General plan model of a reduced intrusion-related gold system. Of note are the wide range of mineralization styles and geochemical variations that vary predictably outward from a central pluton. Scale is dependent on the size of the exposed pluton, which is likely to range from 100 m to 5 km in diameter. Modified from Hart (2007) with relevant examples for mineralization style from the Dublin Gulch property.*

Day 1 - Dublin Gulch reduced intrusion-related gold system

District geology

The Dublin Gulch property is located in the Mayo mining district, in central Yukon, approximately 85 km north of Mayo and 370 km due north of Whitehorse (Fig. 10). The 350 km² Dublin Gulch property encompasses two reduced intrusion-hosted gold deposits, Eagle and Olive, two small Ag-Pb-Zn vein deposits with historical resources, Rex and Peso, and the Mar tungsten skarn deposit (Fig. 12). These deposits and other occurrences are part of a reduced intrusion-related gold system (Fig. 11). The Eagle deposit is actively being mined using open pit and heap leach methods and contains 4.8 Moz of gold (Table 3; Fig. 13).

The property is located on the northern limb of the faulted McQuesten antiform and is underlain by metasedimentary rocks of the Neoproterozoic-Cambrian Yusezyu Formation (Hyland Group) which are thrust over Keno Hill Quartzite and dark coloured shale of the Earn Group (Murphy, 1997) and intruded by small stocks of the Mayo plutonic suite (Hart et *al.*, 2004b; Fig. 4). The Hyland Group comprises variably gritty, micaceous, and massive quartzite and intercalated muscovite, sericite and chlorite phyllite; thin calcareous horizons are also present.

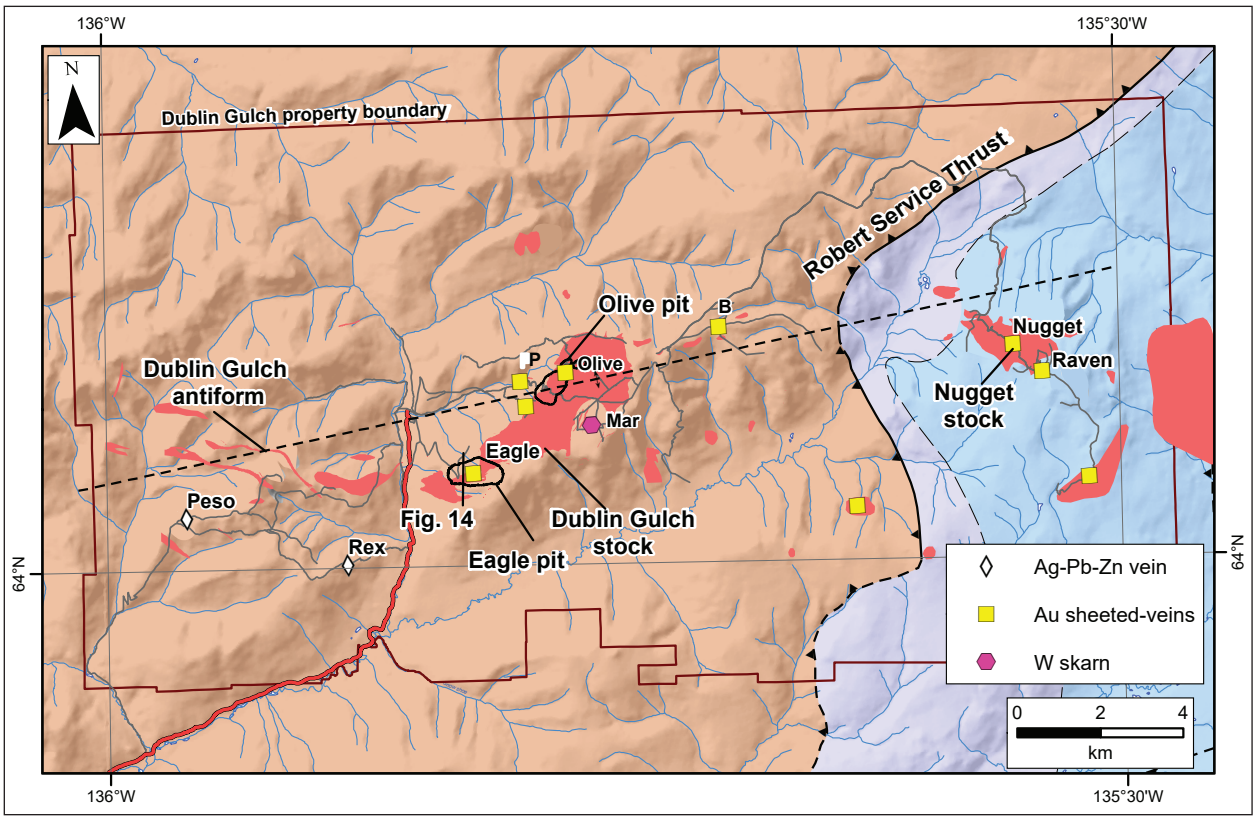

Figure 12. *Dublin Gulch property geology map. Geology from YGS (2020a); intrusions from Victoria Gold company data. Legend same as Figure 4. P = Popeye occurrence, B = Bluto occurrence.*

Table 3. *Summary of the Eagle pre-production in-pit mineral resource, effective date July 1, 2019. This resource has not been depleted for production in 2019/2020. Pre-production resource based on original topo with no depletion from preproduction/ramp up period up. A total of 2.44 Mt at 0.82 g/t Au for 64,500 ounces of gold were extracted from the Eagle deposit as of 15 November 2019. The mineral resource estimate is constrained by a Lerchs-Grossman pit shell using a gold price of US$1,700/oz.*

Classification	Cut-off Grade (g/t Au)	Tonnes (Mt)	Grade (g/t Au)	Contained Au (koz)
Measured	0.15	37	0.71	850
Indicated	0.15	180	0.61	3547
Measured + Indicated	0.15	217	0.63	4397
Inferred	0.15	21	0.52	361

1. Mineral Resources, which are not mineral reserves, do not have demonstrated economic viability. The estimate of Mineral Resources may be materially affected by environmental, permitting, legal, title, taxation, sociopolitical, marketing, or other relevant issues.
2. The quantity and grade of reported Inferred Resources in this estimation are uncertain in nature and there has been insufficient exploration to define these Inferred Resources as an Indicated or Measured Mineral Resource and it is uncertain if further exploration will result in upgrading them to an Indicated or Measured Mineral Resource category.

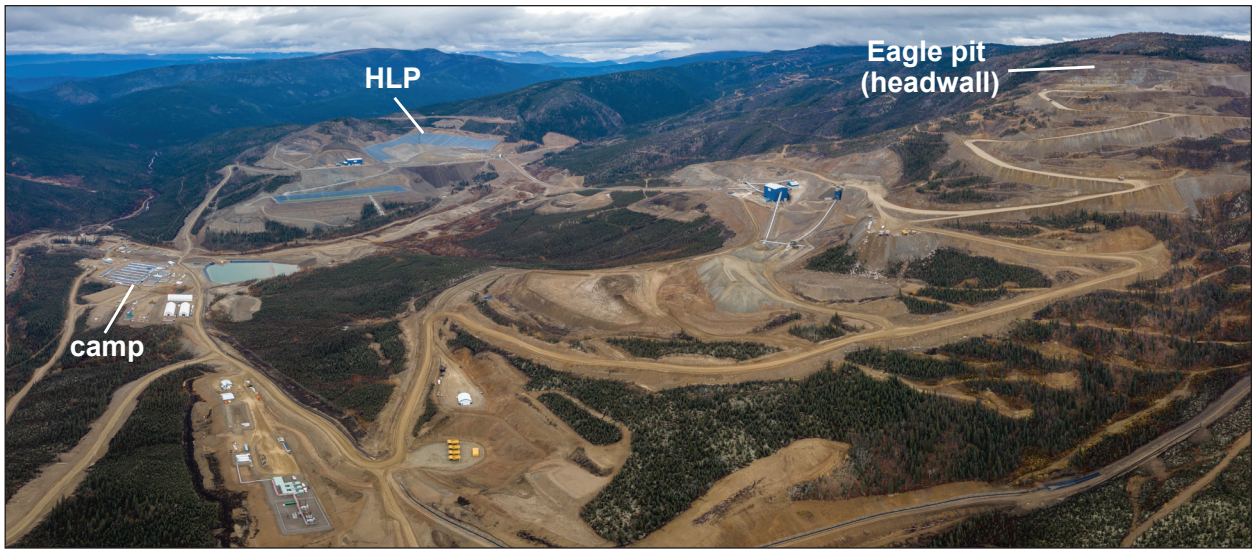

Figure 13. *View looking north of the Eagle mine infrastructure during operations in September 2019. HLP = heap leach pad.*

Mayo suite plutons range in age from 96 to 93 Ma, are intermediate, hornblende ± biotite plutons with low magnetic susceptibility (0.1×10^{-3} SI units) and are metaluminous (Rasmussen, 2013).The largest exposure of the Mayo suite in the area is the Dublin Gulch stock which is mostly granodiorite with subordinate quartz diorite and quartz monzonite. Leucogranite and aplite primarily occur as dikes and sills that cut both the granodiorite and surrounding country rocks. The Dublin Gulch stock has been dated by multigrain U-Pb zircon TIMS analyses at 94.0 ± 0.3 Ma, nominally older than the Re-Os molybdenite age of 93.2 ± 0.3 Ma for mineralization at the Olive deposit (Selby *et al.*, 2003).

The metasedimentary rocks have undergone regional metamorphism to greenschist facies and proximal to the Dublin Gulch stock are contact metamorphosed with a hornfels halo. Within the hornfels halo the coarser clastic components of the Hyland Group have been altered to quartzbiotite-schist; the argillaceous components to sericite-biotite-chlorite schist and the carbonates to marble, wollastonite-quartz skarn and diopside skarn. The hornfels halo extends 80 to 200 m outward from the intrusive rocks.

The Dublin Gulch anticline, located midway between Dublin Gulch and Lynx Creek to the south, has folded the metasedimentary rocks about an axis that trends at an azimuth of 250° and plunges gently to the west-southwest (Fig. 12). The granodiorite stock is an elongate, east-northeast trending body approximately 5 km long and with a maximum width of approximately 2 km. The long axis of the stock is subparallel with the axis of the interpreted Dublin Gulch anticline. Sheet-like sills of granodiorite extend from the stock and cut the metasedimentary strata at low angles. The contact between the stock and the surrounding metasedimentary country rock dips shallowly to steeply to the north and northwest on the northern side of the intrusive, and steeply to the north or south along its southern margin (Fig. 14). No chilled margin is apparent at the contact.

At least four periods of faulting have been documented in the Dublin Gulch area including low-angle thrusting and bedding-plane faults and normal faults with northerly, northeasterly, northwesterly, and easterly strikes. North-striking faults are inferred to have displaced portions of the Dublin Gulch stock, one of which is interpreted to form the eastern boundary of the Eagle deposit.

Veins are typically composed of white or grey quartz with subordinate potassium feldspar, and strike at an azimuth of 060° to 085°. They typically dip between 60° south and vertical, and range in width from 1 mm to more than 10 cm. Contacts are typically sharp. Vein densities range from less than one per metre to more than fifteen per metre, and average three to five per metre. The greatest concentration of veins appears to coincide with both the narrowest constriction as well as the local apex of the intrusion. Sulphides account for less than five percent of vein material and occur in the center, on the margin, and disseminated throughout the veins. The most common sulphide minerals are pyrrhotite, pyrite, arsenopyrite, chalcopyrite, sphalerite, bismuthinite, molybdenite and galena. Sericite-carbonate is generally restricted to narrow vein selvedges although alteration zones of this type also occur with no obvious relation to veins.

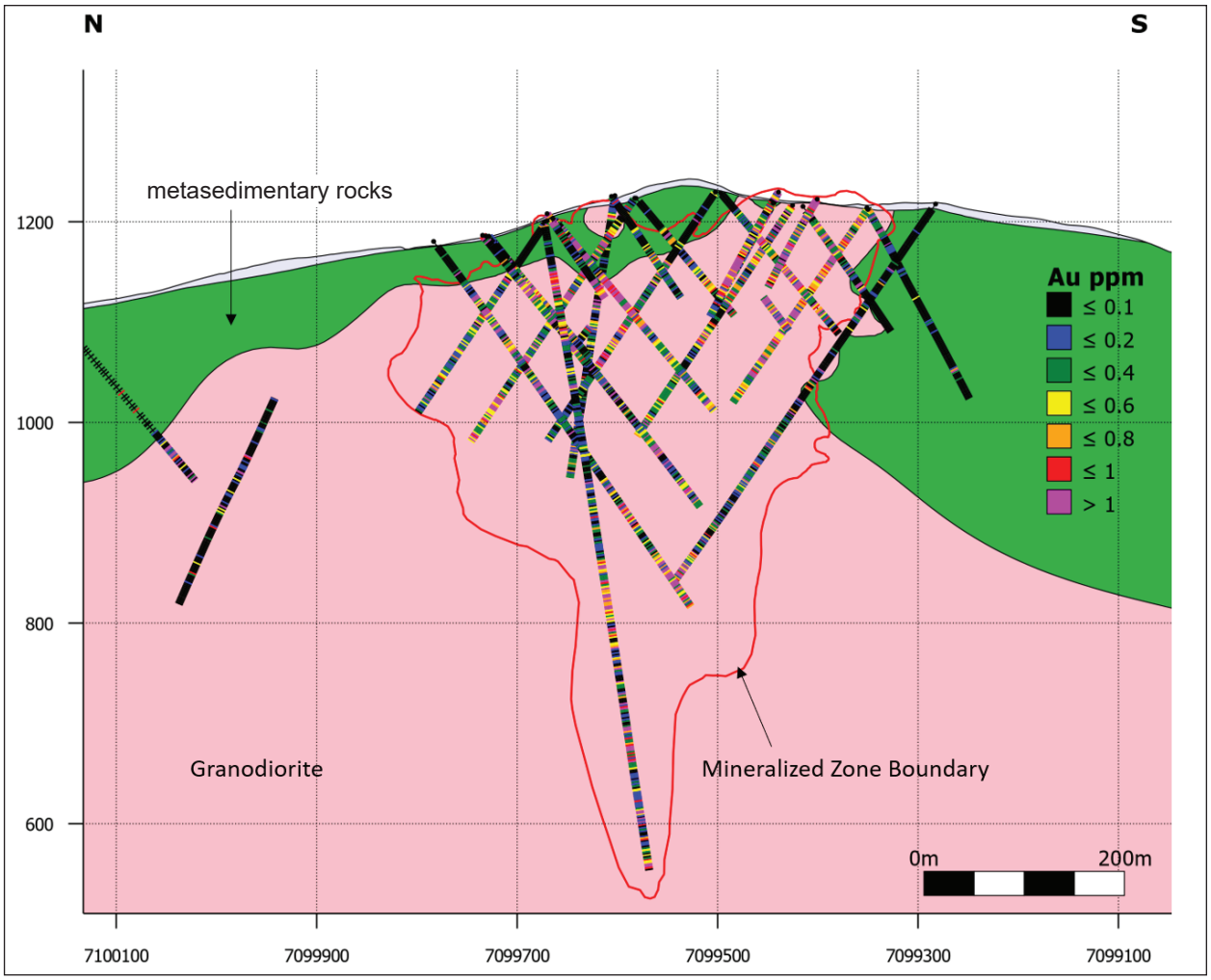

Figure 14. *Representative cross section through the middle of the Eagle deposit. Location shown on Figure 12.*

Vein formation is attributed to rheological contrasts between the intrusion and the surrounding metasedimentary country rocks. Embayments and narrow portions of the stock represent stress shadows that constitute favourable areas for rheological failure leading to the formation of extensional quartz veins. Protrusions in the stock created favourable areas for the development of extensional veining in the adjacent country rocks. Gold mineralization also occurs within the metasedimentary rock package immediately adjacent to the granodiorite. These mineralized rocks may be of potential economic importance.

Deposit geology

Eagle deposit

The Eagle gold deposit [106D 025] is the principal concentration of mineralized rock within the property (Table 3). It occurs at the narrowest exposed portion of the Dublin Gulch stock, near its known western limit. The deposit is approximately 1600 m long (east-west) and 600 m wide north-south. It is near-vertical and has been traced for about 500 m below surface (Fig. 14). Current drilling indicates that ore is relatively continuous along this length and is open in several directions, including at depth. The contact between the stock and surrounding Hyland Group rocks is sharp but irregular and varies between steep attitudes that crosscut foliation within the sedimentary rocks, to shallow southwest dips parallel to foliation.

Within the Eagle gold deposit, gold occurs in subvertical extensional quartz veins that are most abundant on the hanging and footwall contacts of the narrowest portion of the Dublin Gulch granodiorite near its known western limits. Subordinate quantities of gold mineralization occur in quartz veins within the adjacent metasedimentary rocks. Veins strike at an azimuth of 060° to 085°, subparallel to the intrusive contact and are commonly fractured by repeated movement along the host structures.

Gold occurs as isolated grains of elemental gold, most commonly in association with arsenopyrite, and less commonly with pyrite and chalcopyrite. The sulphide content in the veins is typically less than 5%, and is less than 0.5% within the deposit overall. In descending abundance, the principal sulphides observed are pyrrhotite, pyrite, arsenopyrite and chalcopyrite. Minor sphalerite, galena and molybdenite are also present. Scorodite and limonite are common weathering products.

A number of gold-bearing quartz-sulphide veins occur around the margins of the Dublin Gulch stock. These veins are narrow (centimetre-scale), steeply dipping and generally strike at about 070°. Silver-quartz-sulphide veins also occur. These distal veins are infrequent relative to the sheeted vein system within the Dublin Gulch stock and due to their small size, are not a significant part of the mineral resource.

Olive deposit

The Olive deposit is localized at the contact zone on the northwest flank of the Dublin Gulch granodiorite intrusive and located 2.5 km northeast of the Eagle zone. Olive measures approximately 20 to 80 m in width, 900 m in length, and has been drilled to approximately 175 to 250 m in depth. Over 97% of the gold mineralization in the Olive zone is hosted in granodiorite (Table 4).

Compared to Eagle, gold in the Olive deposit is more commonly associated with sulphides and quartz-sulphide veining (Fig. 15) in an interpreted shear-zone setting. An oxidation zone and a transition zone, from near total oxidation to only sulphides, have been defined. Veins can be only sulphides or sulphides with white quartz. Pyrite plus arsenopyrite (or arsenian pyrite) and quartz-pyrite veins are common, within the overall NE trending zone of mineralized rock.

Table 4. *Olive constrained in-pit mineral resource. The effective date for the mineral resource is September 12, 2016. Gold price used for this estimate was US$1,700/oz.*

Classification	Cut-off Grade (g/t Au)	Tonnes (Mt)	Grade (g/t Au)	Contained Au (koz)
Measured	0.4	2	1.19	75
Indicated	0.4	8	1.05	254
Measured + Indicated	0.4	10	1.07	329
Inferred	0.4	7	0.89	210

1. Mineral Resources, which are not mineral reserves, do not have demonstrated economic viability. The estimate of Mineral Resources may be materially affected by environmental, permitting, legal, title, taxation, sociopolitical, marketing, or other relevant issues
2. The quantity and grade of reported Inferred Resources in this estimation are uncertain in nature and there has been insufficient exploration to define these Inferred Resources as an Indicated or Measured Mineral Resource and it is uncertain if further exploration will result in upgrading them to an Indicated or Measured Mineral Resource category

Figure 15. *Mineralized quartz-arsenopyrite vein intersections at the Olive zone. Greenish mineral is scorodite. Veins are emplaced into Mayo suite granodiorite. Core diameter is approximately 5 cm.*

Regional targets

Outside of the Eagle and Olive deposits, gold, silver-lead-zinc and tungsten mineralization is present in a range of geological settings on the Dublin Gulch property. Quartz-arsenopyrite vein-hosted gold mineralization similar to Eagle has been identified at the Shamrock, Steiner, Popeye, and Bluto prospects (Fig. 12). The Mar (Wolf) tungsten deposit [106D 027], located approximately 2 km northeast of Eagle, is a skarn-hosted scheelite (Fig. 16) resource situated within a hornfelsed roof pendant of calcareous Hyland Group rocks in an embayment of the Dublin Gulch stock (Table 5).

Polymetallic vein-hosted silver-lead-zinc mineralization (Fig. 17; Table 6), similar in character to those in the Keno Hill silver district outcrop at Rex-Peso [106D 021], situated 5 km southeast of Eagle and hosted within phyllite and quartzite of the Hyland Group.

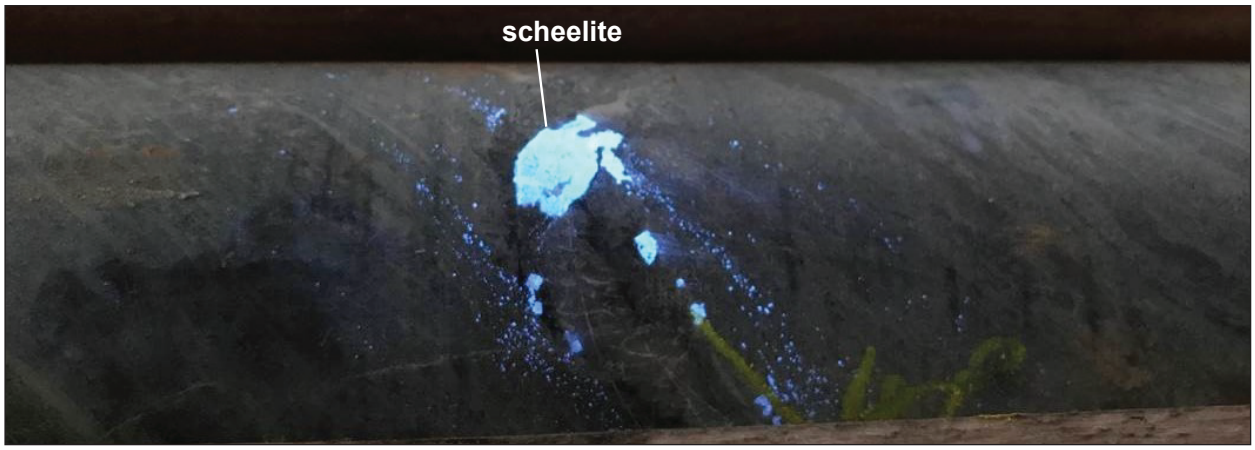

Figure 16. *Scheelite (fluorescent mineral) within a skarn horizon in the Mar tungsten deposit. Diamond drill hole DG17-967C 119.6 m. Core diameter is approximately 5 cm.*

Table 5. *Mar tungsten resource. From 'NI 43-101 Preliminary Assessment Dublin Gulch Property – Mar-Tungsten Zone' released on December 1, 2008.*

Resource Category	% WO_3 Cut-off	Total Mt	% WO_3 Grade	Contained WO_3 (Mlbs)
Indicated	0.1	12.7	0.31	86.2
Inferred	0.1	1.3	0.3	8.9

Table 6. *Rex-Peso historical resource. This historical mineral reserve is taken from a Peso Silver mine company report dated November 10, 1965. It is not NI43-101 compliant. 'Proven' ore is that which was within 30 ft of good surface or underground exposures, 'probable' ore is that which was 30 ft beyond the proven indicated by drill hole intersections. In 1965, the gross value of the Rex-Peso ore in the ground was $6.2 million. Total costs of mining and milling were calculated at $25 per ton of ore with an assumed 90% recovery.*

Classification	Tons	Ag Grade (oz/ton)	Pb Grade %
Proven	91,745	23.7	3.7
Probable	61,885	16.7	3.7

Figure 17. *Mineralized sulphosalt + pyrite + arsenopyrite vein at the Rex deposit. Diamond drill hole DG17-955C 129 m. Core diameter is approximately 5 cm.*

The Nugget zone [106D 019], represents the second largest Cretaceous granodiorite intrusive body on the Dublin Gulch property (second only the Dublin Gulch stock that hosts the Eagle deposit) and consists of a 2.2 by 1.2 km, medium to coarse-grained granodiorite stock on the eastern side of the Lynx Creek valley. The area is underlain by the Devonian to Mississippian Earn Group and the Lower Carboniferous Keno Hill quartzite which are folded and faulted and metamorphosed to greenschist facies (Murphy, 1997). The Raven occurrence [106D 018] is hosted in a shear zone corridor within the Nugget stock, in close proximity to its contact with the metasedimentary rocks (Fig. 18). The Raven occurrence is highlighted by coincident gold + arsenic + bismuth soil anomalies. Trenching in the fall of 2018 uncovered scorodite, bismuthinite and siderite related sulphide veins buried under a metre of overburden. Trench assays from 2018 returned from trace to 124.0 m of 3.50 g/t Au including 58.0 m of 4.68 g/t Au.

Mining and processing

The Eagle deposit is actively being mined using open pit methods. Production rate are expected to average 13.0 million tonnes per year (Mt/a), consisting of 29 500 tonnes per day (t/d) ore and 7500 t/d run-of-mine (ROM) material over a thirteen-year mine life, excluding the initial ramp-up period.

Gold is extracted from ore into a solution by a heap leaching process using an in-valley leach pad (HLP). Heap leach feed consists of crushed ore (116.9 Mt at 0.78 g/t Au) conveyed to the HLPs as well as ROM, uncrushed (32.1 Mt at 0.22 g/t Au) ore, which is hauled directly to the HLP for leaching. Crushed ore is being fed through a three-stage crushing plant to produce an 80% passing (P80) 6.5 mm product. All ROM ore will bypass the crushing plant. Gold is being leached with cyanide solution and recovered by an adsorption-desorption-regeneration carbon plant. A total of 2406 koz of gold will be recovered over a thirteen-year mine life for 77% overall recovery.

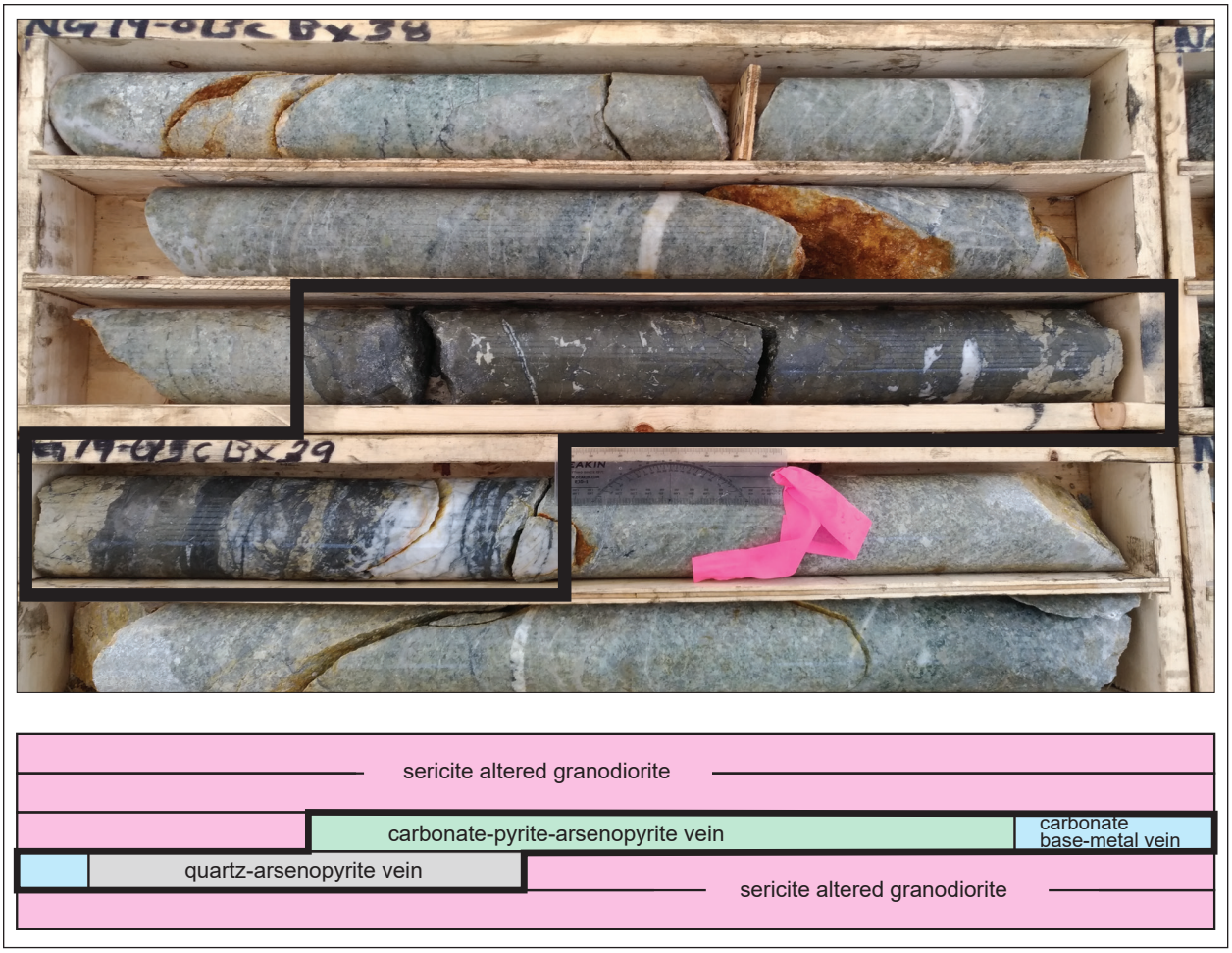

Figure 18. *A typical example of mineralized veins (heavy black outline) at the Raven zone hosted in the Nugget granodiorite intrusion. A strong sericite altered selvage with an initial stage of quartz-arsenopyrite veining that has been overprinted by later carbonate pyrite arsenopyrite and carbonate base metal phases. Shearing and brecciated textures are evident at the contact between the first and later stages of veining indicating mineralization occurred during fault movement. Schematic below photo shows interpretation of vein-types.*

Day 2 - Keno Hill silver district

The Keno Hill silver district is located in central Yukon, some 450 km by road access north of Whitehorse (Fig. 2). The nearest settlement is Keno City located at the head of the Silver Trail Highway that connects to Stewart Crossing on the Klondike Highway. The exploration base for Alexco Resource Corp. is the historic mining town of Elsa on the Silver Trail Highway approximately 40 km north of the town of Mayo. Silver production in the Keno Hill district in excess of 213 million ounces (Moz) is recorded from 4.8 Mt mined at average grade of 44 oz/t (1373 g/t) Ag, 6.7% Pb, 4.1% Zn from 35 mines, with seven producing over 10 Moz each, the largest being Hector-Calumet (96 Moz) and Elsa (30 Moz).

Mining history

Cathro (2006, p. 103) described Keno Hill as "... one of The Great Mining Camps of Canada; it was not only Canada's second largest primary silver producer and one of the richest Ag-Pb-Zn vein deposits ever mined in the world, it was also one of the mainstays of the Yukon economy from the 1920s, after the rapid decline of the Klondike Goldfield, until the early 1960s. At its peak in the 1950s and early 1960s, it supported about 15% of the territorial population. It also produced more wealth than the Klondike, one of the richest placer gold districts in the world. Following a small amount of hand mining between 1913 and 1917, larger scale production was almost continuous from 1919 to 1989, except during the war from 1942 to 1945. Two companies produced most of the ore, Treadwell Yukon Corp. Ltd. from 1925 to 1941, and United Keno Hill Mines Ltd. (UKHM) between 1947 and 1989."

District geology

The Keno Hill mining district is underlain by parautochthonous sedimentary strata deposited along the western margin of ancestral North America (Figs. 1 and 4). Refer to Read *et al.* (2020) for detailed geology of the Keno district.

The main stratigraphic units in the Keno Hill silver district are shown in Figure 19, from structural bottom to top these are:

- Devonian Earn Group comprising predominantly phyllitic grey graphitic metasedimentary rocks, with an upper band of greenish chlorite-muscovite felsic metavolcanic rocks. Minor interbedded quartzite occurs close to the conformable transition to the overlying Keno Hill Quartzite;
- Mississippian Keno Hill Quartzite, the dominant host to the silver-lead-zinc mineralization, with a total estimated structural thickness of about 1900 m, comprises a prominent lower massive blocky Basal Quartzite member (structural thickness about 1100 m) with thin to thick interbeds of quartzite and graphitic schist, and the overlying Sourdough Hill member (structural thickness about 800 m) which has distinctive basal marker horizons of sericitic and graphitic schist, intermediate units of an Upper Quartzite, quartz-eye grits and chloritic schist

that pass into an overlying section that is carbonate rich with some well-defined black limestone beds; and

- To the south, the sequence is structurally overlain across the Robert Service thrust by the Yusezyu Formation of the Neoproterozoic to Cambrian Hyland Group, comprising greenish quartz-rich chlorite-muscovite schist that locally includes clear and blue quartz-grain gritty schist.

Intrusive rocks include:

- The Keno Hill sequence contains numerous Middle Triassic Galena suite (ca. 230 Ma) greenstone sills, locally up to 100 m thick, intruded in the Earn Group and Keno Hill Quartzite. In most of the area the sills reach stratigraphically no higher than within the marker schists at the base of the Sourdough Hill member; but, on the west slope of Aurex Hill, they intrude to a level more than 500 m stratigraphically above the base of the member;
- mid-Cretaceous Mayo suite aplite (ca. 93 Ma) occurring locally as dikes and sills; and
- Late Cretaceous fine-grained lamprophyre (89 Ma) occurring as metre-scale dikes and sills.

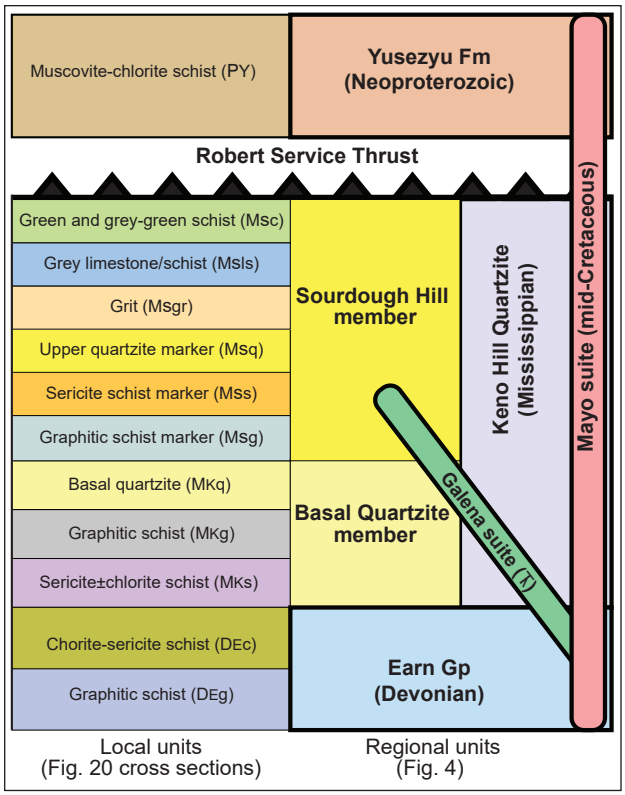

Figure 19. *Detailed local stratigraphy and regional stratigraphy from the Keno Hill district (modified from Read et al., 2020). Bold outlined units match those on Figure 4.*

Extensive Quaternary glacial and alluvial deposits cover the bedrock in the area (Bond, 1998).

Structurally, the area lies within the highly deformed Tombstone strain zone (Murphy, 1997) where at least one and possibly two phases of deformation (ca. 100–110 Ma), accompanied by chlorite grade regional metamorphism and isoclinal folding, produced district scale overturned isoclines (with local structural thickening and thrusting) of Keno Hill Quartzite overlying the Earn Group (Fig. 20). A later post-metamorphic, upright mesoscopic phase of folding produced southeasterly plunging mesoscopic folds in the area, and to the southeast macroscopic folds. The dominant foliation is essentially axial planar to the early folding and subparallel to primary bedding.

A transect from Sourdough hill (in the south) to Keno Hill (in the north) starts with the lower limb of the northerly overturned Galena Hill syncline containing northerly verging mesoscopic folds (Fig. 20 B–B' and C–C'; Read et *al.*, 2020). Along a strike length of

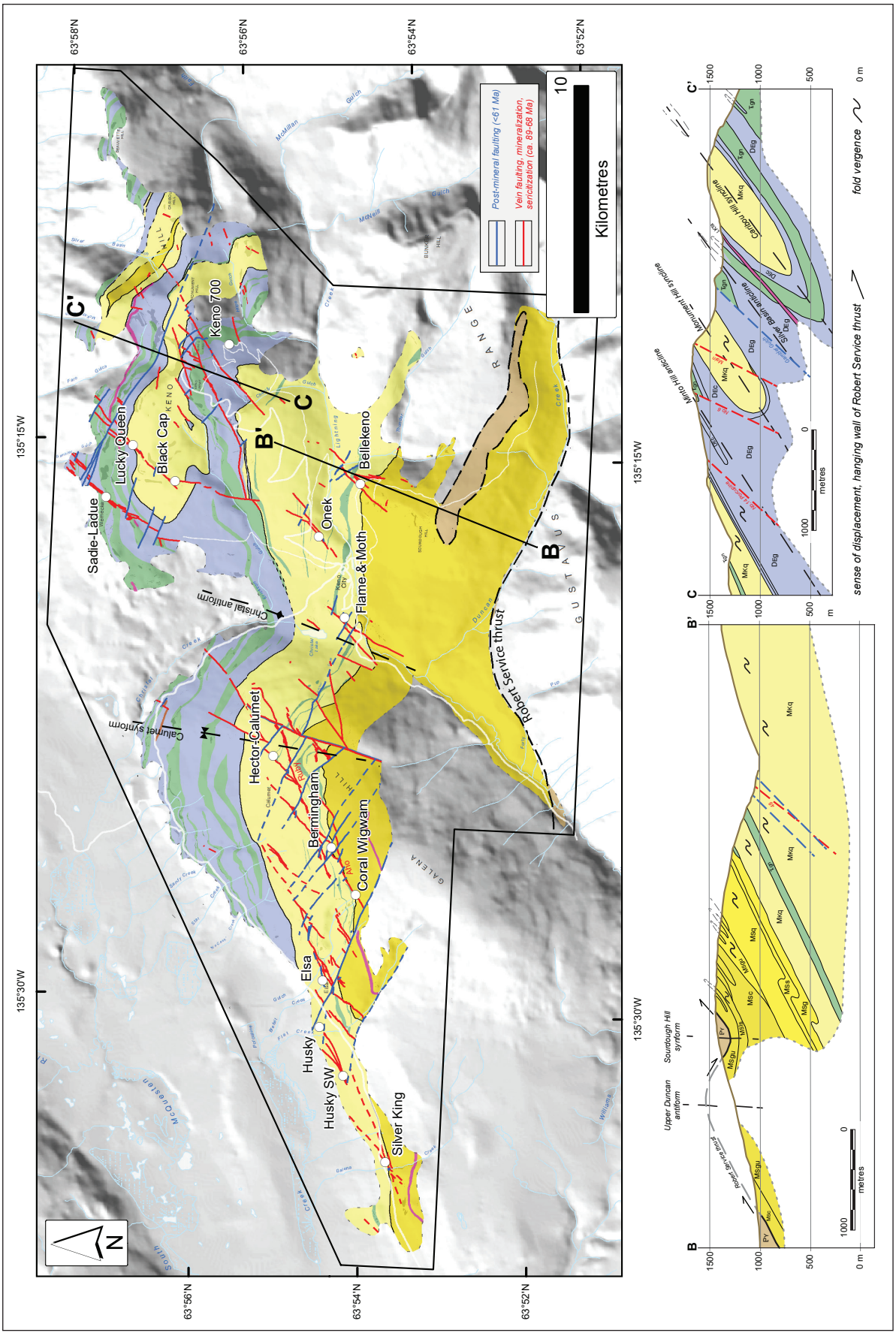

Figure 20. *Simplified geological map of Keno Hill area with main past producers and deposits labelled. Geological units correspond to those on Figure 19. Modified after Read et al. (2020).*

more than 30 km, the Robert Service thrust sets the gritty schist of the Neoproterozoic-Cambrian Yusezyu Formation (PY) against the truncated lower limb of this syncline leaving only a limb composed of the Earn Group and Keno Hill Quartzite (Fig. 20).

When you leave Keno City for Sign Post hill you are on the lower upright limb of the Galena Hill syncline and although gaining in elevation you are driving structurally and stratigraphically downward towards and finally into the schists of the Earn group that core the underlying Minto Hill anticline. At the Sign Post you have passed through the anticlinal core composed of Earn group and are now on the inverted northern limb of the anticline at the boundary between the schist of the Earn group and underlying, but younger Basal Quartzite, which forms the walls of Faro Gulch and cores Monument Hill syncline, the next isoclinal fold to the north. Murphy (1997) laid the groundwork for the development of this detailed stratigraphy. Middle Triassic sills of the Galena suite (=gn), deformed and metamorphosed to greenstone, are widespread to the top of the Basal Quartzite member (Fig. 20). A few post-metamorphic and undeformed aplite sills (LKTa) and lamprophyre dikes (LKTlp) of the Mayo plutonic suite form the only intrusions.

Climbing the southern slope of Keno Hill, you pass from the Basal Quartzite into the underlying Earn Group of the Galena Hill syncline, and near the top at the Sign Post cross the isoclinal Minto Hill anticline with its attenuated lower limb to find Basal Quartzite stratigraphically inverted with schists of the Earn Group overlying the quartzite all dipping moderately to the south (Read *et al.*, 2020). The cliffs on the north side of the Sign Post expose the Basal Quartzite core of the next northerly overturned Monument Hill syncline. Farther to the northeast, and out of sight, the pattern is repeated again with Earn Group appearing in the isoclinal core of Silver Basin anticline followed by the northeasterly overturned Caribou Hill syncline with its Basal Quartzite core. McTaggart (1960) first discovered and depicted this pattern of northerly overturned isoclinal folds.

A second phase of upright southeasterly plunging mesoscopic folds is widespread in the schistose units of the Keno Hill mining camp but macroscopic folds of this post-metamorphic phase occur only to the east of this area. Spatial and probably genetically associated with the movement along the Robert Service thrust is folding of the thrust to develop a klippe of Neoproterozoic rocks of the Hyland Group lying on graphitic schist of the Sourdough Hill member. Calumet synform and Christal antiform are third phase broad, upright concentric folds that developed prior to the formation of vein-faults.

Up to four periods of faulting, including the Robert Service thrust, are recognized. Mineralization developed in a series of north-northeast to northeast striking, southeasterly dipping fault systems named “vein faults” by Boyle (1965) with major movements that typically exceed a displacement of 200 m, and may be continuous over several kilometres in the Basal Quartzite and extend into the Earn Group.

The south-southeast boundary of vein-faults with this magnitude of displacement passes immediately east of the Flame and Moth deposit and the Sadie-Ladue Mine. The movements of vein-faults to the east have an apparent left-lateral offset that does not

exceed 100 m and the orebodies are small, widely scattered within the structure and typically do not exceed 5–10 million ounces of silver. The western boundary of this belt is undefined and must lie west of the Husky and Silver King mines on Galena Hill, where Boyle (1965) recognized three northeast striking fault systems. The absolute timing of formation and periods of subsequent propagation of the mineralized vein-faults is not known.

Post-mineralization faults consist of cross-faults, dipping southwesterly between low and high angles, with oblique normal movement producing an apparent right-lateral offset of the vein faults and parallel faults along one or both walls of the vein faults. The most significant cross-fault is the Brefalt Creek fault, which has displaced, with a right lateral component of 800 m, the Husky vein fault system from the vein system on the north side of the cross-fault at Elsa (Fig. 20). The Brefalt Creek fault has right laterally displaced the aplite dike in the Sourdough Hill member. The north-northeast striking faults, paralleling both walls of the prominent McLeod vein fault east of Hector Calumet prevent the cross-faults on both sides of the vein fault from offsetting the McLeod vein fault system (Read et *al.*, 2021). The east-southeast striking cross-fault extending from the McLeod vein fault to the north-northeast striking Flame and Moth vein fault does not offset the latter because of a parallel fault running along the Flame and Moth's western side. The absence of offset of the vein faults results from conjugate post-mineral fault movement on both the cross and parallel fault sets. Where the parallel set is not present, cross-faults offset the vein faults.

Deposit geology

Style of mineralization

Keno Hill mineralization, comprising polymetallic silver-lead-zinc quartz-carbonate veins (Figs. 20 and 21), developed in moderately steep southeasterly dipping vein-faults, with deposits hosted either by the competent Basal Quartzite member of the Mississippian Keno Hill Quartzite or in some instances the Devonian Earn Group where greenstone sills form part of the wall rock.

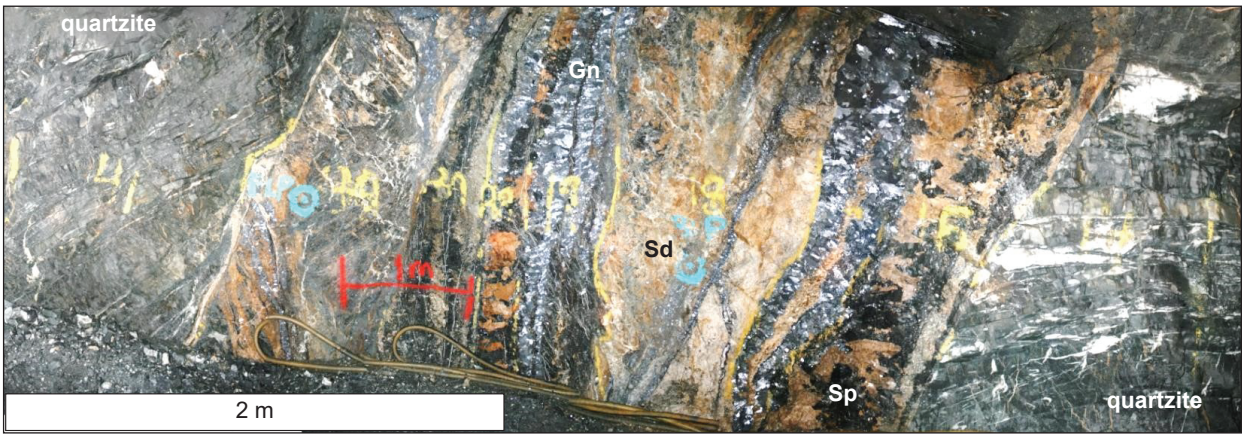

Figure 21. *Bellekeno 48 vein with bands of galena (Gn), black sphalerite (Sp) and buff siderite (Sd) developed across approximate width of 5 m.*

The Keno Hill deposits do not readily fit into a recognized mineral deposit model, and attempts to classify a "deposit type" for the mineralization are questionable since the source(s) of metals and conditions related to ore-deposition are poorly understood. Beaudoin and Sangster (1992) classified the Keno Hill as sediment-hosted veins, likened to the silver bearing deposits at Coeur d'Alene, USA and the Kokanee Range, Canada. A genetic relationship between silver-lead-zinc and intrusion-related gold mineralization has also been postulated (Mair *et al.*, 2006). The mineralization has been more recently classified as belonging to the Lithogene genetic group (Greybeal and Vikre, 2010) which invokes a depositional environment of remobilized metals, with no magmatic contribution or associated gold. Current information however, shows that this classification is not correct, as there was some magmatic component to mineralizing fluids (Hantelmann, 2013) and early gold was associated with mineralization. Furthermore, there appears to be a district-wide mineralogical zoning around the mid-Cretaceous Roop Lakes pluton suggesting it may be genetically related to vein mineralization (Lynch, 1989).

Minerals and controls on mineralization

The primary reference to the description of the mineralogy of the Keno Hill deposits is Boyle (1965). In general, common gangue minerals include (manganiferous) siderite and, to a lesser extent, quartz and calcite. Common silver-bearing minerals are shown in Figure 22:

- argentiferous galena $(Pb,Ag,Sb,Bi)_2S_2$;
- tetrahedrite $((Ag,Cu)_{10}(Fe,Zn)_2Sb_4S_{13})$;
- argentiferous tetrahedrite (freibergite) $(Ag_6(Cu_4Fe_2)(Sb4S_{13-X}))$;
- pyrargyrite Ag_3SbS_3;
- polybasite $(Cu(Cu,Ag)_6Ag_9Sb_2S_{11})$;
- stephanite (Ag_5SbS_4);
- native silver (Ag);
- electrum (Au,Ag);
- acanthite (AgS_2);
- canfieldite (Ag_8SnS_6); and
- treasurite $(Ag_7Pb_6Bi_{15}S_{32})$.

Hantelmann (2013, 2014a,b) completed a comprehensive study that established a 12-stage vein paragenesis of mineral deposition from the Bellekeno and Flame & Moth deposits. The Flame & Moth contains abundant (Stage 1) quartz-arsenopyrite-pyrite (-gold) material, as well as greater amounts of pyrite, tourmaline and tin minerals not present at Bellekeno, suggesting that mineralization may have been active over an extended period of time and that it formed at high depositional temperature perhaps suggesting closer depositional proximity to a magmatic input. Vein textures are commonly dominated by multiphase brecciation and re-healing (Fig. 21).

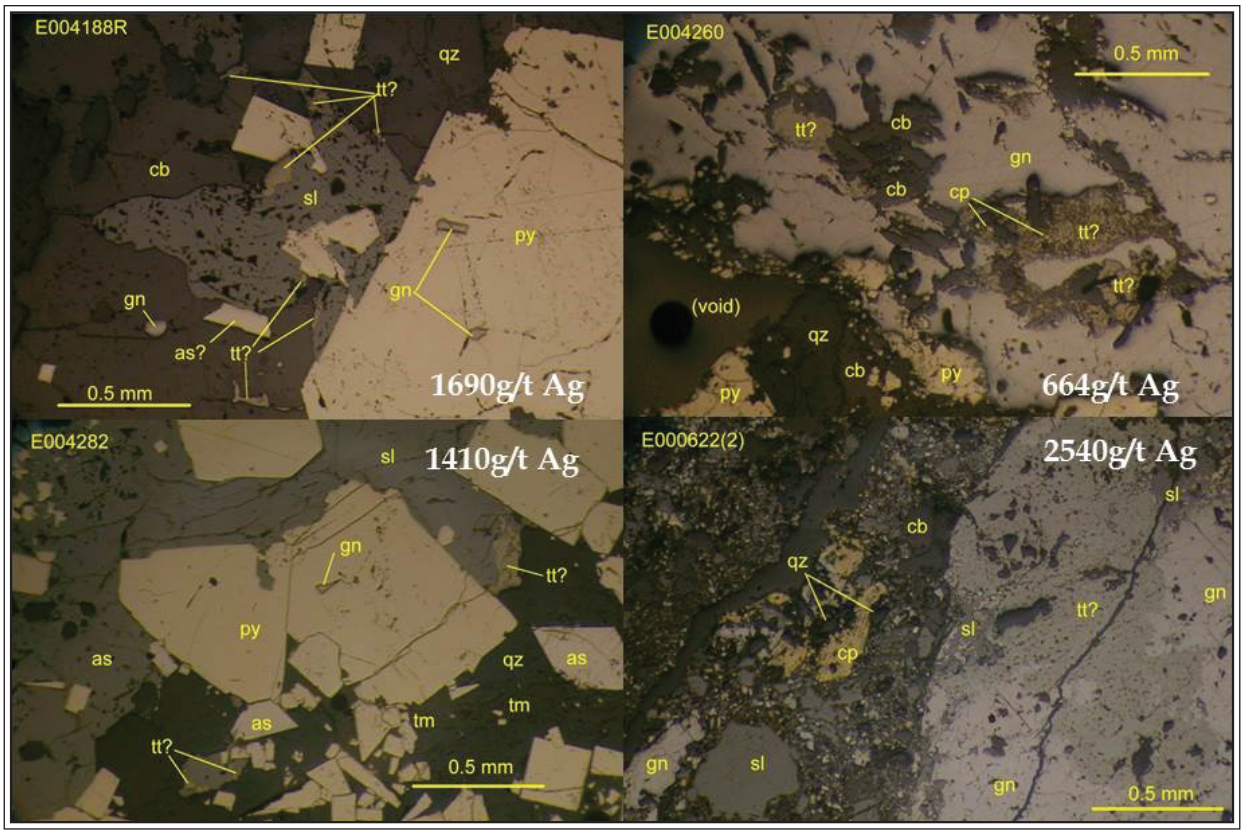

Figure 22. *Photomicrographs of high grade silver ore from the Flame vein. as = arsenopyrite, cb = carbonate, cp = chalcopyrite, gn = galena, qz = quartz, py = pyrite, tm = tourmaline, tt = tetrahedrite, sl = sphalerite.*

The primary control on mineralization was the presence of dilation zones in the pre-mineral faults where multiple pulses of deposition occurred from fluids as they depressurized or boiled during repeated reactivation and breccia formation along the host fault structures. Fundamental to understanding the process is the recognition of the incremental propagation of the host fault structures, the faults that link the segments forming bends in the vein-fault surface and the parts of the structures that present dilational zones. The Bellekeno vein-fault varies in width between several centimetres to over five metres (Fig. 23) and is best mineralized at releasing linkages in more competent stratigraphy (Fig. 24; Iles, 2013, 2016).

The secondary control on mineralization was the presence of a metal pregnant (mesothermal) fluid to fill the dilational spaces and physiochemical conditions to permit deposition, inferred to be predominantly through processes of depressurization or boiling. The actual source or path of the mineral depositing fluids has long been a matter of conjecture, but is inferred from detailed petrology and geochemical analysis to be at least in part magmatic, most likely related to late phases of Mayo suite intrusions.

Figure 23. *Complete drill hole intercept of K-12-0432 (311.34–319.32 m) showing the quartz and siderite vein types. Composite assay over 6.99 m true width 1180 g/t Ag (37.9 oz/t), 1.5 g/t Au, 2.1% Pb, 7.5% Zn.*

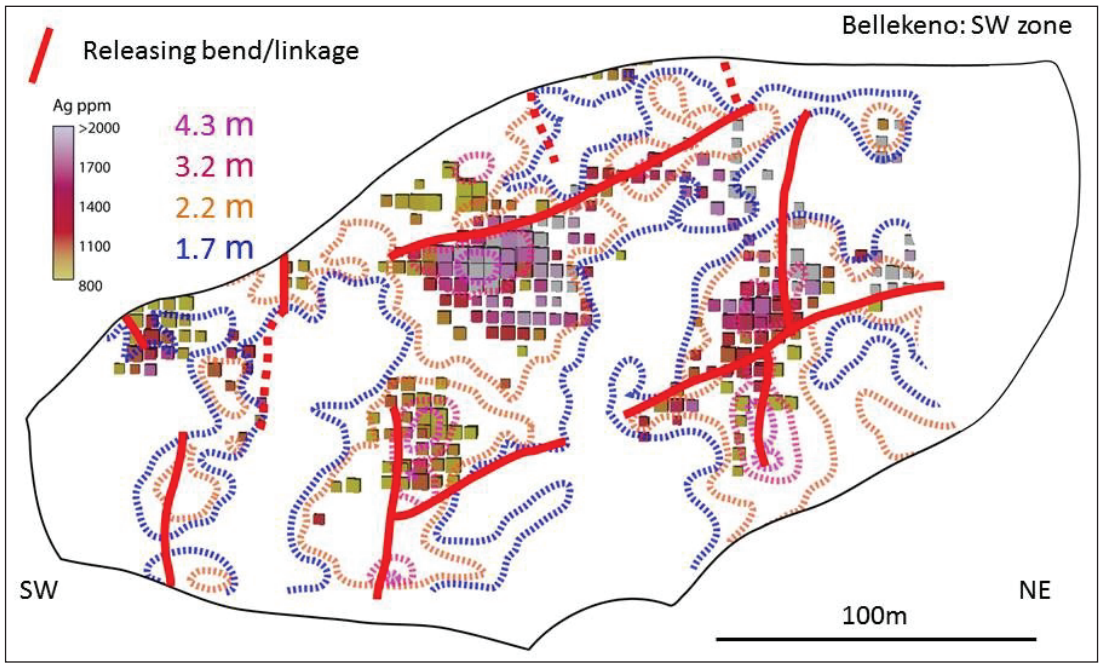

Figure 24. *Long-section of Bellekeno SW zone (looking NW) showing releasing fault linkages, contoured vein thickness and ore blocks. Moderate southwest plunging bends reflect stratigraphic contrasts between incompetent graphitic schist packages and competent thicker quartzite bands.*

Vein formation

Veins developed in two sets of faults striking in the northeast quadrant and dipping southeasterly. Boyle (1965) named them “vein faults”; the northerly striking set called “transverse” and the easterly set “longitudinal”. These two sets intersect, and both sets commonly contain the same paragenetic mineral assemblages from “early” to “late” implying conjugate movement on the intersecting sets. However, the silver-bearing minerals of the “late” stage are selectively more abundant, continuous and yield thicker sections in the transverse rather than the longitudinal vein faults. The difference in grade and thickness of mineralization results from the hanging wall fault block, created by the intersecting vein fault sets, moving in a direction that lies in the plane of the longitudinal vein fault away, even slightly, from its line of intersection with the transverse fault. This conjugate fault movement selectively develops open space for vein filling along the transverse vein faults and restricts space for vein development on the longitudinal vein faults (Read, et *al.*, 2021).

The richest linked transverse and longitudinal vein fault sets are the transverse Hector Calumet linked by the longitudinal Ruby to the transverse Bermingham that is finally linked by the longitudinal Aho to the transverse Coral Wigwam (Fig. 20).

Age of mineralization

The age of the Keno Hill mineralization has not been directly determined, rather the age of mineralization is constrained by cross-cutting relationships and alteration dates. The youngest rocks in the district that are cut by the mineralization are reported to be quartz-feldspar porphyry dikes (Boyle, 1965). Murphy (1997) concluded that the mineralized vein-faults formed during the late stage cooling of the Mayo suite intrusions, following the intrusion of some dikes and emplacement of higher temperature gold bearing fluids. This is consistent with the findings of Tupper and Bennett (2010) who obtained two LA-ICPMS U-Pb zircon ages of *ca.* 93 Ma for aplite dikes in Duncan Creek just south of the Flame & Moth deposit indicating the presence of Mayo suite intrusions at Keno Hill. The Roop Lake stock, approximately 20 km east of the Keno Hill silver district is the largest intrusion in the area and has a U-Pb zircon CA-TIMS age of 94.20 ± 0.02 Ma (YGS, 2020b).

$^{40}Ar/^{39}Ar$ dating of biotite flakes from a pre-mineral lamprophyre exposed at the Formo prospect givse a weighted mean age of 89.02 ± 0.28 Ma, a maximum age for siderite-sphalerite-galena style of mineralization (Read, 2010). The $^{40}Ar/^{39}Ar$ age coupled with a K/Ar date of 87.0 ± 3 Ma on sericite alteration of Ag-Pb-Zn vein wallrock (Sinclair et *al.*, 1980), constrains the age of vein formation to 89 to 84 Ma.

Current resources and mining plans

Alexco acquired the Keno Hill property in 2006 and operated the Bellekeno mine between 2011 and 2013, producing 5.6 Moz silver, 44.5 Mlb lead and 16.3 Mlb zinc from 242 000 tonnes ore at an average grade of 779 g/t (25.0 oz/t) Ag, 9.5% Pb and 5.1% Zn.

Over the last fourteen years Alexco has maintained a systematic exploration approach and has been rewarded with discovery and documentation of 30 million ounces of silver in probable mineral reserves, 74 million ounces of silver in indicated mineral resources (inclusive of probable mineral reserves) and a further 24 million ounces of silver in inferred mineral resources. In the last six years more than 58 million ounces of silver in indicated mineral resources, mainly from Flame & Moth and Bermingham, have been added to the mineral resource base at an average silver grade in excess of 800 g/t (26 oz/t) and a discovery cost of under $0.55 per ounce.

In 2019, Alexco announced positive results of a pre-feasibility study for the Keno Hill silver district, which contemplates production of approximately 1.2 million tonnes at an average grade of approximately 805 g/t silver, 2.98% lead, and 1.13% zinc from four deposits (Bellekeno, Flame & Moth, Bermingham and Lucky Queen; Fig. 25). The average processing rate during the 8-year mine life is estimated at 430 tonnes per day, and Keno Hill is expected to produce approximately 4 million ounces of silver annually, contained in high-quality lead and zinc concentrates.

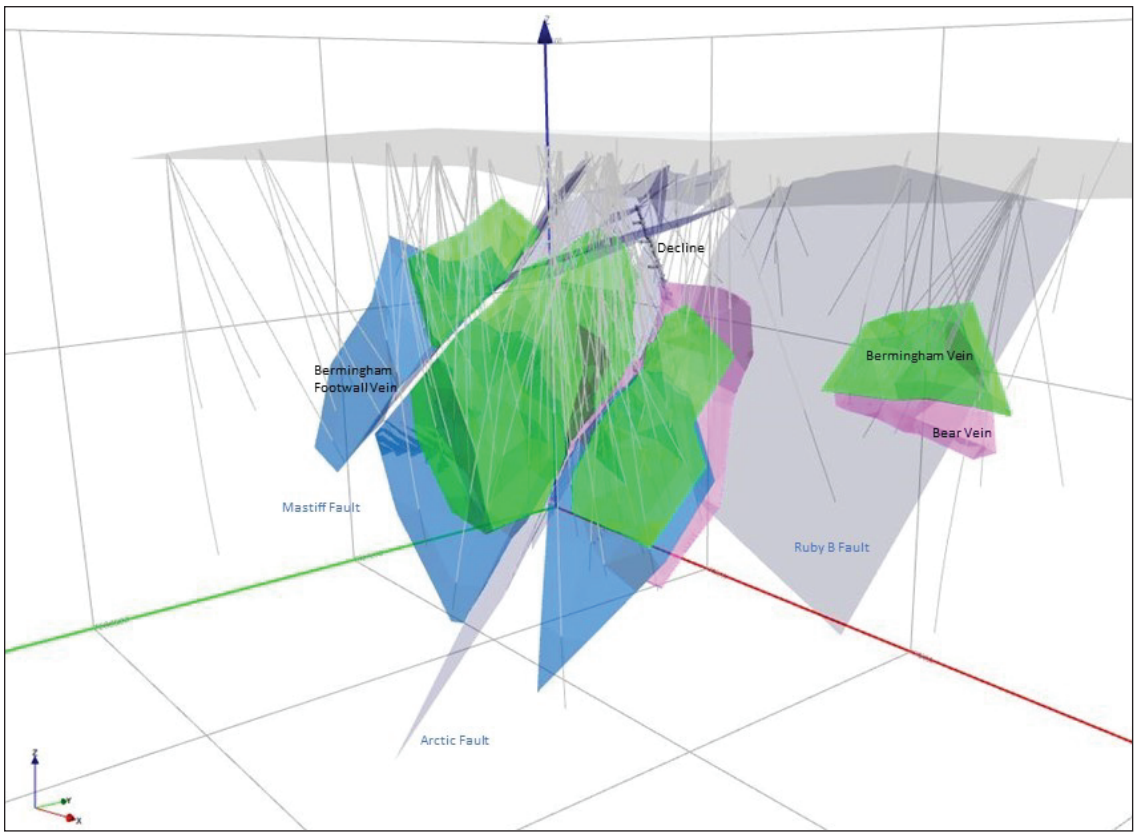

Figure 25. *Vein structures in the Bermingham area (oblique view to northwest).*

Days 3 and 4 - Carmacks Copper belt

Carmacks Copper belt geology

Days 3 and 4 of the field trip (Fig. 26) will focus on the Carmacks copper belt, an informally named, northwest trending belt 20 km wide and 80 km long, containing approximately 20 copper (gold ± silver, molybdenum) occurrences in west-central Yukon (Fig. 27). The two deposits in the belt, both of which are subjects of this field trip, are the Minto deposit [115I 021 and 022] in the northwest, and the Carmacks Copper (Williams Creek) deposit [115I 008] in the southeastern part of the belt. Several other copper (± gold) occurrences, including the Stu [115I 011], are located between these two deposits or within mafic volcanic rocks of the Late Triassic Povoas Formation to the northeast (Fig. 27). Carmacks copper belt occurrences are primarily hosted within a latest Triassic to Early Jurassic Minto suite (205 to 194 Ma) granitoid batholith intruded into the Yukon-Tanana/Stikinia contact (Sack *et al.*, 2020). This batholith is mapped as the Yukon River, Minto and Granite Mountain plutons, but these bodies are likely connected at depth beneath Upper Cretaceous volcanic cover (Fig. 27). The area is dissected by Cretaceous and younger faults, including the northwest-trending Hoochekoo fault (Tempelman-Kluit, 1984) which modified the original intrusive contact between the Granite Mountain and Minto plutons and Late Triassic mafic volcanic rocks of Stikinia (Sack *et al.*, 2020).

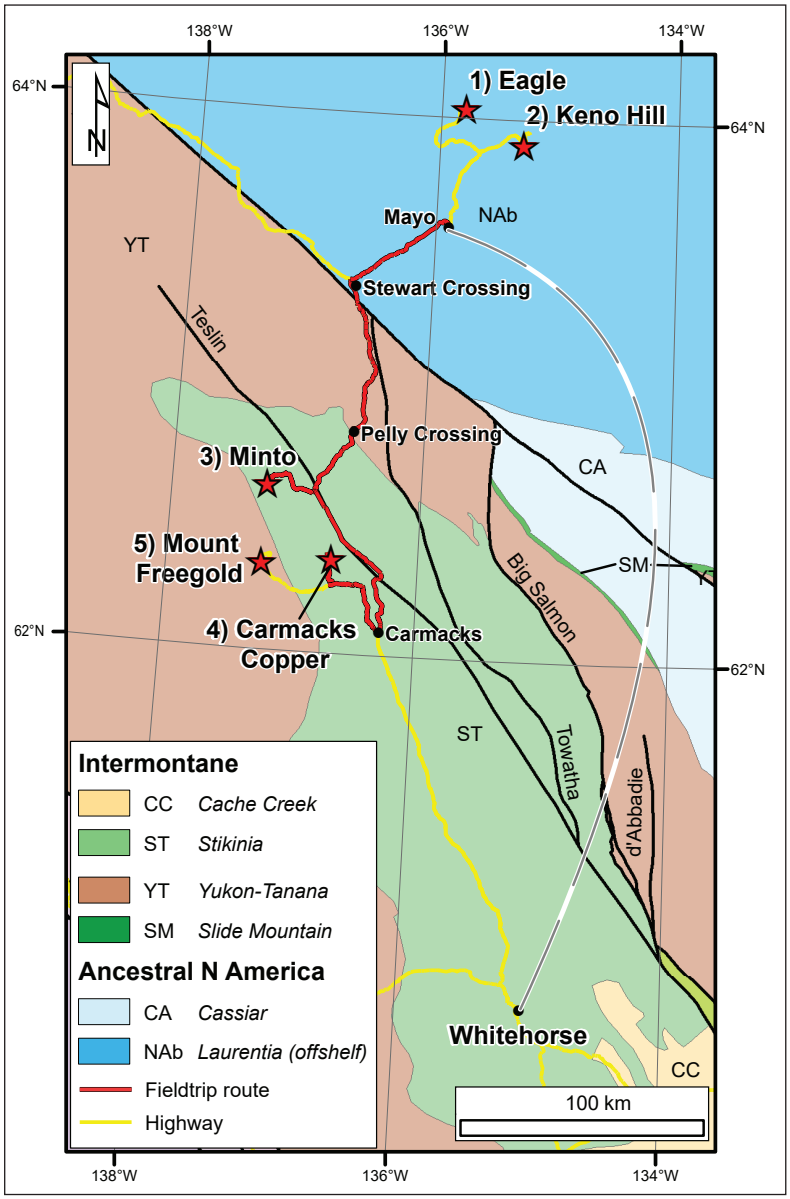

Figure 26. *Field trip route for Days 3 and 4. Numbered locations refer to order of field trip days in Table 1. Dashed grey line illustrates flight from Whitehorse to Mayo.*

Carmacks Copper belt deposits are enigmatic in that they are relatively small, high-grade Cu-Au-Ag deposits with ore primarily found as semi-massive sulphide-bearing rafts of variably deformed and metamorphosed schist or gneiss within Minto suite plutons. The best understood occurrence in the belt is the Carmacks Copper deposit which is described in detail below, but broadly is interpreted as a metamorphosed Late Triassic porphyry deposit (Kovacs, 2018; Kovacs *et al.*, 2020), an interpretation that likely applies to the other copper occurrences hosted within Minto suite plutons. If this is correct, Late Triassic volcanic rocks in the area may also be prospective, but for more classic Late Triassic porphyry deposits.

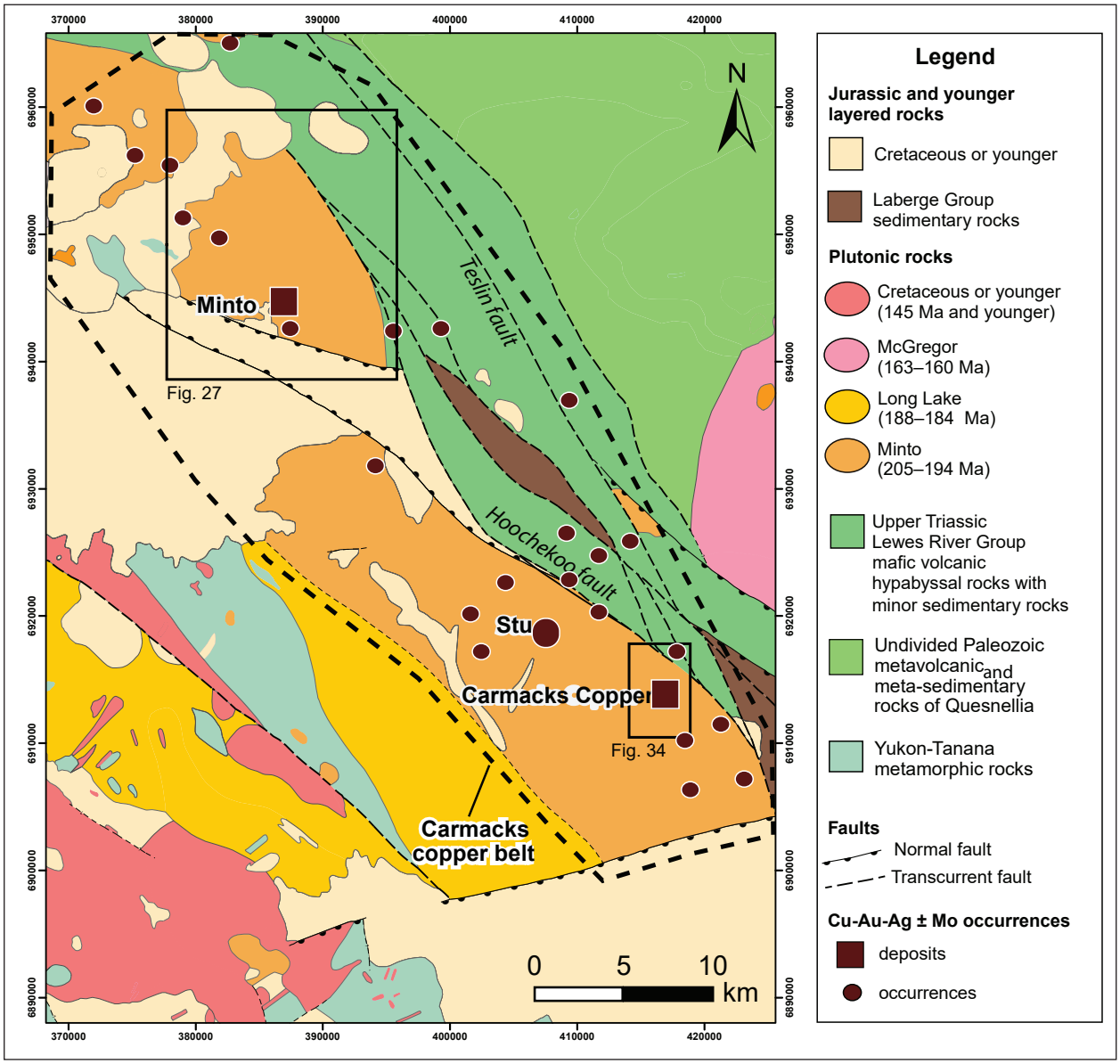

Figure 27. *Geology of the Carmacks Copper belt area, geology from YGS (2020a).*

Day 3 – Minto mine

Deposit geology

The Minto copper-gold-silver mine is located in central Yukon, 75 km northwest of the village of Carmacks (Fig. 26). The Minto property comprises several deposits that have a combined geologic resource of more than 1.6 Blbs of copper, 800 koz of gold and 8 Moz of silver, and a combined average grade of 1.2% Cu, 0.4 g/t Au and 4 g/t Ag in 63 Mt (Table 7). The mine is accessed via the Klondike Highway to a seasonal barge crossing the Yukon River and then via a private 27 km road to the mine site. Mineralized rocks were discovered on the property in 1971 and the mine was in production between 2007 and 2018. In 2018, the mine temporarily closed while ownership changed and in late 2019 the mine reopened under its current owner, Pembridge Resources.

The Minto pluton has an exposed surface area of 170 km² and the local geology of the area is shown in Figure 28. The Minto pluton intrudes the Upper Triassic augite-phyric basaltic rocks of the Lewes River Group (Stikine terrane) to the east and north, and presumably the Late Devonian-Early Mississippian metaplutonic rocks of the Simpson Range plutonic suite (Yukon-Tanana terrane) to the west (Tempelman-Kluit, 1984). The contact between the Minto pluton and Yukon-Tanana rocks is covered by younger volcanic rocks, and the exact nature of that contact is unknown. The northern end of the Minto pluton is covered by Pliocene and younger basalt flows of the Selkirk Volcanic Group (Tempelman-Kluit, 1984). The eastern margin of the Minto pluton is locally faulted against rocks of the Lewes River Group along the dextral Ingersoll fault (Tempelman-Kluit, 1984). The southern margin of the Minto pluton is unconformably overlain by volcanic and sedimentary rocks of the Upper Cretaceous Carmacks Group, as demonstrated locally by a clast-supported cobble to boulder conglomerate that includes clasts of mineralized Minto rocks (Hood, 2012). The southern margin of the pluton is defined by an unnamed normal fault (Tempelman-Kluit, 1984).

Table 7. *Global Minto resource recalculated from Mercer and Sagman (2012) for Minto South, Ridgetop, Minto North and Minto East deposits (their Tables 1-2 through 1-5 respectively). Minto Main deposit estimate is from SRK (2008; their Table 1-5, Dec. 2007 Model). The Dec. 2007 model was done after approximately 6 months of mining and does not include mined out material; it is considered a slight underestimate. Each estimate uses a cut-off grade of 0.5% Cu. M&I = Measured & Indicated.*

	Tonnes (000)	Cu (%)	Au (ppm)	Ag (ppm)	Cu (lbs)	Cu (tonnes)	Au (oz)	Au (tonnes)	Ag (oz)	Ag (tonnes)
Total M&I	54 513	1.21	0.45	4.4	1,449,715,364	657 579.29	771,233	21.9	7,696,197	218.2
Total Inferred	8491	0.81	0.24	2.9	151,741,000	68 828.50	64,300	1.8	787,000	22.3
Global Resource (M&I plus Inf)	63 004	1.15	0.42	4.2	1,601,456,364	726 407.80	835,533	23.7	8,483,197	240.5

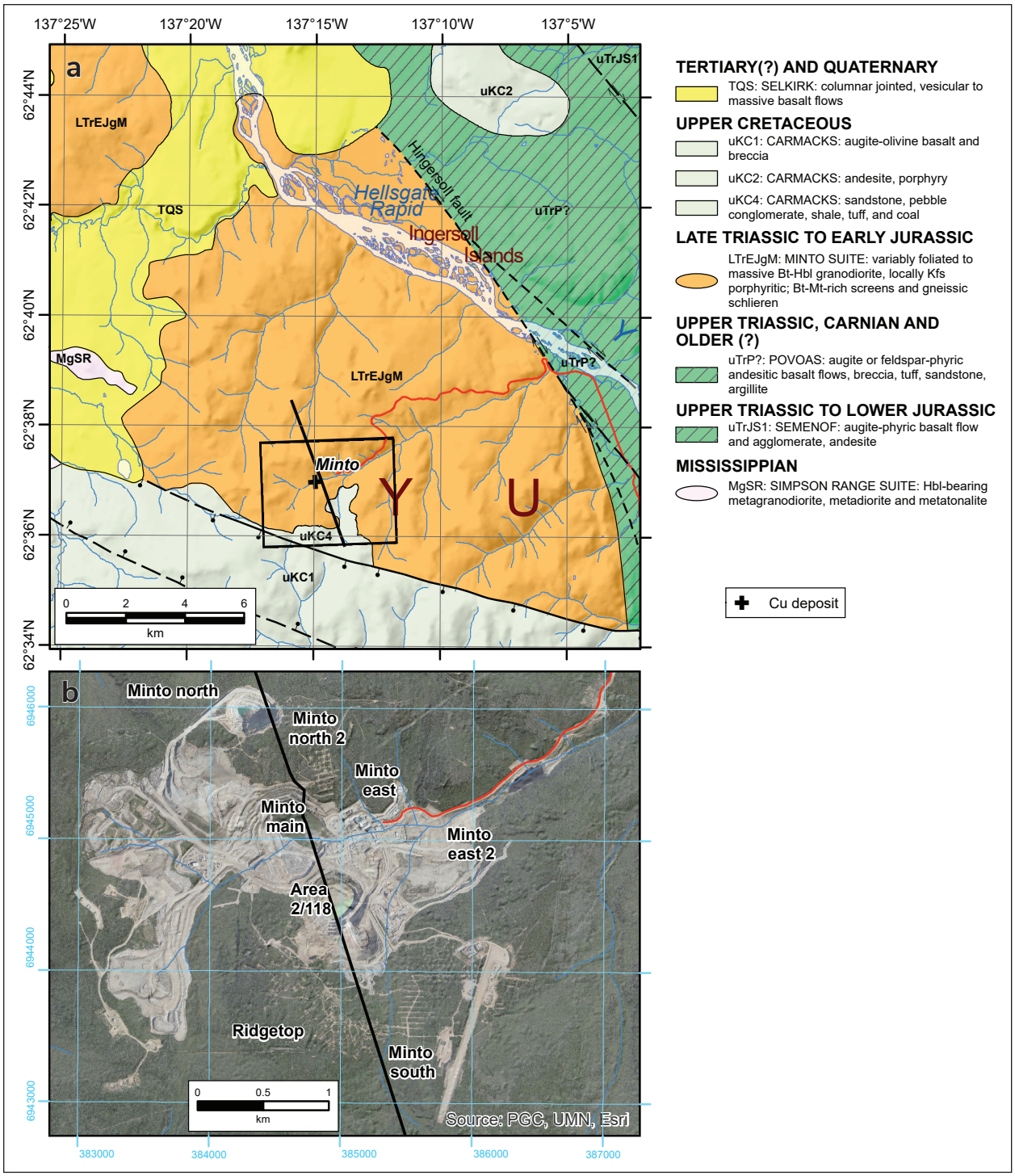

Figure 28. (a) *Simplified geology of the Minto pluton, geology from YGS (2020a).* ***(b)*** *Aerial orthophotograph showing location of the various orebodies at the Minto mine (30 August 2017; https://www.geomaticsyukon.ca/data). Location of cross sections in Fig. 31 shown.*

The deposits are hosted by the Minto pluton, an Early Jurassic granitoid composed of medium to coarse-grained, K-feldspar phyric to equigranular, unfoliated granodiorite (Fig. 29; Hood, 2012; Sack *et al.*, 2020; Tafti, 2005). The actual composition and texture varies from crowded K-feldspar megacrystic syenite to equigranular tonalite or quartz diorite. In general, the granodiorite contains approximately 30 to 50% plagioclase, 10 to 50% K-feldspar, 20 to 25% quartz, and 10 to 15% biotite ± hornblende (Hood, 2012). Accessory minerals include magnetite, epidote, titanite, apatite and zircon, all

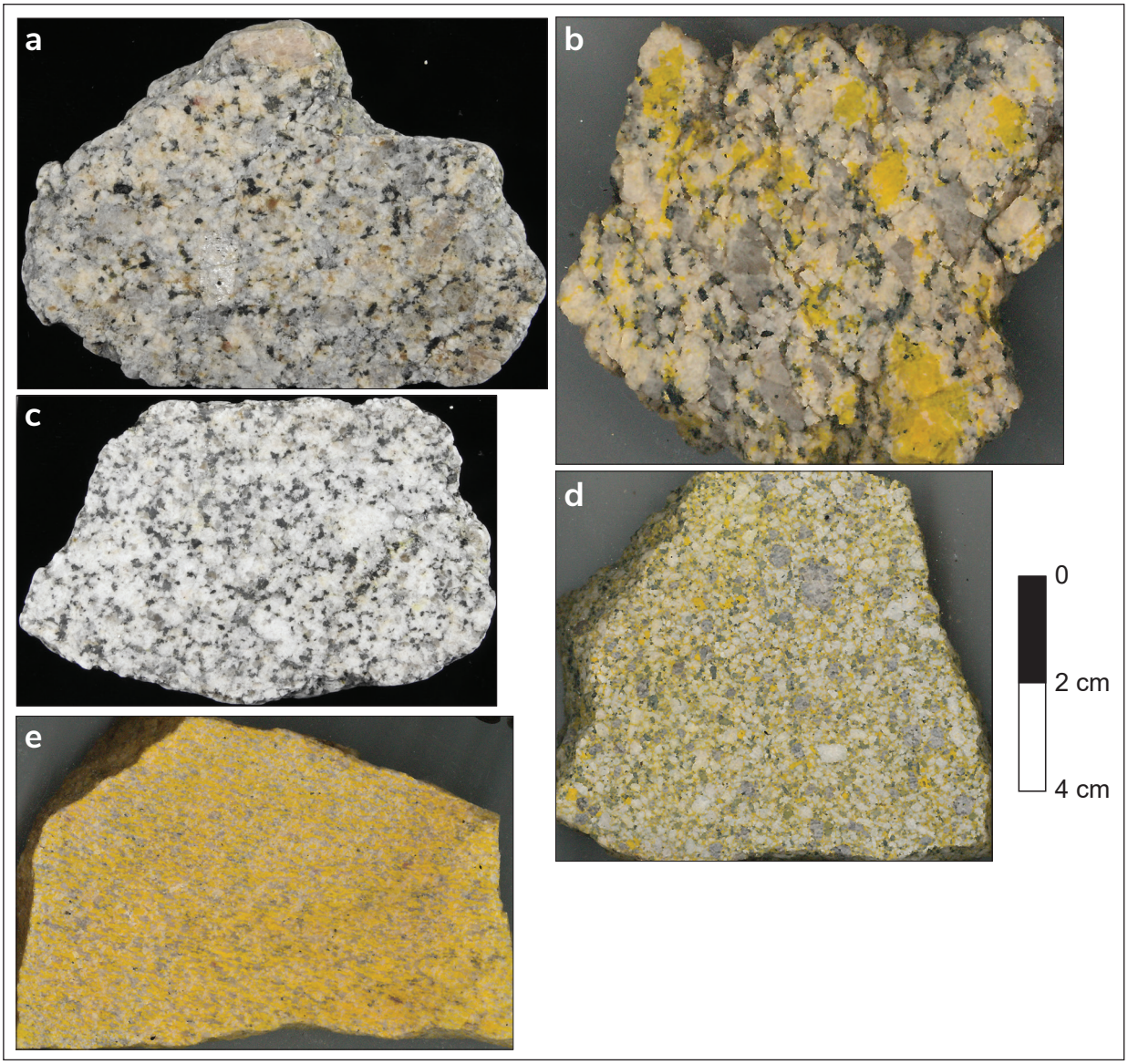

Figure 29. *Representative samples from the Minto pluton (from Sack et al., 2020).*
(a) and (b) *Coarse-grained, porphyritic granodiorite; a-11RAYJC040A, b-11RAYJC039A.*
(c) and (d) *Medium-grained equigranular monzodiorite; c-11RAYJC042A, d-11RAYJC038A.*
(e) *aplite; 11RAYJC041B. Fresh polished surface (left) and a cobaltinitrite-stained surface (right). Note K-feldspar is yellow.*

of which have sharp euhedral crystal faces in thin section (Hood, 2012). K-feldspar occurs most commonly as phenocrysts 1 to 3 cm long, with inclusions of biotite, plagioclase, hornblende, epidote and zircon commonly along growth zones (Hood, 2012). Biotite and hornblende are the most common mafic minerals; they are typically <1 cm, and comprise up to 5 to 15% of the granodiorite (Hood, 2012). Both magmatic epidote and secondary epidote are present; magmatic epidote has sharp euhedral boundaries with mafic phases and growth zoning (as described by Zen and Hammarstrom, 1984).

The Minto deposits have been studied and described by Pearson and Clark (1979), Tafti (2005) and Hood (2012). The mineralized rocks comprise alternating mafic and felsic layers that are moderately to strongly foliated and recrystallized, these rocks have been partially melted and migmatized (Fig. 30). Individual orebodies of foliated rock are up to tens of metres thick and form gently dipping horizons, which can be traced laterally for

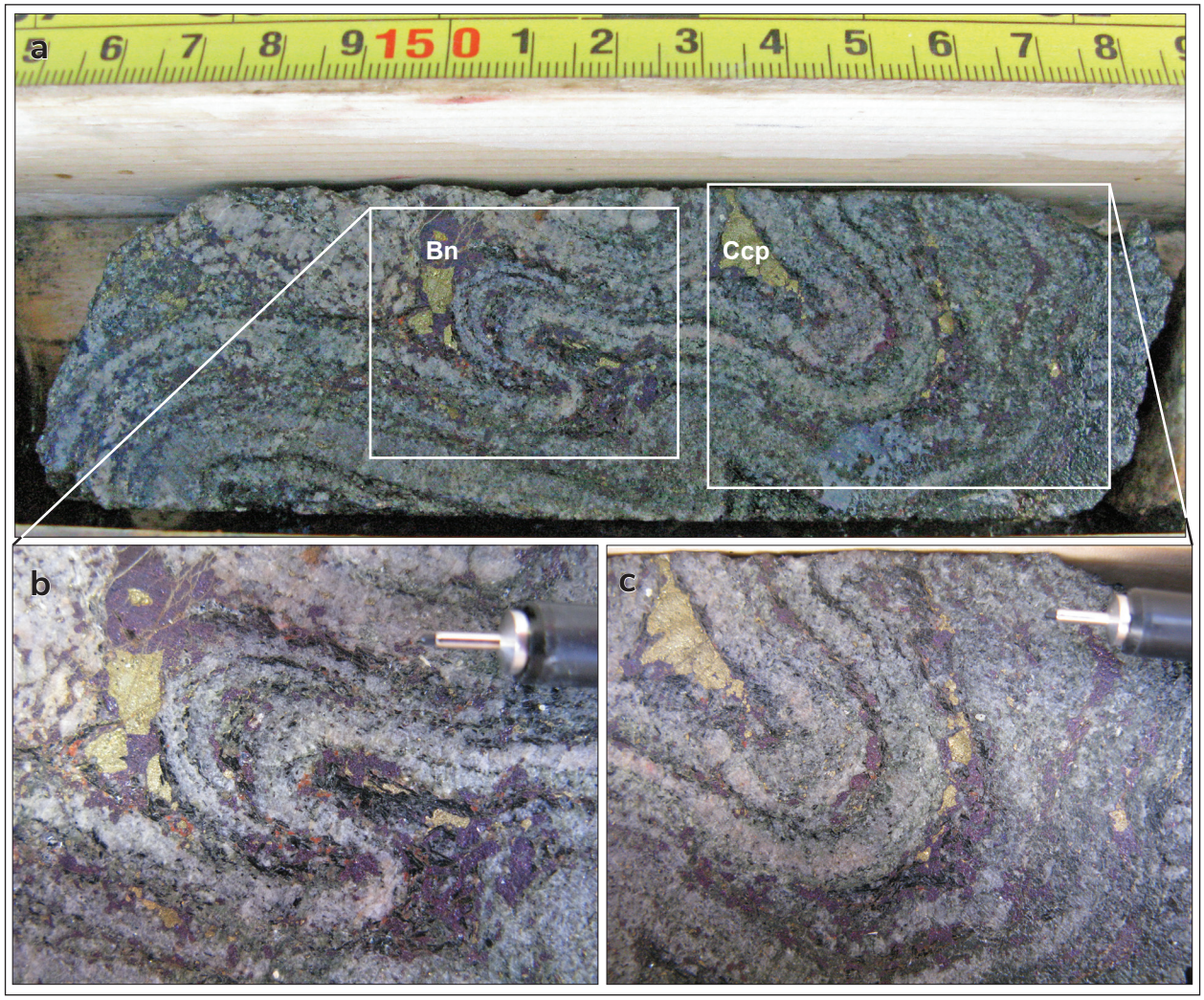

Figure 30. *Ptygmatic folding within migmatitic mineralized rocks in diamond drill hole 09SWC390 at approximately 81 m depth, Minto North deposit. Copper sulphides (chalcopyrite and bornite) locally remobilized and concentrated in fold hinges. Photo credit: J. Chapman (GSC).*

more than one kilometre in diamond drill core; these horizons are stacked in parallel to subparallel sequences (Fig. 31; Mercer and Sagman, 2012). Individual mafic layers are millimetres to centimetres thick and consist of moderately aligned biotite, hornblende, epidote, magnetite and titanite; these layers are separated by thicker felsic layers that are centimetres to tens of centimetres and composed of medium to coarse-grained quartz and plagioclase with lesser amounts of biotite, hornblende, epidote, magnetite and titanite (Hood, 2012). Higher grade ore typically occurs within thicker layered, coarser grained and more siliceous rocks, while lower grade ore is often associated with thin, discontinuously layered and more mafic rocks (Mercer and Sagman, 2012). Contacts between foliated and unfoliated rocks are typically sharp, marked by rapid change in grain-size, with foliation and gneissic banding commonly at high angle to contacts with unfoliated rocks; locally, K-feldspar phenocrysts from unfoliated granodiorite impinge on foliation (Fig. 32). These observations suggest an intrusive relationship between unmineralized and mineralized rocks (Hood, 2012). As described at the Carmacks Copper

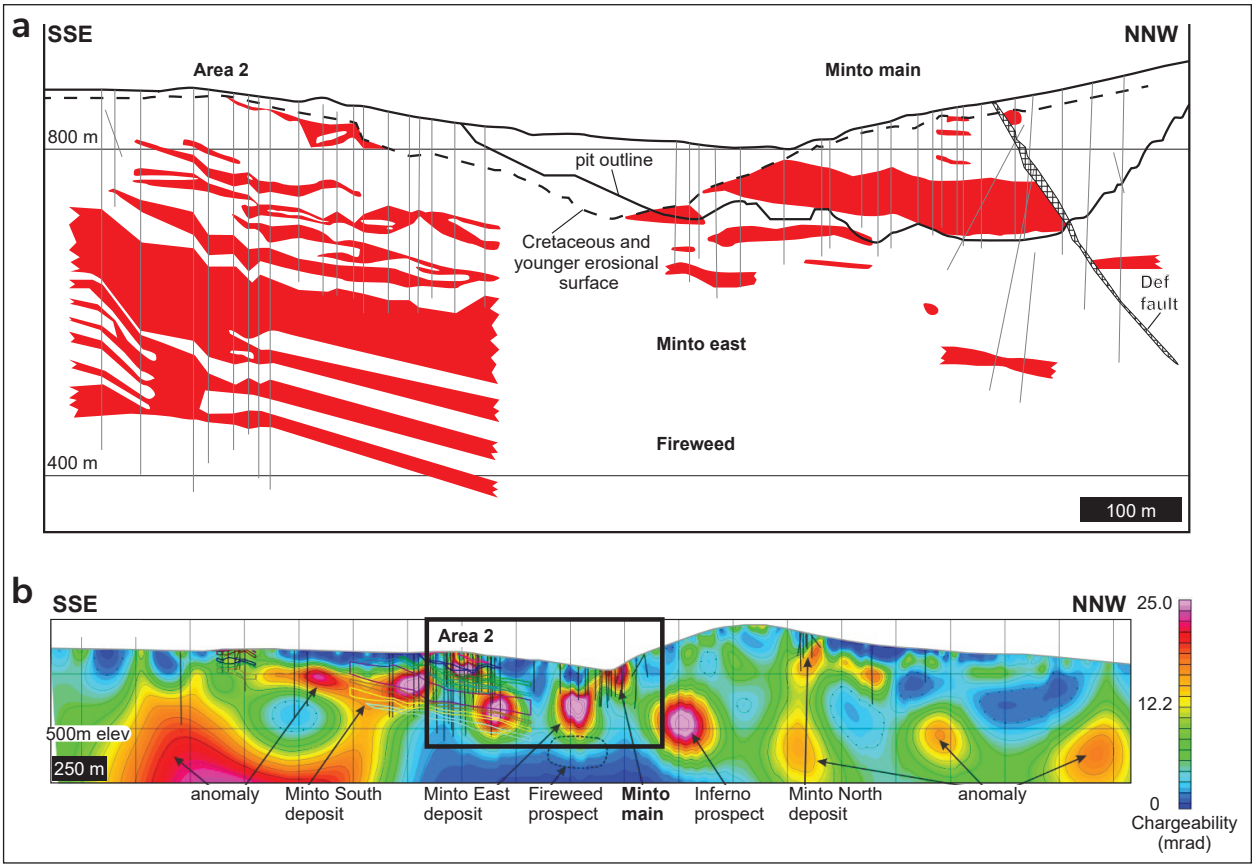

Figure 31. *Vertical sections across the Minto property, location shown in Figure 28.* ***(a)*** *Geology of the Minto deposit prior to mining development, ca. 2007 (after Hood et al., 2009). Copper mineralization occurs in shallow dipping bands of foliated and gneissic rocks (red).* ***(b)*** *Titan-24 survey Line 3. Smooth IP chargeability from DC resistivity (Mercer and Sagman, 2012). Note correspondence of high chargeability anomalies with known deposits. Location of (a) shown by heavy box.*

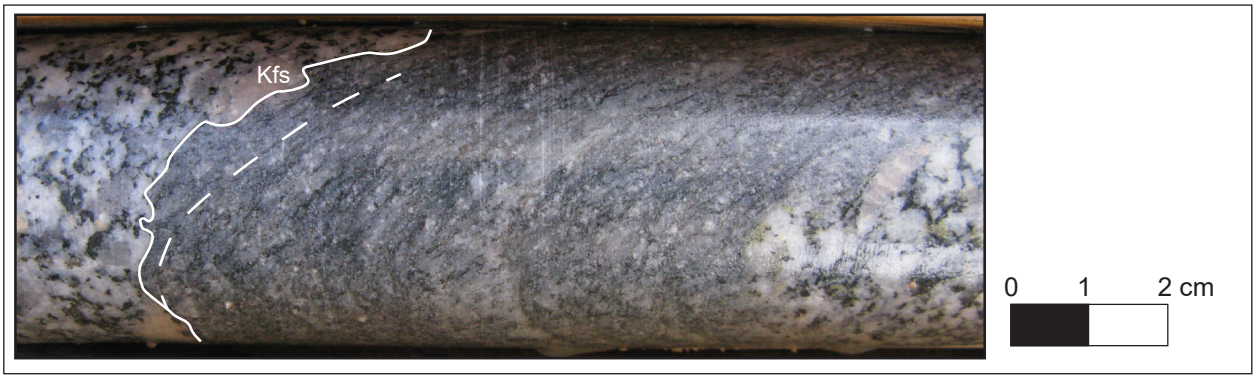

Figure 32. *Contact relationship between foliated and unfoliated rocks in the Minto North deposit; diamond drill hole 09SWC457 at approximately 23 m depth. Truncation of foliation (dashed white line) by the irregular contact (solid white line) between foliated and unfoliated rocks. Also, note the K-feldspar phenocryst impinging upon foliated rocks. Photo credit: J. Chapman (GSC).*

deposit (Kovacs, 2018; Kovacs et *al*., 2020), the mineralized horizons at Minto appear to represent migmatized rafts intruded by the main phase granodiorite of the Minto pluton. However, this process is generally more advanced at Minto and gneissic horizons were commonly inferred to be derived from plutonic protoliths in previous studies (e.g., Hood, 2012; Tafti, 2005).

Hypogene ore minerals in the Minto deposits are mainly chalcopyrite and bornite, with rare chalcocite and minor pyrite (Mercer and Sagman, 2012). The sulphides occur as disseminated and foliaform stringers along foliation planes and commonly display a net-texture suggesting recrystallization of original ore minerals (N. Kovacs, pers. comm., 2018). Magnetite and biotite are commonly abundant in association with ore sulphides (Fig. 33). Magnetite content decreases from migmatized rafts (median = 35.7×10^{-3} SI units; metatexite), to foliated granodiorite (median = 8.25×10^{-3} SI units; assimilation zone), and finally to unfoliated granodiorite (median = 0.37×10^{-3} SI units; Fig. 33). The magnetite and biotite enrichment and K-feldspar replacement of plagioclase observed in the ore zones are interpreted as part of a strong potassic alteration associated with the Minto mineralization (Hood, 2012; Mercer and Sagman, 2012). Supergene mineralization consisting of chalcocite, malachite and minor azurite and native copper, is localized near surface extensions of the orebodies (commonly beneath exposure of the Upper Cretaceous conglomerate), and along late faults such as the DEF fault.

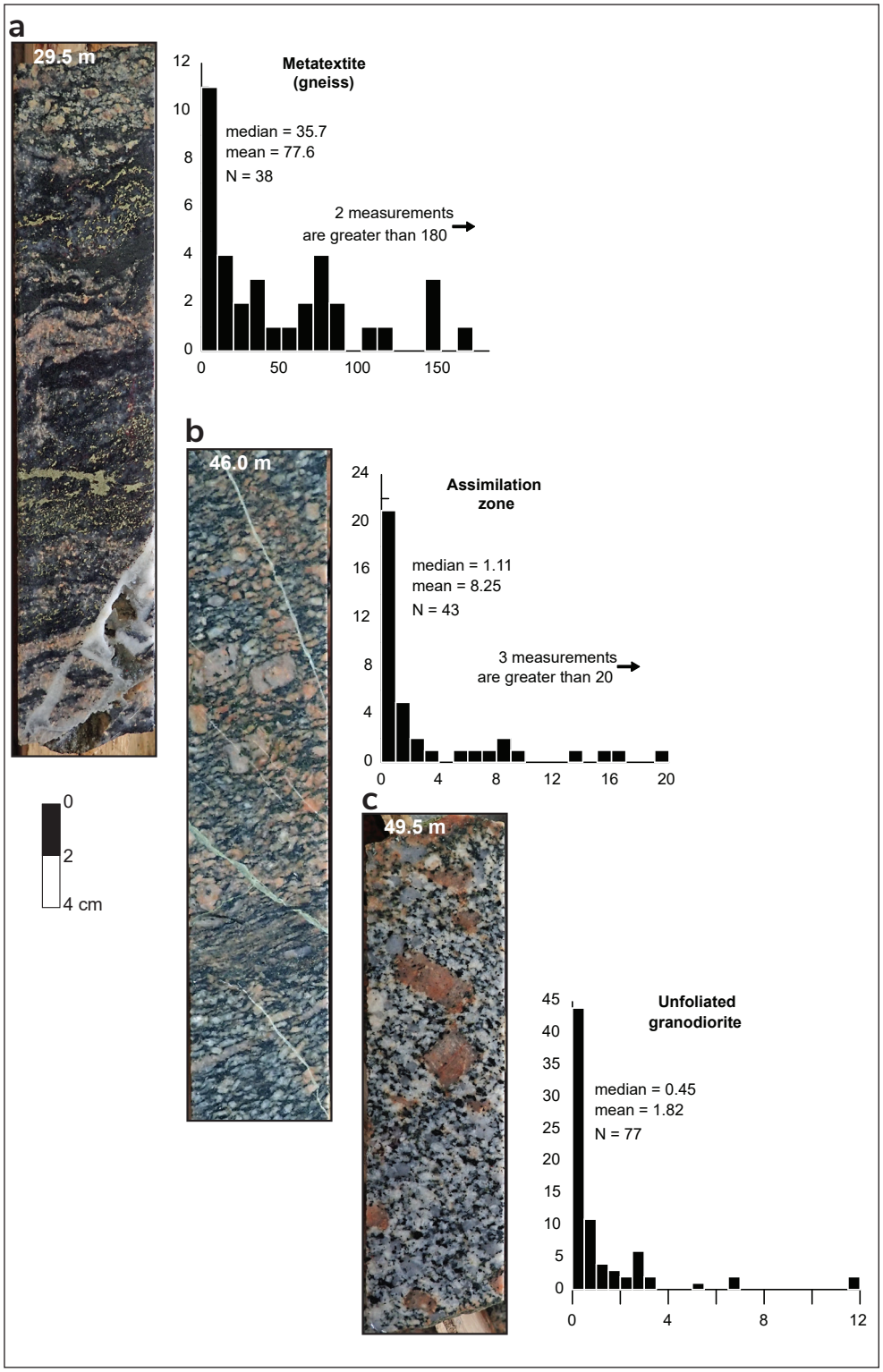

Figure 33. *Transition from mineralized to unmineralized rock over 20 m drilled distance (from Sack et al., 2020). Core photos from the Copper Keel West underground orebody, Minto deposits, diamond drill hole UG18-003.* ***(a)*** *Foliated and mineralized metatexite with 5.4% Cu, 29.5 m depth.* ***(b)*** *Unmineralized assimilation zone with both foliated rock and 2 cm K-feldspar phenocrysts, 46.0 m depth.* ***(c)*** *K-feldspar porphyritic unfoliated granodiorite without mineralization, 49.5 m depth. Metatexite is interpreted as highly metamorphosed protolith rock whereas the unfoliated granodiorite is the engulfing intrusion; assimilation zone is interpreted as the transition between the two (N. Kovacs, personal communication, 2018). Magnetic susceptibility histogram beside each photo uses data from diamond drill core in the H.S. Bostock core library (Sack et al., 2017). Note the decrease in magnetic susceptibility from metatexite to assimilation zone to unfoliated granodiorite. X-axes x10^{-3} SI units; Y-axes number of measurements.*

Age of mineralization

The age of the Minto pluton is best constrained by U-Pb zircon dates from Hood (2012) and Sack et *al.* (2020) that range from ca. 205 to 195 Ma (Fig. 34). The age of mineralization is best constrained by molybdenite with ages between 202 and 196 Ma (Hood, 2012). Hood (2012) documented deformed and undeformed molybdenite grains but interpreted only one mineralization age. We interpret these data in a manner similar to that of Kovacs et *al.* (2020) at the Carmacks Copper deposits. Kovacs et *al.* (2020) found an older population of deformed grains and a younger age population of undeformed molybdenite grains and interpreted the dates from each as an original Late Triassic mineralization age and a subsequent Early Jurassic migmatization age, respectively. Because Re-Os dating is a separation and solution technique, it is not possible to completely constrain the generation of molybdenite being dated and these are best thought of as mixed ages and thus approximations. For the Minto deposits, we prefer the interpretation that the older 202 Ma age represents a Late Triassic mineralization age, but one that has a significant contribution from the younger migmatization event. This interpretation is consistent with the overall more migmatized nature of the Minto rafts compared to those at Carmacks Copper.

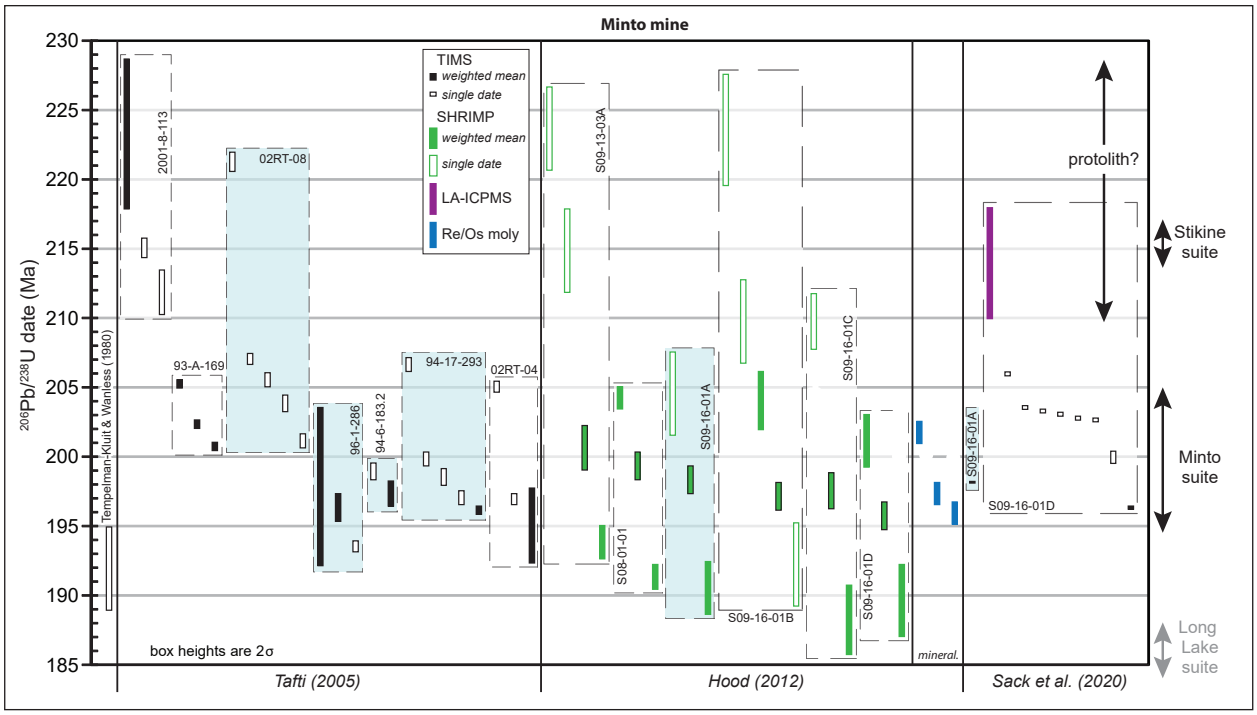

Figure 34. *Summary of $^{206}Pb/^{238}U$ zircon dates from the Minto pluton (from Sack et al., 2020). All samples were collected at the Minto mine. Dates by Tafti (2005) and Tempelman-Kluit and Wanless (1980) were analyzed by ID-TIMS on multi-grain zircon fractions. Hood (2012) dated single grains by SIMS at the GSC; the weighted mean $^{206}Pb/^{238}U$ date for the dominant population in SIMS analyses is outline in black. Hood (2012) also dated molybdenite in mineralized samples by Re/Os (blue bars). New CA-TIMS dates are shown at right (reanalysis of 2 samples analyzed by Hood, 2012; Sack et al., 2020).*

Mining and processing methods

The Minto Mine has been in operation since 2007. Operations consisted solely of open pit mining from 2007 until 2013 when underground mining began. Surface mining was finished in 2018 and since then the Minto deposit has been mined using an underground long-hole open stope method.

The mining method requires a series of parallel sill drifts to be developed along the strike of the deposit, following the footwall contact. From these sill drifts, a long-hole rig drills rings of 3" diameter up-holes into the deposit above, stopping at the hanging wall contact. After drilling is completed, the rings are loaded, blasted, and then mucked out from the sill drift. Mucking is via remote-controlled load-haul-dump machines (LHDs). The broken ore from the stopes is mucked by LHDs to remuck bays, or loaded directly onto trucks, which carry ore from the mine to a small stockpile adjacent to the portal. The surface mining fleet then takes ore to the stockpiles or to the mine crusher on a daily basis.

Copper is recovered through a crushing-grinding-flotation circuit. The underground ore is crushed at first to produce mill feed. Initially, grinding is carried out in a 16.5 ft diameter by 5 ft long Semi-Autogenous Grinding (SAG) grinding mill. After the SAG, secondary grinding is carried out in two 12.5 ft diameter by 10 ft long overflow type ball mills. Each ball mill operates in closed circuit with a bank of three 15" hydrocyclones. The grinding circuit produces a flotation circuit feed with a product size of 250 µm P80.

Rougher flotation is achieved using three 1400 ft^3 tank cells. The rougher tailing is further treated in a bank of four 500 ft^3 flotation cells. The rougher-scavenger tailing is the final tailing from the flotation plant and it is thickened to about 50% solids by weight before being pumped from the plant to the storage area. Both the rougher and rougher/scavenger concentrates are pumped to a bank of four foot cleaner cells. The cleaner concentrate is forwarded on to a bank of six re-cleaner cells, which is the final concentrate from the plant.

Gold and silver are recovered via two streams in the mill process. A portion of the gold and silver are recovered using a centrifugal gravity concentrator installed in the cyclone underflow in the grinding circuit. Precious metals are also recovered to the final copper concentrate. The contained gold and silver in the gravity and flotation concentrates are sold separately from each other.

Day 4 - Carmacks Copper deposit

Deposit geology

The Carmacks Copper deposits (Williams Creek; [115I 008]) are located 40 km northwest of Carmacks (Fig. 26). Access to the property is via the Freegold road along the 25 km long Carmacks Copper access road. The first discovery in the Carmacks copper belt occurred in 1970 when Grant Abbott, future Director of the Yukon Geological Survey, was an undergraduate student working for local exploration company Archer Cathro. Legend has it he took his lunch break on a hill looking over Williams Creek, after his customary nap, he realized that he was surrounded by green weathering rocks! We will visit his lunch site on our property tour, it is the location of the discovery trench at the Main zone of the Carmacks Copper deposit.

The Carmacks Copper deposits were the first mineralized rocks of this kind found in the Carmacks copper belt (Abbott, 1971) with their discovery sparking an exploration rush in the district; most known occurrences were initially found during this rush in the 1970s. An initial resource estimate was produced for the Carmacks Copper deposits in 1989 and ground was cleared for the leach pad before property development stalled in the early 1990s. An updated resource estimate in 2016 and 2018 defined 34 Mt of sulphide and oxide ore with an average grade just below 1% Cu, 0.3 g/t Au and 3 g/t Au and a contained metal content of 500 Mlbs of Cu, 300,000 oz Au and 3.5 Moz Ag (Table 8).

At Carmacks Copper the orebodies are similar to those at Minto with three distinct differences:

1. supergene processes have affected the upper portion of the orebodies and locally remobilized copper into surrounding Granite Mountain batholith rocks. The ore is primarily oxide minerals though significant sulphide ore is present at depth;
2. orebody orientation is more variable at Carmacks Copper with the majority of ore occurring in steeply dipping, northwest striking bodies; and
3. ore is mostly hosted by rafts of foliated mafic schist and amphibolite as compared to gneiss and migmatite at Minto. The degree of migmatization at Carmacks Copper seems to be less intense than at Minto.

Combined, zones 1, 7 and 4 make up the largest deposit on the property with a 700 m strike length and up to 100 m in width (Fig. 35; JDS, 2016). Mineralization in zone 4 is interpreted as an apparent 250 m sinistral offset of zones 1 and 7 across a post-mineralization brittle fault (Kovacs, 2018). The main area zones are oxidized to approximately 200 m below surface and hypogene mineralization extends to at least 450 m down dip; mineralization is open at depth (Fig. 36; JDS, 2016). Zones 12 and 13 have a combined strike length of 1.2 km and the widest part of zone 13 is up to 100 m.

Table 8. *Carmacks Copper mineral resource summary. 2016 resources recalculated from JDS (2016), 2018 from April 9, 2018 Copper North Mining Corp. news release. Contained Cu calculated using Total Cu as metallurgical work indicates >100% recovery of soluble copper, indicating the leach method is more aggressive than the soluble copper assay method (J. Milton written communication, December 2018).*

Deposit	Class	Cut-off	Tonnes (000)	Total Cu (%)	Soluble Cu (%)	Sulphide Cu (%)	Au (ppm)	Ag (ppm)	Cu (lbs)	Cu (Tonnes)	Au (oz)	Au (Tonnes)	Ag (oz)	Ag (Tonnes)	Type	Year calculated
Main (1,4,7)	Measured	0.25% CuT	4031	1.10	0.90	0.20	0.59	5.65	79,942,167	36 261	84,044	2.4	803,432	22.8	Oxide + Transition	2016
	Indicated	0.25% CuT	7949	1.04	0.83	0.20	0.40	4.05	146,144,039	66 290	110,863	3.1	1,134,623	32.2		
	Inferred	0.25% CuT	90	0.73	0.53	0.20	0.13	1.82	1,043,888	474	404	0.0	5,774	0.2		
	M+I+Inf	**0.25% CuT**	**12 070**	**1.06**	**0.85**	**0.20**	**0.46**	**4.57**	**227,130,094**	**103 025**	**195,311**	**5.5**	**1,943,830**	**55.1**		
	Measured	0.25% CuT	695	0.80	0.02	0.77	0.26	2.50	11,798,024	5352	6,374	0.2	61,289	1.7	Sulphide	
	Indicated	0.25% CuT	3645	0.74	0.03	0.71	0.21	2.30	57,054,463	25 880	27,000	0.8	295,720	8.4		
	Inferred	0.25% CuT	4031	0.71	0.01	0.70	0.18	1.90	62,207,763	28 217	25,594	0.7	270,160	7.7		
	M+I+Inf	**0.25% CuT**	**8371**	**0.73**	**0.02**	**0.71**	**0.20**	**2.12**	**131,060,250**	**59 448**	**58,969**	**1.7**	**627,168**	**17.8**		
South (2000S, 12,13)	Measured	0.15% CuOx	3409	0.46	0.34	0.12	0.12	1.80	34,571,528	15 681	14,430	0.4	216,448	6.1	Oxide + Transition	2018
	Indicated	0.15% CuOx	895	0.50	0.36	0.14	0.12	2.20	9,865,675	4475	3,788	0.1	69,455	2.0		
	Inferred	0.15% CuOx	389	0.34	0.27	0.07	0.12	1.65	2,915,830	1323	1,647	0.0	22,641	0.6		
	M+I+Inf	**0.15% CuOx**	**4693**	**0.46**	**0.34**	**0.12**	**0.12**	**1.86**	**47,353,033**	**21 479**	**19,865**	**0.6**	**308,543**	**8.7**		
	Measured	0.25% CuT	1136	0.59	0.11	0.49	0.13	2.30	12,271,797	5566	5,209	0.1	92,164	2.6	Sulphide	
	Indicated	0.25% CuT	3280	0.63	0.07	0.56	0.13	2.30	40,494,460	18 368	15,041	0.4	266,107	7.5		
	Inferred	0.25% CuT	4281	0.54	0.05	0.49	0.12	1.90	46,246,093	20 977	18,121	0.5	286,915	8.1		
	M+I+Inf	**0.25% CuT**	**8697**	**0.58**	**0.07**	**0.52**	**0.13**	**2.10**	**99,012,350**	**44 911**	**38,371**	**1.1**	**645,186**	**18.3**		
	Global resource (M+I+Inf all zones)		**33 831**						**504,555,727**	**228 863**	**312,515**	**8.9**	**3,524,728**	**99.9**		

The continuity of zones 12 and 13 has not been demonstrated and in zone 12, the rafts bifurcate and split into several parallel splays offset by post-mineralization faulting (JDS, 2016). Zone 2000S is between the main area and zone 13, and has a 300 m strike length and 30 m width. The oxidation in zones 2000S, 12 and 13 extends to 40 to 80 m below surface (JDS, 2016). In zones 1, 7 and 2000S the orebodies are defined by roughly elongate, ellipsoidal shells that strike northwest and dip steeply to the east (Kovacs, 2018). In contrast, the orebody in zone 4 is flat lying (Kovacs, 2018) and those at zones 12 and 13 also strike northwest but dip moderately (~45°) to the east.

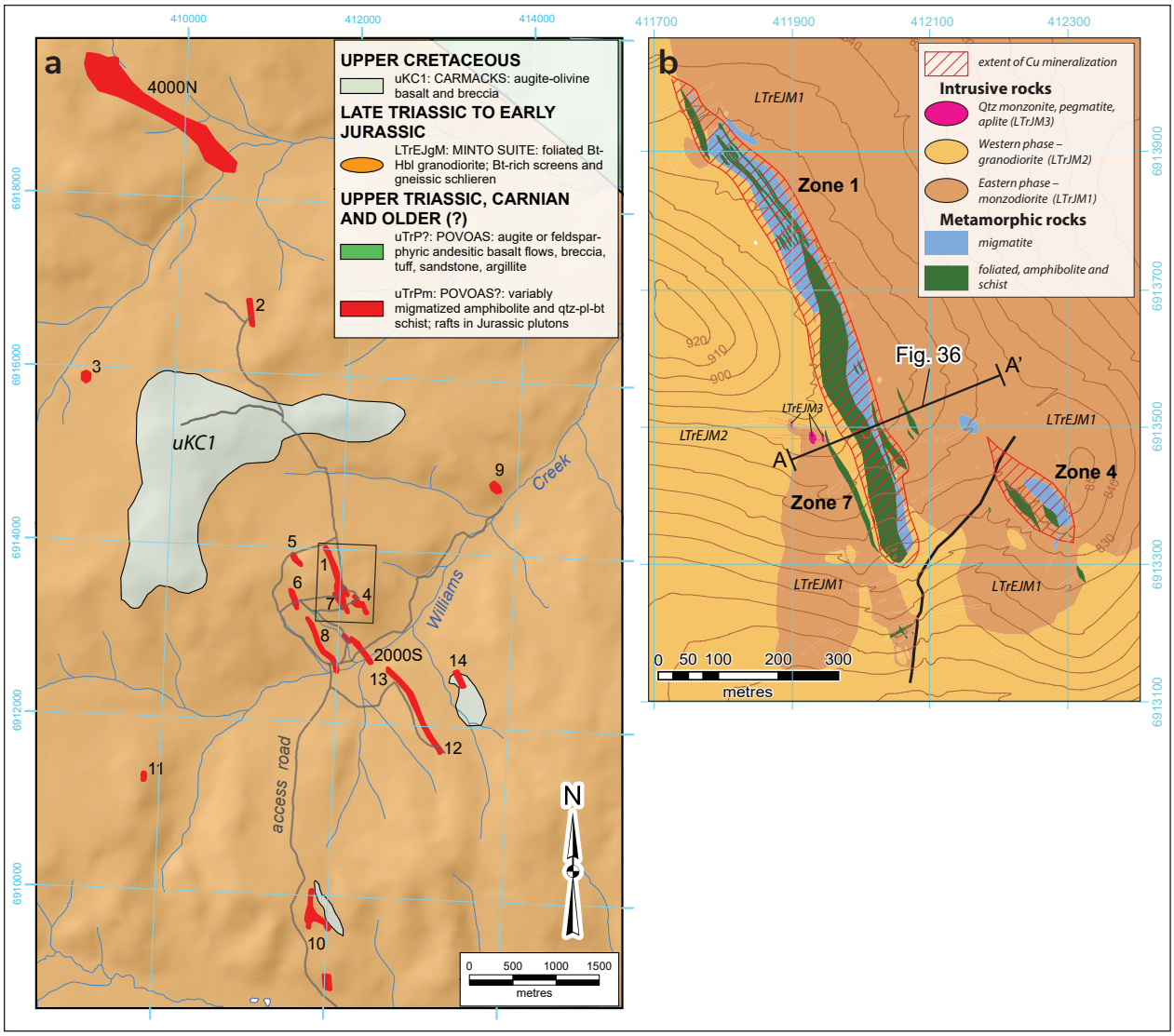

Figure 35. (a) *Detailed geological map showing distribution of mineralized rafts of amphibolite and intermediate schist within granodiorite at the Carmacks Copper deposit; (Kovacs et al., 2020).* ***(b)*** *Detailed map of the Main zones at the Carmacks Copper deposit (after Kovacs, 2018). This map shows the phases of the Granite Mountain batholith and the relationship between migmatized and relatively intact metamorphic rafts in the main deposit area.*

The majority of the resource at Carmacks Copper is within the upper oxidized portion of the orebodies (Fig. 37) where weathering has created 1 to 3% pore space and supergene minerals commonly line and in-fill cavities as irregular and coliform masses, fill fractures and rim sulphides (JDS, 2016). The majority of the copper in the supergene portions is in malachite, cuprite, azurite and tenorite, with trace amounts of covellite, digenite, djurlite and native copper (Fig. 37; JDS, 2016). Non-copper-bearing supergene minerals include limonite, goethite, specular hematite and gypsum (JDS, 2016).

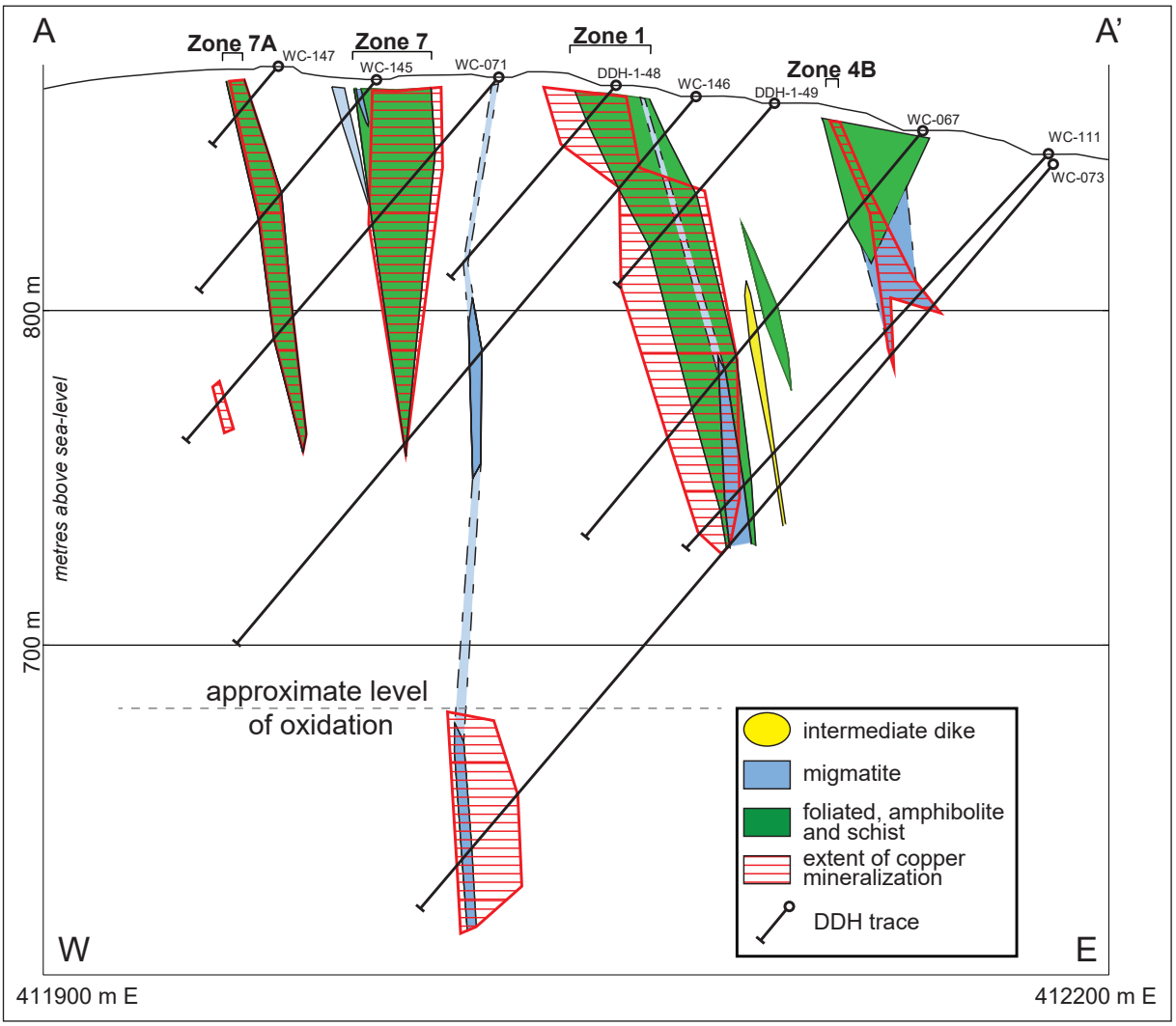

Figure 36. *Cross section 200N (50 m thick, oriented 066) through southern part of the main area; NAD 83, Zn 8, looking north. Location of cross section shown on Figure 35. White area is unfoliated granodiorite and monzodiorite. Faded colours indicate our interpretation which utilizes surface mapping and terminology of Kovacs (2018). Extent of Cu mineralization based on total copper and oxide copper assays. Intermediate dike is likely related to the Upper Cretaceous Carmacks volcanics. Modified from Casselman (2007). DDH = diamond drill hole.*

Figure 37. *Supergene copper mineralization at zone 1, Carmacks Copper deposits.* ***(a)*** *'Discovery trench', showing abundant supergene copper, most obvious is blue-green malachite but azurite and tenorite are also common. Approximate location of* ***(b)*** *shown in centre left. (b) Close-up of quartz-plagioclase-biotite schist, migmatite and a late dike. Supergene copper mineralization coating all three rock types; hammer head 13 cm.* ***(c)*** *Reflected light image of a hypogene copper mineral (bornite) weathering to a supergene copper mineral (covellite) with specular hematite (from trench 91-11; Tafti, 2005).*

Hypogene copper-bearing minerals in the Carmacks Copper deposit are bornite and chalcopyrite (Kovacs, 2018; Tafti, 2005). Non-copper-bearing hypogene minerals include magnetite, pyrite, pyrrhotite and carbonate with trace amounts of native gold and bismuth, molybdenite, bismuthinite, and arsenopyrite (JDS, 2016). In zones 1 and 7, hypogene copper mineralization is zoned from bornite in the north to chalcopyrite, and finally to minor pyrite-pyrrhotite in the south (JDS, 2016). Gold is associated with bornite and as a result, gold values are higher in the northern half of the main area (average 0.75 g/t Au) and lower in the southern half (average 0.27 g/t Au; JDS, 2016). In the lower hypogene portions of the orebodies, sulphide minerals have three distinct textural and rock associations (Fig. 38). The least metamorphosed amphibolite and schist contain either disseminated chalcopyrite and pyrite or foliaform chalcopyrite and bornite, whereas migmatized portions of the rafts are characterized by net-textured bornite and chalcopyrite (Kovacs, 2018). Disseminated and foliaform sulphides are interpreted as the earliest mineralization (*i.e.*, pre-Granite Mountain batholith) whereas net-textured sulphides have been partially melted and locally remobilized, likely as a result of the Granite Mountain batholith engulfing the rafts (Kovacs *et al.*, 2020).

Age of mineralization

The age of the Early Jurassic Granite Mountain batholith is best constrained by U-Pb zircon ages from Tafti (2005), Kovacs *et al.* (2020) and Sack *et al.* (2020) with most weighted mean ages between 200 and 194 Ma (Fig. 39). The age of mineralization at the Carmacks Copper deposits is thoroughly described in Kovacs *et al.* (2020). In brief, Re-Os analysis primarily of deformed molybdenite grains suggests initial mineralization occurred in the Late Triassic, *ca.* 212–215 Ma slightly after igneous crystallization of the host amphibolite as interpreted from the oldest zircon cores in the rocks. Cryptic zircon rims in mineralized rocks show they were metamorphosed *ca.* 205 Ma. Subsequent to metamorphism, Re-Os ages of primarily undeformed and isotopically reset molybdenite grains are as young as 198 Ma indicating the mineralized rafts were engulfed and migmatized by the host Early Jurassic Granite Mountain batholith.

Planned mining and processing methods

The mine plan for the Carmacks Copper project consists of a 6.5 year mine life through open pit mining. Four mining phases are designed for the Carmacks project. The design is based on 10 m mining benches in a double bench configuration with 25 m wide walls and 25 m wide main road at a maximum grade of 10%. Mineralized material production is envisioned to be 1.775 million tonnes per year at an average rate of 4860 tonnes per year with a peak total material rate is 13 million tonnes per year.

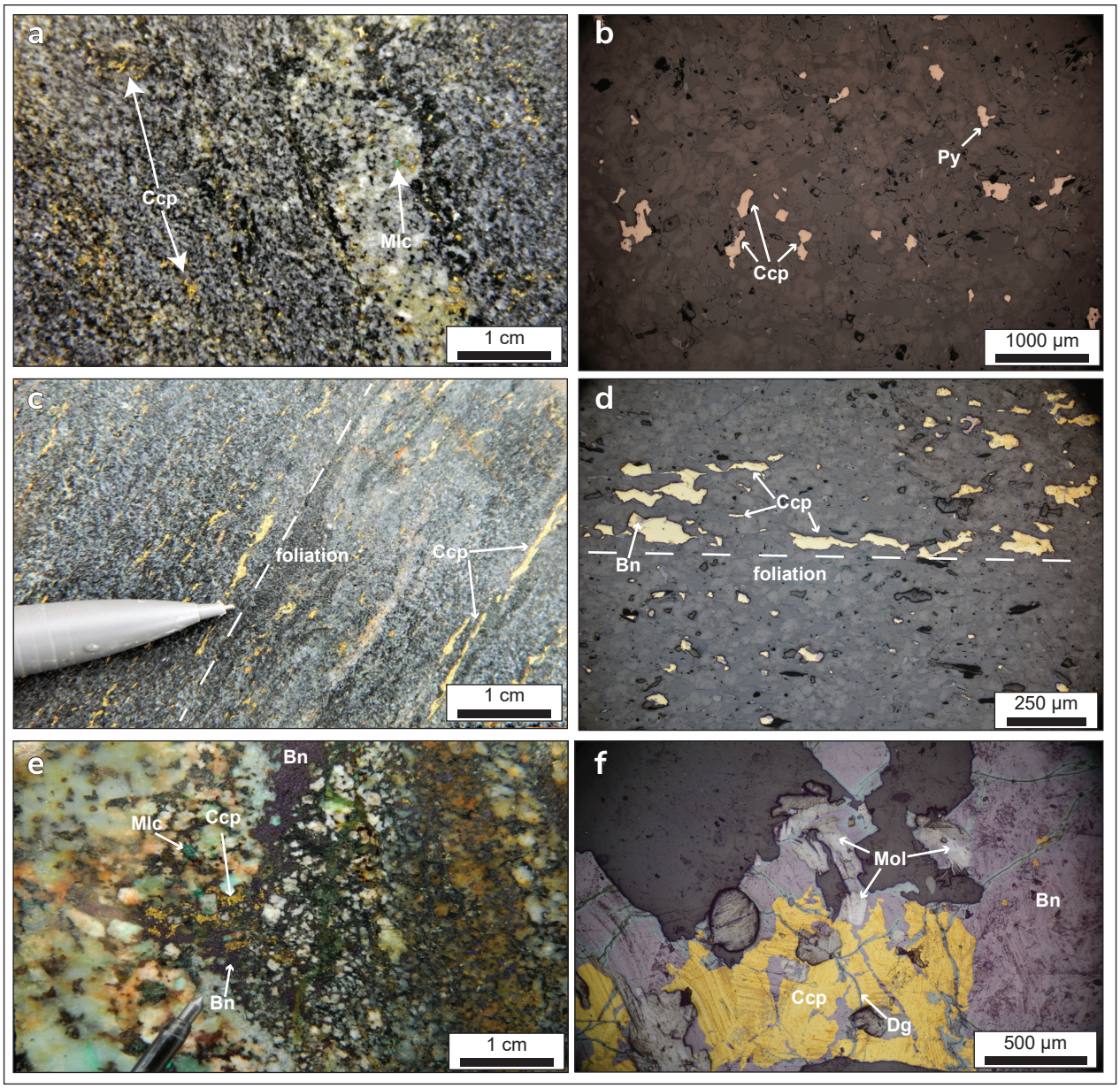

Figure 38. *Disseminated, foliaform and net-textured hypogene copper mineralization at the Carmacks Copper deposits. All images from Kovacs (2018).* ***(a)*** *Disseminated chalcopyrite mineralization in the quartz-plagioclase-biotite schist, CN15024-44.5 m.* ***(b)*** *Reflected light photomicrograph of disseminated chalcopyrite ± pyrite, CN15024-54.88 m.* ***(c)*** *Foliaform chalcopyrite mineralization in the amphibolite, WC005-254.4 m.* ***(d)*** *Reflected light photomicrograph of foliaform chalcopyrite-bornite mineralization in amphibolite, WC005-254.4 m.* ***(e)*** *Net-textured bornite-chalcopyrite mineralization in diatexite migmatite, WC002-148 m.* ***(f)*** *Reflected light photomicrograph of net-textured bornite-chalcopyrite mineralization in migmatite, WC008-174.31 m.*

Initial metallurgical testing program on the Carmacks Copper project focused on the recovery of acid soluble copper mineralization. Based on the current PEA, mineralized material will be crushed and ground to 80% <664 µm using a jaw crusher followed by a SAG mill in closed circuit with hydrocyclones followed by leaching the copper into solution with sulphuric acid. Copper is then recovered using solvent extraction and electrowinning (SX-EW). Tailings from the copper leach circuit will be processed through a Carbon in Leach (CIL) circuit, where gold and silver are leached into solution with sodium cyanide and adsorbed onto activated carbon. The precious metals are then recovered through elution, electrowinning and refining. An adsorption, desorption and refining (ADR) circuit will be implemented to concentrate the gold/silver into doré bars. The resulting tailings residue then passes through an Inco SO2-Air circuit for destruction of the residual cyanide, followed by filtration and placement as dry stack tailings.

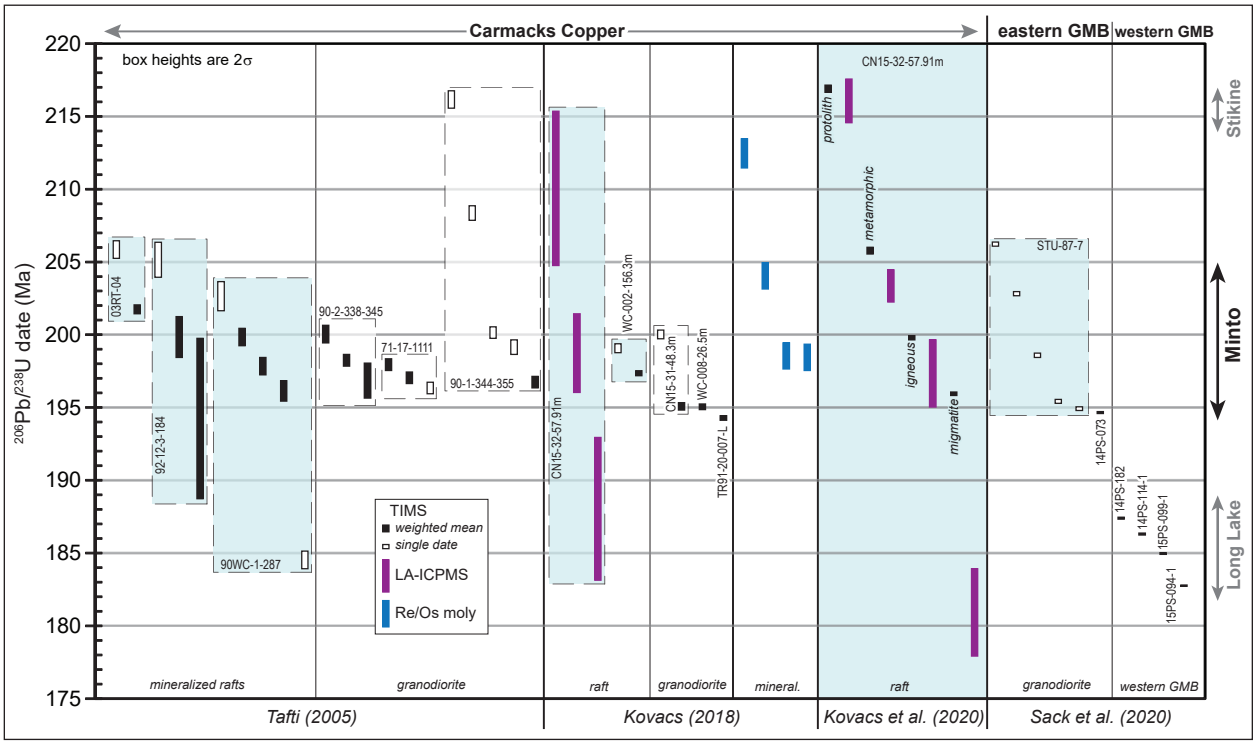

Figure 39. *Summary of $^{206}Pb/^{238}U$ zircon dates from the Granite Mountain batholith. The majority of samples dated were collected at the Carmacks Copper deposit (Kovacs et al., 2020; Tafti, 2005). New CA-TIMS dates from the eastern margin of Granite Mountain batholith collected for this study are shown at right (eastern GMB). We also show younger dates from the western portion of the batholith for comparison at far right (western GMB). Re-Os dates from molybdenite in ore at the Carmacks Copper deposits are also shown for comparison (Kovacs, 2018). Samples shown with blue shading were collected from mineralized foliated rafts at the Carmacks Copper and Stu occurrences. Double arrows along the right edge of the diagram indicate age ranges of the Stikine (217–214 Ma), Minto (205–194 Ma) and Long Lake (188–184 Ma) suites from Sack et al. (2020).*

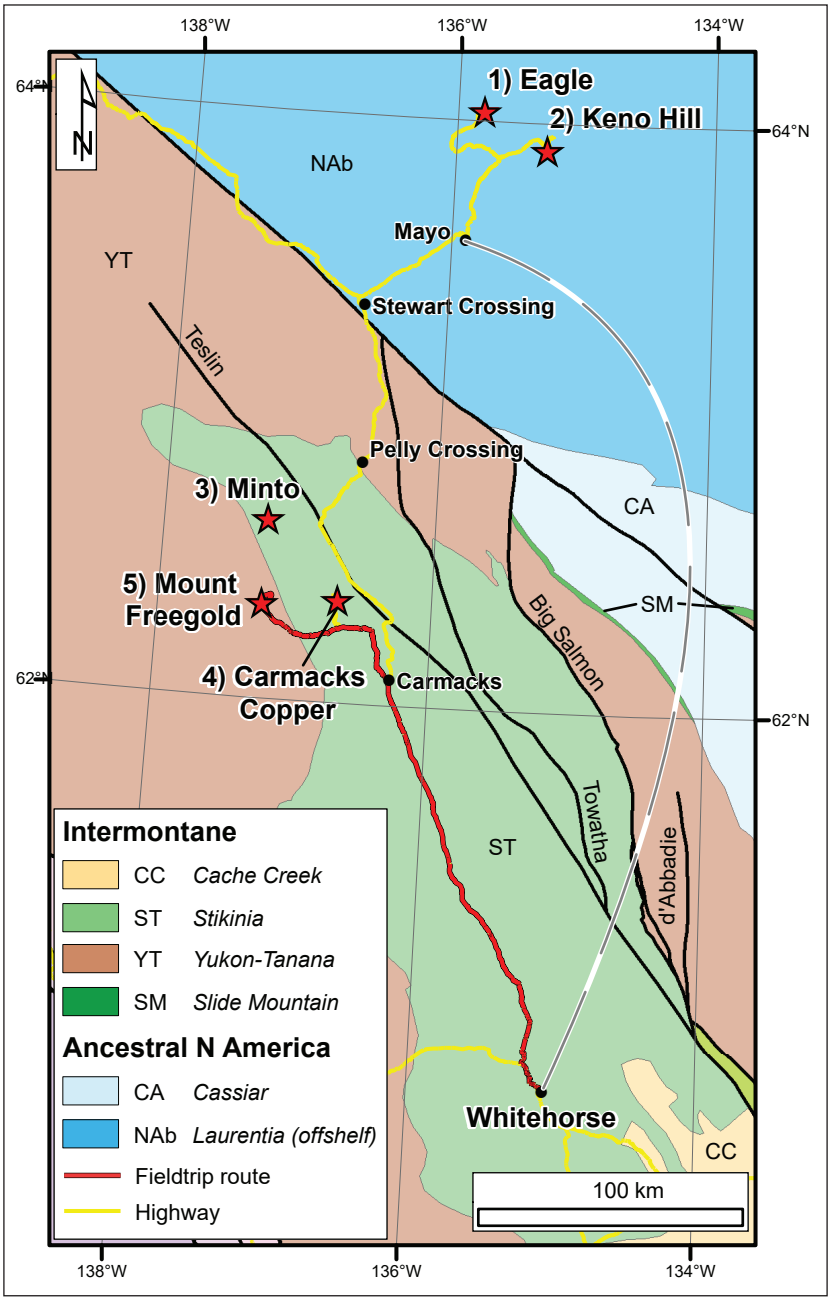

Figure 40. *Field trip route for Day 5. Numbered locations refer to order of field trip days in Table 1. Dashed grey line illustrates flight from Whitehorse to Mayo.*

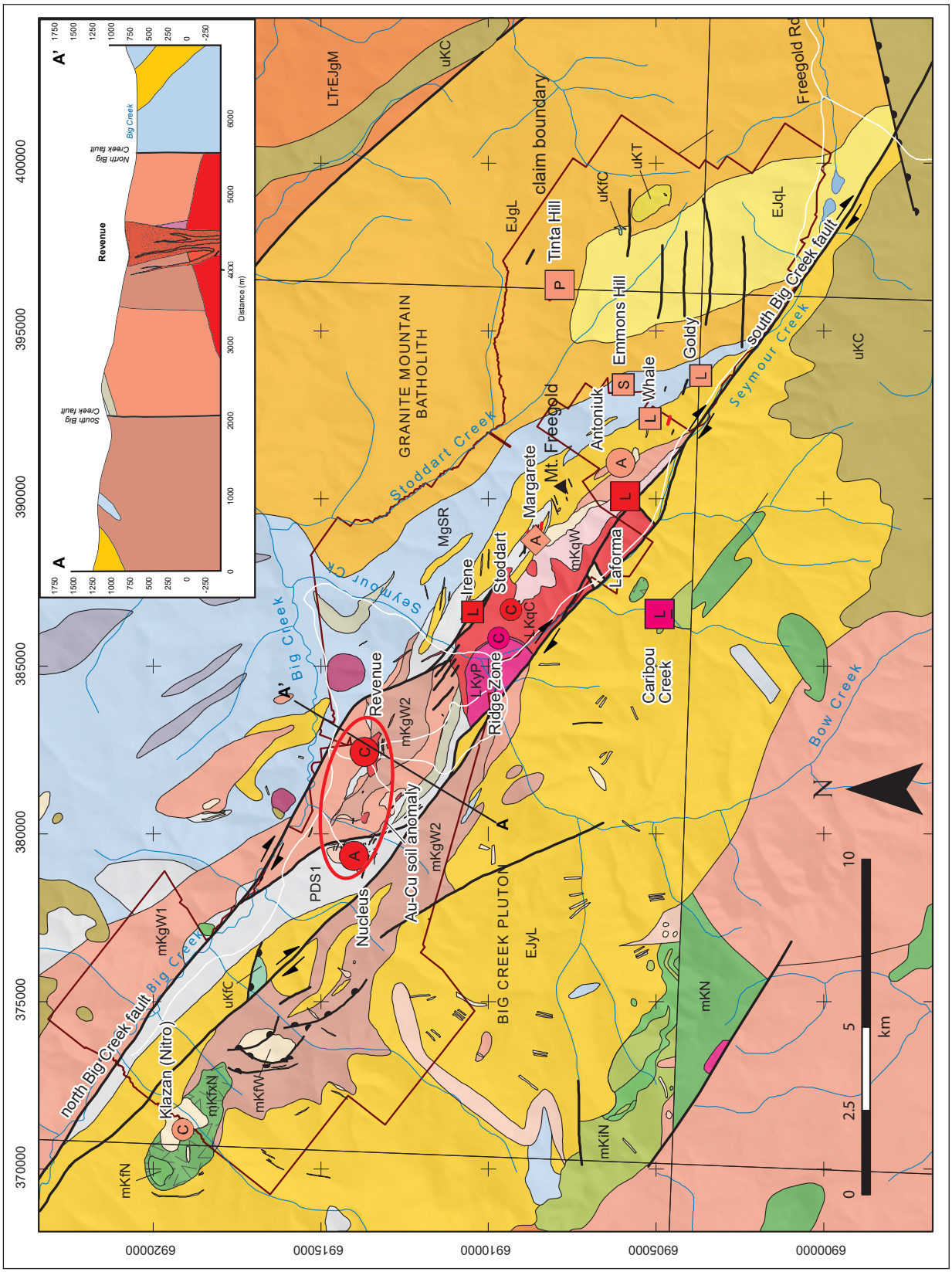

Figure 41. *Geology of the Freegold Mountain Project, showing the Big Creek Fault structure and associated stepover faults in the Revenue-Nucleus area (Friend et al., 2018). Cross section is looking northwest and is from Allan and Friend (2018). Legend on next page.*

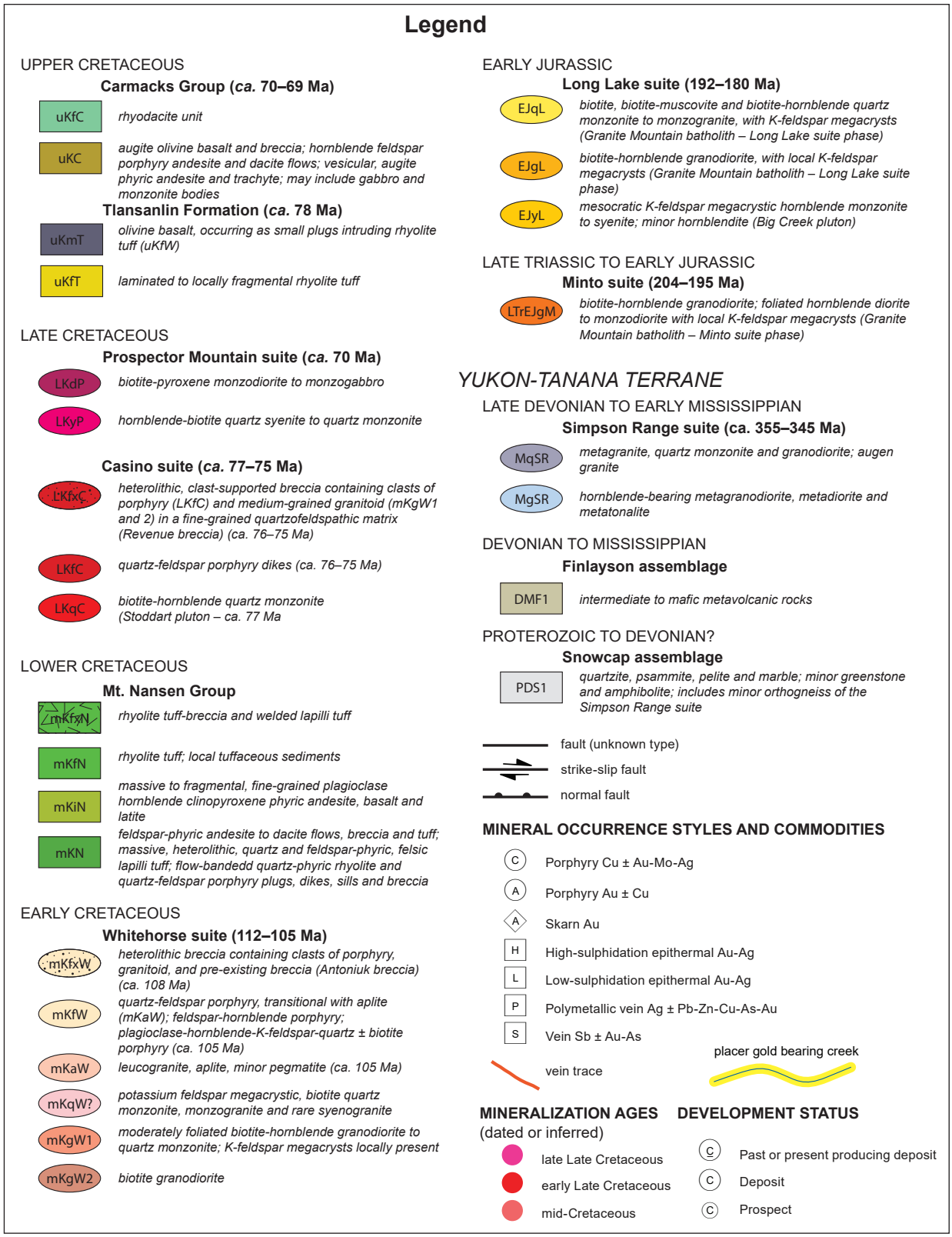

Figure 41. continued

Table 9. *Current mineral resource estimates at the Freegold Mountain property, recalculated in February 2020 by SIM Geological Inc. Nucleus and Revenue resources use a 0.30g/t AuEq cut-off for open pit and 1.00 g/t AuEq cut-off for underground; Tinta uses a 0.35g/t AuEq cut-off for open pit and 1.80 g/t AuEq cut-off for underground.*

		Average Grade								Contained Metal							
	Tonnes (million)	AuEq (g/t)	Au (g/t)	Cu (%)	Ag (g/t)	Mo (%)	W (%)	Pb (%)	Zn (%)	AuEq (koz)	Au (koz)	Cu (Mlbs)	Ag (koz)	Mo (klbs)	W (klbs)	Pb (klbs)	Zn (klbs)
Indicated																	
Nucleus	31	0.75	0.65	0.07	0.7	na	na	na	na	748	651	44	698	na	na	na	na
Revenue	11.4	0.69	0.38	0.12	2.4	0.02	0.01	na	na	252	140	30	895	4089	2082	na	na
Total Indicated	**42.4**	**0.73**	**0.58**	**0.08**	**1.2**					**1000**	**791**	**74**	**1593**	**4089**	**2082**		
Inferred																	
Nucleus	9.4	0.63	0.56	0.04	0.7	na	na	na	na	189	169	9	217	na	na	na	na
Revenue	27.5	0.77	0.51	0.12	2.5	0.01	0.01	na	na	677	446	73	2203	5478	2867	na	na
Tinta	2.2	3.08	1.29	0.17	44.7	na	na	0.63	1.29	220	92	8	3195	na	na	31	63
Total Inferred	**39**	**0.86**	**0.56**	**0.1**	**4.5**					**1085**	**707**	**90**	**5614**	**5499**	**3094**	**31**	**63**

The Mount Freegold project is a 200 km² block of claims that contains three deposits with NI43-101 resources totaling 1 million ounces of gold equivalent indicated, and 1.1 million ounces of gold equivalent inferred. The property also contains numerous prospective gold and copper showings. Access from Whitehorse is via the North Klondike highway to the village of Carmacks, then via the government-maintained Mount Freegold road (Fig. 40). Triumph Gold Corporation currently holds the property. The main exploration camp is located at kilometre 82 of the Mount Freegold road, near the Revenue and Nucleus deposits.

Mount Freegold district geology

The Mount Freegold district is a northwest elongate cluster of approximately 15 mid to Late Cretaceous porphyry, epithermal and skarn mineral occurrences located along a 20 km portion of the Big Creek fault system (Allan and Friend, 2018; Friend et *al.*, 2018; Fig. 41). The Big Creek fault system is a 130 km long, steeply dipping, northwest striking dextral

fault system that extends along the northeastern margin of the mid-Cretaceous Dawson Range batholith (Fig. 5). The spatial coincidence of Cretaceous magmatism, magmatic-hydrothermal occurrences and the Big Creek fault suggests a strong structural control on magmatism and mineralization in the area. In particular, the location of the Mount Freegold district coincides with a major stepover between two strands of the Big Creek fault, which has resulted in a structurally complex zone that hosts the Nucleus and Revenue deposits, the two largest deposits in the district (Table 9; Fig. 41).

The Mount Freegold district sits on Paleozoic Yukon-Tanana terrane metamorphic basement comprising metasiliciclastic rocks of the Snowcap assemblage, metavolcanic rocks of the Finlayson assemblage, both intruded by metaplutonic rocks of the Simpson Range suite (Fig. 41). These metamorphic rocks are intruded by mostly undeformed latest Triassic to Early Jurassic Minto and Long Lake suite plutonic rocks. Cretaceous magmatism in the district broadly occurred as two pulses, the first during 108 to 105 Ma when relatively large (up to 50 km²) stocks of northwest elongate, calc-alkaline granodiorite of the Whitehorse suite were emplaced. These plutonic rocks are coeval with minor epithermal and polymetallic vein and skarn occurrences, including Antoniuk [115I 111], Tinta Hill [115I 058] and Goldy [115I 182], that are hosted by the Paleozoic metamorphic and early Mesozoic plutonic rocks in the southeastern end of the district (Friend *et al.*, 2018; Fig. 41). The second Cretaceous magmatic pulse occurred during the Late Cretaceous, *ca.* 79 to 66 Ma, when relatively smaller volumes of Casino suite plutonic rocks (*ca.* 79–72 Ma) were emplaced as dikes, plugs and intrusive breccia complexes (Friend *et al.*, 2018). This stage of magmatism is coeval with the majority of mineralization in the district, including that at the Nucleus [115I 107] and Revenue [115I 042] deposits where the age of mineralization is constrained by several Re-Os molybdenite ages of *ca.* 75 Ma (Allan and Friend, 2018). Late Cretaceous magmatism ended with emplacement of the volumetrically minor, slightly alkalic Prospector Mountain plutonic suite (*ca.* 72–66 Ma) and eruption of the widespread bimodal Carmacks Group volcanic rocks (*ca.* 70 Ma). Mineralization is associated with Prospector Mountain rocks regionally, for example, at the Cyprus porphyry occurrence [115I 066] in the Mount Nansen district, 25 km south of the Mount Freegold district (Selby and Creaser, 2001). However, locally this age of mineralization seems to be poorly represented, with the lone example possibly being the Ridge zone near the Seymour Creek stock (Friend *et al.*, 2018).

The Big Creek fault system was active from at least the mid-Cretaceous to the Paleogene over a span of 50 to 60 m.y. In the mid-Cretaceous it likely influenced the emplacement of Whitehorse suite rocks, as evidenced by the elongation of these bodies parallel to the strike of the system. Uranium-lead in calcite dating shows that there was also movement along the fault system in the Late Cretaceous, coeval with emplacement of Casino suite

plugs and porphyry-epithermal mineralization; the latest movement occurred post-mineralization in the Paleocene to early Eocene (Mottram et *al.*, 2020).

Age of mineralization

Geochronologic data limit the main mineralizing event to the Late Cretaceous: approximately 76–72 Ma (Bineli Betsi and Bennett, 2010; M. Friend, pers. comm., 2019; Mottram, pers. comm., 2019, Creaser, pers. comm., 2018; Bineli Betsi et *al.*, 2013). Mineralization is roughly coeval with early movement on the Big Creek fault and emplacement of Casino suite rocks including quartz-feldspar porphyry dikes, the Revenue diatreme, and the Stoddart pluton (Fig. 41).

Nucleus deposit

The Nucleus Au-Ag-Cu deposit lies immediately west of a stepover fault that connects the north and south Big Creek fault strands (Fig. 41). The deposit is hosted in tightly-folded Yukon-Tanana metavolcanic schist and gneiss. Microgranite, a term applied to an aplitic phase of the Revenue granite, forms a small roughly tabular stock that overlaps with the northern end of the deposit. The Nucleus resource occurs in a complex region of intersecting dikes of microgranite, Revenue granite, and quartz-feldspar-porphyry, that parallel west and northwest-trending faults. Mineralization at Nucleus is consistent with an early stage of skarn development, overprinted by a multiphase epithermal gold system. Mineralization styles include polyphase quartz-chalcopyrite-pyrite-arsenopyrite veins, mineralized hydrothermal and fault breccia, and semi to massive-sulphide lenses. A copper and gold oxide blanket of irregular thickness covers the deposit.

Revenue deposit

The Revenue deposit consists of porphyry style mineralization, which until recent years was considered spatially related to the Revenue diatreme, primarily along its southern contact with the Revenue granite. The Revenue diatreme is an east-trending, ovoid, groundmass to clast-supported, pyroclastic breccia that was emplaced along the contact of two phases of the Revenue granite, which is sometimes marked by a screen of Yukon-Tanana country rock. The diatreme hosts low-grade copper and gold throughout, with higher-grade domains associated with late replacement and hydrothermal-breccia styles of mineralization. The Revenue resource contains copper, molybdenum, tungsten, gold and silver occurring as disseminated sulphides, stockwork veins, and breccias with sulphide cement (Campbell et *al.*, 2015; Sim, 2020). Since 2017 Triumph has discovered a number of other porphyry-related breccia and stockwork zones outboard of the Revenue diatreme.

Exploration

In 2016 the resources on the Mount Freegold property area were considered too

low-grade to attract a capital investment for a mine and mill, so the focus of exploration was turned to the potential for additional, higher-grade mineralization. Compilation of soil geochemistry showed a 6 km long multi-element gold, silver, copper and molybdenum anomaly that encompassed Nucleus, Revenue and numerous other lesser-explored showings (Fig. 41). Review of drill core data revealed low-temperature alteration (illite-kaolinite) at Nucleus and related to the Revenue diatreme, but higher temperature potassic alteration and mineralization associated with quartz stockwork in several locations outboard of the resource areas, within the soil anomaly. Subsequent exploration east of the diatreme has resulted in multiple intersections of the highest-grading porphyry copper rocks found to date on the property. It is now understood that emplacement of the Revenue diatreme occurred during the latest stage of an evolving magmatic-hydrothermal system. Exploration focused on the earlier stages of porphyry

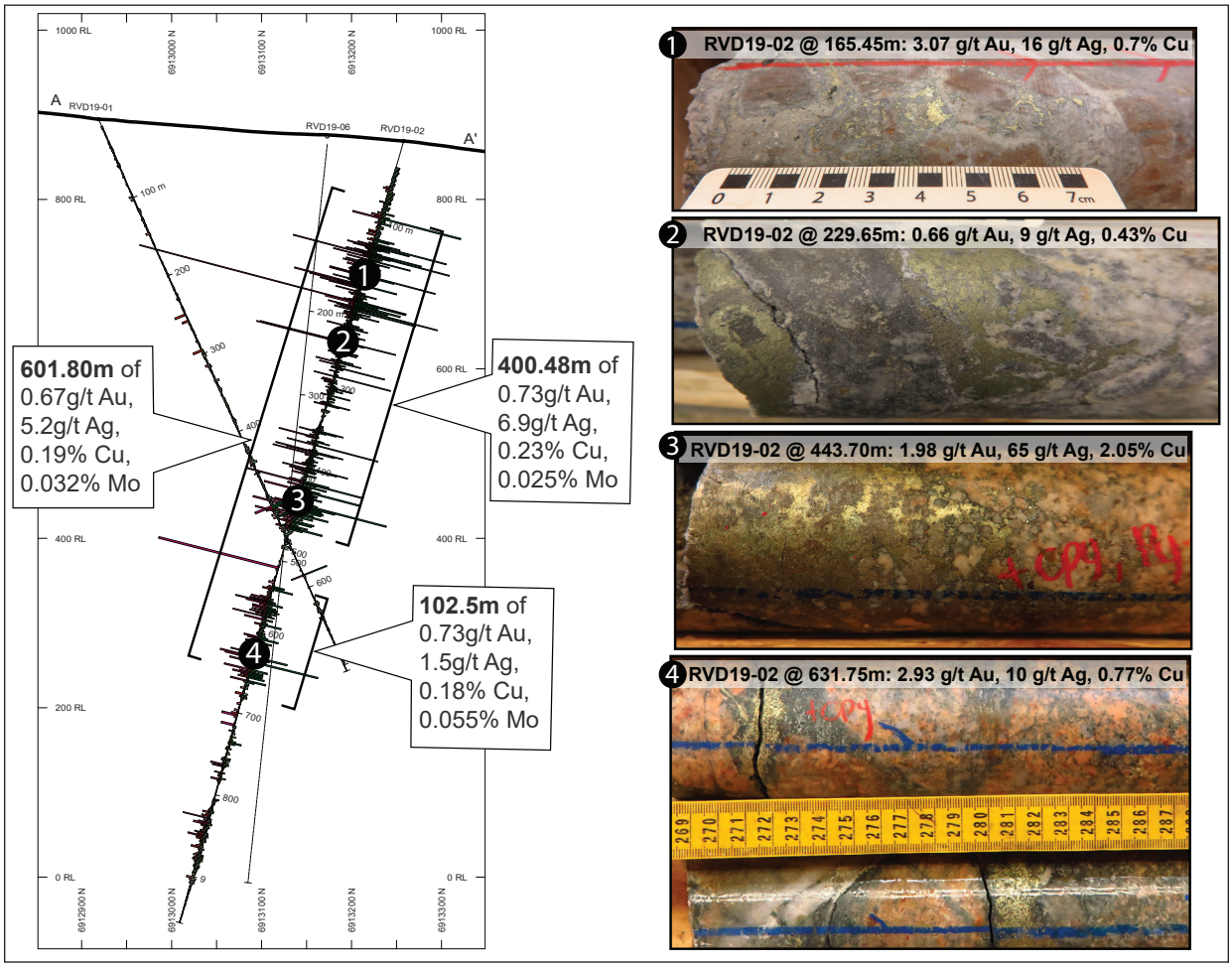

Figure 42. *Cross section 383000E, looking west, with photographs of representative core from hole RVD19-02. Section is located east of the Revenue diatreme in the WAu breccia body. RVD19-02 includes an intersection over 400 m of mineralized rock before transitioning to over 100 m of high-temperature magnetite-potassic intrusive breccia. Red bars show gold assay data and green show copper. Section is 50 m thick.*

related mineralization has yielded exploration successes in recent years (e.g., RVD18-19 with 316 m of 1.1 g/t Au, 5 g/t Ag. 0.27% Cu and 0.02% Mo).

Recent new discoveries include the WAu breccia, a Au-Ag-Cu-Mo-W rich hydrothermal breccia pipe immediately southeast of the Revenue diatreme with significant concentrations of Pb, Zn, and Co, and the Blue Sky breccia, a Au-Cu rich steeply-dipping pipe-like hydrothermal breccia. Both breccia bodies overprint domains of Cu-Mo-Au mineralized stockwork quartz veins, and are overprinted by varying densities of late polymetallic veins that contain coarse visible gold. The Blue Sky breccia is mainly characterized by high temperature potassic alteration (biotite ± potassium feldspar) with local phyllic overprints, while the WAu breccia is mainly affected by low temperature

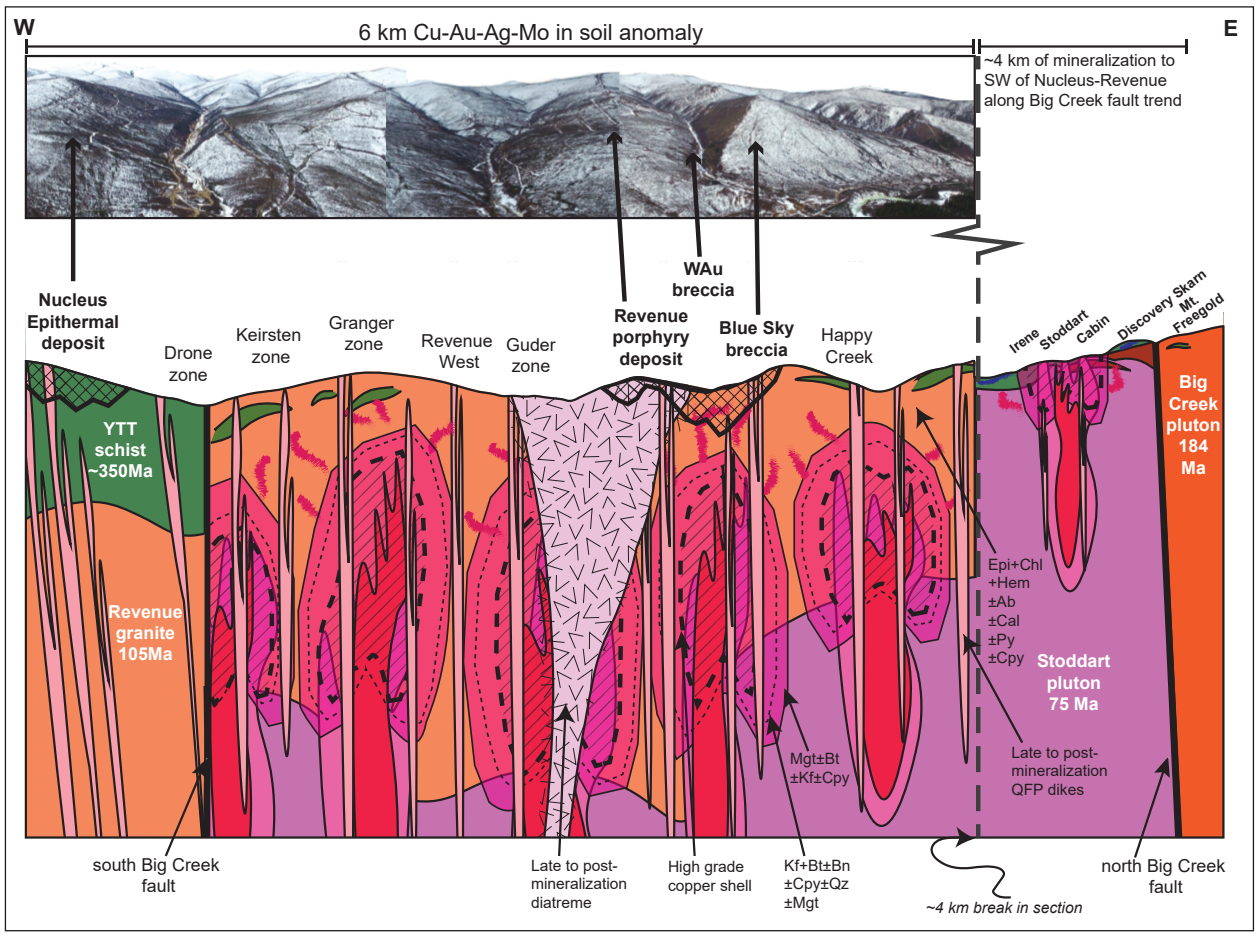

Figure 43. *Panorama looking north with a schematic cross section below showing multiple porphyry centres (represented in red with pink mineralized shells), emanating from a causative intrusion (purple) and emplaced in a passive host (orange). Epi = epidote, Chl = chlorite, Hem = hematite, Ab = albite, Cal = calcite, Py = pyrite, Cpy = chalcopyrite, Kf = K-feldspar, Bt = biotite, Bn = bornite, Qz = quartz, Mgt = magnetite.*

illite-kaolinite alteration to a depth of approximately 450 m, where it begins to transition to higher-temperature potassic alteration (Fig. 42). A portion of the Blue Sky breccia was high enough grade (e.g., over 1 g/t gold equivalent) to be incorporated into an underground resource, which is now part of the otherwise pit-constrained Revenue Au-Cu-Mo-W-Ag deposit (Table 9). Mineralization in both breccia bodies consists of chalcopyrite and molybdenite in stockwork veins, disseminations, and breccia infill. A late stage of quartz-carbonate veins with galena, sphalerite, scheelite, bismuth-tellurides and sometimes significant native gold overprints the breccia mineralization.

The Revenue-Nucleus area conforms to a generalized copper-gold porphyry system model where volatiles are driven-off of a crystallizing magma intruding at shallow crustal levels (Fig. 43). The epithermal deposit at Nucleus, is considered the distal expression of the larger magmatic-hydrothermal system. The Revenue diatreme is the latest mineralizing event in the area as it crosscuts earlier stockwork veining, the WAu breccia, and contains mineralized clasts. The six-kilometre-long soil anomaly that encompasses the Revenue and Nucleus deposits is currently being explored for multiple buried porphyry centres. The deposits themselves, as well as other mineralized rocks found across the area of interest, are considered to be high-level expressions of these buried porphyry centers. In 2019, deep drilling to the east of the diatreme and beneath the WAu breccia intersected one such porphyry centre starting at a depth of approximately 550 m, where a chalcopyrite-magnetite intrusive breccia in intensely potassic-altered granite, grading 0.73 g/t Au, 1.5 g/t Ag, 0.18% Cu, and 0.055% Mo was intersected over 102.5 m (Fig. 42). Beneath the chalcopyrite-magnetite breccia an aplitic intrusive breccia was intersected; it is interpreted to be an apical domain of a causative intrusion. In a drill hole eight hundred metres to the west, a clast of porphyritic rock with bornite-bearing A-veins as well as clasts with unidirectional solidification textures and clotty chalcopyrite, over a 15 m interval within the diatreme were identified. These mineralized clasts are thought to represent a second, as of yet untested porphyry centre.

Mineralized porphyry centres appear to extend southward along the belt of mid to Late Cretaceous intrusions to Mount Freegold 4 km away. At Mount Freegold, the Stoddart porphyry [115I 121] is a drilled prospect with numerous 100 m long >0.1% Cu intersections and there are a number of other undrilled porphyry prospects, as well as variably tested epithermal vein and skarn showings.

Relevant papers

Thompson *et al.* (1999) – redox conditions of magma and metal mobility

Cathro (2006) – History and geology of Keno Hill silver camp

Sack *et al.* (2017) – Minto deposit description

Kovacs *et al.* (2020) – Carmacks Copper description and geochronology

Friend *et al.* (2018) – Mount Freegold district geology

References

Abbott, J.G., 1971. Geology of the Williams Creek prospect. Unpublished BSc thesis, University of British Columbia, 53 p.

Abbott, J.G. and Turner, R.J.W., 1990. Character and paleotectonic setting of Devonian stratiform sediment-hosted Zn, Pb Ba deposits, Macmillan Fold Belt, Yukon. *In:* Field Trip Guidebook, 8th IAGOD Symposium: Mineral deposits of the northern Canadian Cordillera, Yukon-eastern British Columbia, J.G. Abbott and R.J.W. Turner (eds.), *also* Geological Survey of Canada, Open File 2169, p. 99–136.

Allan, M.A. and Friend, M., 2018. Bedrock geological map of the Mount Freegold district, Dawson Range (NTS 115l/6 and parts of 115l/2, 3, 5, 7, 10, 11, 12). Yukon Geological Survey, Open File 2018-2.

Armstrong, R.L., 1988. Mesozoic and early Cenozoic magmatic evolution of the Canadian Cordillera. Geological Society of America Special Papers, vol. 218, p. 55–92.

Beaudoin, G. and Sangster, D.F., 1992. A descriptive model for silver-lead-zinc veins in clastic metasedimentary terranes. Economic Geology, vol. 87, p. 1005–1021.

Berman, R.G., Ryan, J.J., Gordey, S.P. and Villeneuve, M., 2007. Permian to Cretaceous polymetamorphic evolution of the Stewart River region, Yukon-Tanana terrane, Yukon, Canada: P–T evolution linked with in situ SHRIMP monazite geochronology. Journal of Metamorphic Geology, vol. 25, p. 803–827.

Bineli Betsi, T. and Bennett, V., 2010. New U-Pb age constraints at Freegold Mountain: Evidence for multiple phases of polymetallic mid- to Late Cretaceous mineralization. *In:* Yukon Exploration and Geology 2009, K.E. MacFarlane, L.H. Weston and L.R. Blackburn (eds.), Yukon Geological Survey, p. 57–84.

Bineli Betsi, T., Lentz, D., Chiaradia, M., Kyser, K. and Creaser, R., 2013. Genesis of the Au–Bi–Cu–As, Cu–Mo ± W, and base–metal Au–Ag mineralization at the Mountain Freegold (Yukon, Canada): constraints from Ar–Ar and Re–Os geochronology and Pb and stable isotope compositions. Mineralium Deposita, vol. 48, p. 1–27.

Bond, J., 1998. Surficial geology of Keno Hill sheet 105M/14. Indian and Northern Affairs Canada, Geoscience Map 1998-4.

Bordet, E., Crowley, J.L. and Piercey, S. J., 2019. Geology of the eastern Lake Laberge area (105E), south-central Yukon. Yukon Geological Survey, Open File 2019-1, 120 p.

Boyle, R.W., 1965. Geology, geochemistry and origin of the lead-zinc-silver deposits of the Keno-Galena Hill area, Yukon Territory. Geological Survey of Canada, Bulletin 111, 302 p.

Campbell, J., Sexton, A., Armitage, A. and Studd, D., 2015. Technical report on the Freegold Mountain project, Yukon, Canada: Resource estimates. Northern Freegold Resources Ltd., February 28, 2015.

Casselman, S. (compiler), 2018. Yukon mineral deposits summary 2018. Yukon Geological Survey, 30 p.

Casselman, S., 2007. Assessment Report for the Carmacks Copper project (Volume 1). Yukon Mining Assesment Report 094996.

Cathro, R.J., 2006. Great Mining camps of Canada 1: The history and geology of the Keno Hill Silver Camp, Yukon Territory. Geoscience Canada, vol. 33, p. 103–134.

Clark, A.D., 2017. Tectonometamorphic history of mid-crustal rocks at Aishihik Lake, southwest Yukon. Unpublished MSc thesis, Simon Fraser University, 153 p.

Cobbett, R., Colpron, M., Crowley, J.L., Cordey, F., Blodgett, R.B. and Orchard, M.J., 2021. Late Devonian magmatism and clastic deposition in the upper Earn Group (central Yukon) mark the transition from passive to active margin along western Laurentia. Canadian Journal of Earth Sciences, vol. 58, p. 471–494, doi: 10.1139/cjes-2020-0161.

Colpron, M. (compiler), 2006. Tectonic assemblage map of Yukon-Tanana and related terranes in Yukon and northern British Columbia. Yukon Geological Survey, Open File 2006-1.

Colpron, M. and Friedman, R.M., 2008. U-Pb zircon ages for the Nordenskiold formation (Laberge Group) and Cretaceous intrusive rocks, Whitehorse trough, Yukon. *In:* Yukon Exploration and Geology 2007, D.S. Emond, L.R. Blackburn, R.P. Hill and L.H. Weston (eds.), Yukon Geological Survey, p. 139–151.

Colpron, M. and Nelson, J.L., 2009. A Palaeozoic Northwest Passage: incursion of Caledonian, Baltican and Siberian terranes into eastern Panthalassa, and the early evolution of the North American Cordillera. *In:* Earth Accretionary Systems in Space and Time, P.A. Cawood and A. Kröner (eds.), Geological Society of London, Special Publications 318, p. 273–307.

Colpron, M. and Nelson, J.L., 2021. Northern Cordillera: Canada and Alaska. *In:* Encyclopedia of Geology, volume 4, Regional Geology|Americas, S.A. Elias and D. Alderton (eds.), Elsevier Science, p. 93–106.

Colpron, M., Nelson, J.L. and Murphy, D.C., 2006, A tectonostratigraphic framework for the pericratonic terranes of the northern Cordillera. *In:* Paleozoic Evolution and Metallogeny of Pericratonic Terranes at the Ancient Pacific Margin of North America, Canadian and Alaskan Cordillera, M. Colpron and J.L. Nelson (eds.), Geological Association of Canada, Special Paper 45, p. 1-23.

Colpron, M., Nelson, J.L. and Murphy, D.C., 2007. Northern Cordilleran terranes and their interactions through time. GSA Today, vol. 17, p. 4–10.

Friend, M., Allan, M.A. and Hart, C.J.R., 2018. New contributions to the bedrock geology of the Mount Freegold district, Dawson Range, Yukon (NTS 115I/2, 6 and 7). *In:* Yukon Exploration and Geology 2017, K.E. MacFarlane (ed.), Yukon Geological Survey, p. 47–68.

Gabrielse, H., Murphy, D.C. and Mortensen, J.K., 2006. Cretaceous and Cenozoic dextral orogen-parallel displacements, magmatism and paleogeography, north central Canadian Cordillera. *In:* Evidence for Major Lateral Displacements in the North American Cordillera, J.W. Haggart, J.W.H. Monger and R.J. Enkin (eds.), Geological Association of Canada, Special Paper 46, p. 255–276.

Gaidies, F., Morneau, Y.E., Petts, D.C., Jackson, S.E., Zagorevski, A. and Ryan, J.J., 2021. Major and trace element mapping of garnet: Unravelling the conditions, timing and rates of metamorphism of the Snowcap assemblage, west-central Yukon. Journal of Metamorphic Geology, vol. 39, p. 133–164, doi: 10.1111/jmg.12562.

Gordey, S.P. and Anderson, R.G., 1993. Evolution of the northern Cordilleran miogeocline, Nahanni map area (105I), Yukon and Northwest Territories. Geological Survey of Canada, Memoir 428, 214 p.

Gordey, S.P., Abbott, J.G., Tempelman-Kluit, D.J. and Gabrielse, H., 1987. "Antler" clastics in the Canadian Cordillera. Geology, vol. 15, p. 103–107.

Greybeal, F.T. and Vikre, P.G., 2010. A review of silver rich mineral deposits and their metallogeny. Society of Economic Geology, Special Publication 15, p. 85–117.

Hantelmann, J.J., 2013. The paragenesis and geochemistry of the Bellekeno Ag-Pb-Zn vein, Keno Hill district, Yukon. Unpublished MSc thesis, University of Alberta, 292 p.

Hantelmann, J., 2014a. Report on the petrography and fluid Inclusion analyses of the Flame vein system in the Keno Hill district, Yukon, Canada. Alexco Resources Ltd., Internal Report.

Hantelmann, J.J., 2014b. Keno Hill district Ag-Pb-Zn vein mineral assemblages and pargenesis. Alexco Resources Ltd., Internal Report.

Hart, C.J.R., 2007. Reduced Intrusion-related gold systems. *In:* Mineral Deposits of Canada: A Synthesis of Major Deposit-types, District Metallogeny, the Evolution of Geological Provinces, and Exploration Methods, W.D. Goodfellow (ed.), Geological Association of Canada, Mineral Deposits Division, Special Publication 5, p. 95–112.

Hart, C.J.R., 1997. A transect across northern Stikinia: Geology of the northern Whitehorse map area, southern Yukon Territory (105D/13-16). Exploration and Geological Services Division, Yukon Region, Indian and Northern Affairs Canada, Bulletin 8, 112 p.

Hart, C.J.R., Goldfarb, R.J., Lewis, L.L. and Mair, J.L., 2004a. The northern Cordillera mid-Cretaceous plutonic province: Ilmenite/magnetite-series granitoids and intrusion-related mineralization. Resource Geology, vol. 54, p. 253–280.

Hart, C.J.R., Mair, J.L., Goldfarb, R.J. and Groves, D.I., 2004b. Source and redox controls on the metallogenic variations in intrusion-related ore systems, Tombstone-Tungsten Belt, Yukon Territory, Canada: Transactions of the Royal Society of Edinburgh. Earth Sciences, vol. 95, p. 339–356.

Hood, S., 2012. Mid-crustal Cu-Au mineralisation during episodic pluton emplacement, hydrothermal fluid flow, and ductile deformation at the Minto deposit, YT, Canada. Unpublished MSc thesis, University of British Columbia, 231 p.

Hood, S., Hickey, K., Colpron, M. and Mercer, B., 2009. High-grade hydrothermal copper-gold mineralization in foliated granitoids at the Minto mine, central Yukon. *In:* Yukon Exploration and Geology 2008, L.H. Weston, L.R. Blackburn and L.L. Lewis (eds.), Yukon Geological Survey, p. 137–146.

Iles, S., 2013. A new model for the structural control of vein-fault mineralisation at the Bellekeno mine, Keno Hill. Alexco Resources Ltd., Internal Report.

Iles, S., 2016. A new model for the structural-stratigraphic control of vein-fault mineralisation at Keno Hill, Yukon. *In:* Geological Association of Canada/Mineralogical Association of Canada (GAC/MAC) 2016, Abstract vol. 39, Whitehorse, Yukon, June 1–3, 2016, p. 38.

JDS, 2016. NI 43-101 Preliminary economic assessment technical report on the Carmacks project, Yukon, Canada. Report prepared for Copper North Mining Corp., 227 p.

Kovacs, N., 2018. Genesis and post-ore modification of the migmatized Carmacks Copper Cu-Au-Ag porphyry deposit, Yukon, Canada. Unpublished MSc thesis, University of British Columbia, 291 p.

Kovacs, N., Allan, M.M., Crowley, J.L., Colpron, M., Hart, C.J.R., Zagorevski, A. and Creaser, R.A., 2020. Carmacks Copper Cu-Au-Ag deposit: mineralization and post-ore migmatization of a Stikine arc porphyry copper system in Yukon, Canada. Economic Geology, vol. 115, p. 1413–1442.

Logan, J.M. and Mihalynuk, M.G., 2014. Tectonic controls on Early Mesozoic paired alkaline porphyry deposit belts (Cu-Au ± Ag-Pt-Pd-Mo) within the Canadian Cordillera. Economic Geology, vol. 109, p. 827–858.

Lynch, J.V.G., 1989. Large-scale hydrothermal zoning reflected in the tetrahedrite-freibergite solid solution, Keno Hill Ag-Pb-Zn district, Yukon. The Canadian Mineralogist, vol. 27, p. 383–400.

Mair, J.L., Hart, C.J.R. and Stephens, J.R., 2006. Deformation history of the northwestern Selwyn Basin, Yukon, Canada: Implications for orogen evolution and mid-Cretaceous magmatism. Geological Society of America Bulletin, vol. 118, p. 304–323.

McTaggart, K.C., 1960. The geology of Keno and Galena Hills. Geological Survey of Canada, Bulletin 58, 37 p.

Mercer, B. and Sagman, J., 2012. Phase VI Preliminary Feasibility Report Minto Mine. Minto Explorations Ltd., 368 p.

Mezger, J.E., Creaser, R.A., Erdmer, P. and Johnston, S.T., 2001. A Cretaceous back-arc basin in the Coast Belt of the northern Canadian Cordillera: evidence from geochemical and neodymium isotope characteristics of the Kluane metamorphic assemblage, southwest Yukon. Canadian Journal of Earth Sciences, vol. 38, p. 91–103.

Mihalynuk, M.G., Nelson, J. and Diakow, L.J., 1994. Cache Creek terrane entrapment: Oroclinal paradox within the Canadian Cordillera. Tectonics, vol. 13, p. 575–595.

Monger, J.W.H. and Gibson, H.D., 2019. Mesozoic-Cenozoic deformation in the Canadian Cordillera: The record of a "Continental Bulldozer"? Tectonophysics, vol. 757, p. 153–169.

Monger, J.W.H. and Price, R.A., 2002. The Canadian Cordillera: Geology and tectonic evolution. Canadian Society of Exploration Geophysicists Recorder, vol. 27, p. 17–36.

Mortensen, J.K., 1992. Pre-Mid-Mesozoic tectonic evolution of the Yukon-Tanana terrane, Yukon and Alaska. Tectonics, vol. 11, p. 836–853.

Mottram, C.M., Kellett, D.A., Baressi, T., Zwingmann, H., Friend, M., Todd, A. and Percival, J.B., 2020. Syncing fault rock clocks: Direct comparison of U-Pb carbonate and K-Ar illite fault dating methods. Geology, vol. 48, p. 1179–1183,

Moynihan, D.P., Strauss, J.V., Nelson, L.L. and Padget, C.D., 2019. Upper Windermere Supergroup and the transition from rifting to continent-margin sedimentation, Nadaleen River area, northern Canadian Cordillera. Geological Society of America Bulletin, vol. 131, p. 1673–1701.

Murphy, D., 1997. Geology of the McQuesten River region, northern McQuesten and Mayo map areas, Yukon Territory (115P/14, 15, 16; 105M/13, 14). Indian and Northern Affairs Canada, Exploration and Geological Services Division, Yukon, Bulletin 6, 122 p.

Murphy, D., Mortensen, J.K., Piercey, S.J., Orchard, M.J. and Gehrels, G., 2006. Mid-Paleozoic to early Mesozoic tectonostratigraphic evolution of Yukon-Tanana and Slide Mountain terranes and affiliated overlap assemblages, Finlayson Lake massive sulphide district. *In:* Paleozoic evolution and metallogeny of pericratonic terranes at the ancient Pacific margin of North America, Canadian and Alaskan Cordillera, M. Colpron and J.L. Nelson (eds.), Geological Association of Canada, Special Paper 45, p. 75–106.

Nelson, J.L., Colpron, M. and Israel, S., 2013. The Cordillera of British Columbia, Yukon, and Alaska: Tectonics and metallogeny. *In:* Tectonics, Metallogeny and discovery: The North American Cordillera and similar accretionary settings, M. Colpron, T. Bissig, B.G. Rusk, and J.F. Thompson (eds.), Society of Economic Geologists, Special Publication No. 17, p. 53–109.

Nelson, J.L., Colpron, M., Piercey, S.J., Dusel-Bacon, C., Murphy, D.C. and Roots, C.F., 2006. Paleozoic tectonic and metallogenic evolution of the pericratonic terranes in Yukon, northern British Columbia and eastern Alaska. *In:* Paleozoic Evolution and Metallogeny of Pericratonic Terranes at the Ancient Pacific Margin of North America, Canadian and Alaskan Cordillera, M. Colpron and J.L. Nelson (eds.), Geological Association of Canada, Special Paper 45, p. 323–360.

Pearson, W.N. and Clark, A.H., 1979. The Minto copper deposit, Yukon Territory; a metamorphosed orebody in the Yukon crystalline terrane. Economic Geology, vol. 74, p. 1577–1599.

Piercey, S.J. and Colpron, M., 2009. Composition and provenance of the Snowcap assemblage, basement to the Yukon-Tanana terrane, northern Cordillera: Implications for Cordilleran crustal growth. Geosphere, vol. 5, p. 439–464.

Rasmussen, K.L., 2013. The timing, composition and petrogenesis of syn- to post-accretionary magmatism in the northern Cordilleran miogeocline, eastern Yukon and southwest Northwest Territories. Unpublished PhD thesis, University of British Columbia, 810 p.

Read, P.B., 2010. Stratigraphy, structure and exploration opportunities, Sourdough, Galena and Part of Keno hills. Unpublished report for Alexco Resource Corp.

Read, P.B., McOnie, A. and Iles, S., 2020. Geology of the Keno Hill district, Yukon. Yukon Geological Survey, Open File 2020-42, scale 1:25 000 and 1:2 500, 2 sheets.

Read, P.B., McOnie, A. and Iles, S., 2021. Keno Hill mining camp. Yukon Geological Survey, Miscellaneous Report MR-21, 35 p.

Roots, C.F., 1997. Geology of the Mayo map area, Yukon Territory (105M). Indian and Northern Affairs Canada, Exploration and Geological Services Division, Yukon, Bulletin 7, 82 p.

Sack, P.J., Colpron, M., Crowley, J.L., Ryan, J.J., Allan, M.M., Beranek, L.P., Joyce, N.L., Mortensen, J.K., Israel, S. and Chapman, J.B., 2020. Atlas of Late Triassic to Jurassic plutons in the Intermontane terranes of Yukon. Yukon Geological Survey, Open File 2020-1.

Sack, P.J., Kerr, R. and McIlveen, D., 2017. Update on the Minto deposit (Yukon MINFILE 115I021, 022). *In:* Yukon Exploration and Geology Overview 2016, K.E. MacFarlane (ed.), Yukon Geological Survey, p. 75–87, plus digital appendices.

Selby, D. and Creaser, R.A., 2001. Late and mid-Cretaceous mineralization in the northern Canadian Cordillera: Constraints from Re-Os molybdenite dates. Economic Geology, vol. 96, p. 1461–1467.

Selby, D., Creaser, R.A., Heaman, L.M. and Hart, C. J. R., 2003. Re-Os and U-Pb geochronology of the Clear Creek, Dublin Gulch, and Mactung deposits, Tombstone gold belt, Yukon, Canada: Absolute timing relationships between plutonism and mineralization. Canadian Journal of Earth Sciences, vol. 40, p. 1839–1852.

Sim, R. and Davis, B.M., 2020. Freegold Mountain project, Yukon, Canada: NI 43-101 Technical Report. Report prepared for Triumph Gold Corporation, February 2020.

Simard, R.-L., 2003. Geological map of southern Semenof Hills (part of NTS 105E/1, 7, 8), south-central Yukon. Yukon Geological Survey, Open File 2003-12.

Sinclair, A.J., Tessari, O.J. and Harakal, J.E., 1980. Age of Ag–Pb–Zn mineralization, Keno Hill – Galena Hill area, Yukon Territory. Canadian Journal of Earth Sciences, vol. 17, p. 1100–1103.

Tafti, R., 2005. Nature and origin of the Early Jurassic copper (-gold) deposits at Minto and Williams Creek, Carmacks copper belt, western Yukon: Examples of deformed porphyry deposits. Unpublished MSc thesis, University of British Columbia, 227 p.

Tempelman-Kluit, D.J., 1970. Stratigraphy and structure of the "Keno Hill Quartzite" in Tombstone River – Upper Klondike River map-areas, Yukon Territory (116B/7, 8). Geological Survey of Canada, Bulletin 180, 102 p.

Tempelman-Kluit, D. and Wanless, R. K., 1980. Zircon ages for the Pelly Gneiss and Klotassin granodiorite in western Yukon. Canadian Journal of Earth Sciences, vol. 17, p. 297–306.

Tempelman-Kluit, D. J., 1984. Geology of Laberge (105E) and Carmacks (115I) map areas, Yukon. Geological Survey of Canada, Open File 1101.

Tempelman-Kluit, D.J., 2009. Geology of Carmacks and Laberge map areas, central Yukon: Incomplete draft manuscript on stratigraphy, structure and its early interpretation (ca. 1986). Geological Survey of Canada, Open File 5982, 399 p.

Thompson, R.I., Root, C.F. and Mustard, P.S., 1992. Geology of Dawson map area (116B,C) (northeast of Tintina Trench). Geological Survey of Canada, scale 1:50 000.

Thompson, J.F.H., Sillitoe, R.H., Baker, T., Lang, J.R. and Mortensen, J., 1999. Intrusion-related gold deposits associated with tungsten-tin provinces. Mineralium Deposita, vol. 34, p. 323–334.

Tupper, D. and Bennett, V., 2010. Observations of polymetallic Ag-Pb-Zn (± Au ± In) mineralization at the Eagle and Fisher vein-faults, airborne total field magnetics and identification of Tombstone age-equivalent aplite dykes in the Galena Hill area, Keno City, Yukon. *In:* Yukon Exploration and Geology 2009, K.E. MacFarlane, L.H. Weston and L.R. Blackburn (eds.), Yukon Geological Survey, p. 305–330.

Vice, L., 2017. Late Cretaceous to Paleocene evolution of the Blanchard River assemblage, southwest Yukon; implications for Mesozoic accretionary processes in the northwestern. Unpublished MSc thesis, Simon Fraser University, 242 p.

Vice, L., Gibson, H.D. and Israel, S., 2020. Late Cretaceous to Paleocene tectonometamorphic evolution of the Blanchard River assemblage, southwest Yukon: New insight into the terminal accretion of Insular terranes in the northern Cordillera. Lithosphere, vol. 2020, doi.org/10.2113/2020/2298288.

Wheeler, J. O., 1961. Whitehorse map-area, Yukon Territory (105D). Geological Survey of Canada, Memoir 312, 156 p.

Yukon Geological Survey (YGS), 2020a. Yukon Digital Bedrock Geology. Yukon Geological Survey, https://data.geology.gov.yk.ca/Compilation/3#InfoTab, [accessed January 10, 2020].

Yukon Geological Survey (YGS), 2020b. Yukon Geochronology database. Yukon Geological Survey, https://data.geology.gov.yk.ca/Compilation/22#InfoTab, [accessed February 23, 2020].

Yukon Geological Survey (YGS), 2020c. Yukon MINFILE - A database of mineral occurrences. Yukon Geological Survey, https://data.geology.gov.yk.ca/Compilation/24#InfoTab, [accessed February 14, 2020].

Yukon Geological Survey (YGS), 2020d. A digital atlas of terranes for the northern Cordillera. Yukon Geological Survey, https://data.geology.gov.yk.ca/Compilation/2, [accessed January 20, 2020].

Zen, E. and Hammarstrom, J.M., 1984. Magmatic epidote and its petrologic significance. Geology, vol. 12, p. 515–518.